Discrete Generalized Multigroup Theory and Applications

By
Lei Zhu

B.Eng. Engineering Physics, Tsinghua University, 2005

M.S. Nuclear Engineering, Texas A&M University, 2008

Submitted to the Department of Nuclear Science and Engineering in Partial Fulfillment of the Requirement for the Degree of

Doctor of Philosophy in Nuclear Science and Engineering

at the

MASSACHUSETTS INSTITUTE OF TECHNOLOGY

February 2012

Signature of Author: _____
Department of Nuclear Science and Engineering
November 8, 2011

Certified by: _____
Benoit Forget – Thesis Supervisor
Assistant Professor of Nuclear Science and Engineering

Certified by: _____
Kord S. Smith – Thesis Reader
KEPCO Professor of the Practice of Nuclear Science and Engineering

Accepted by: _____
Mujid S. Kazimi
TEPCO Professor of Nuclear Engineering
Chair, Department Committee on Graduate Students

Discrete Generalized Multigroup Theory and Applications

By
Lei Zhu

Submitted to the Department of Nuclear Science and Engineering
on November 8, 2011, in Partial Fulfillment of the
Requirements for the degree of Doctor of Philosophy in
Nuclear Science and Engineering

ABSTRACT

This study develops a fundamentally new discrete generalized multigroup energy expansion theory for the linear Boltzmann transport equation. Discrete orthogonal polynomials are used, in conjunction with the traditional multigroup representation, to expand the energy dependence of the angular flux into a set of flux moments. The leading (zeroth) order equation is identical to a standard coarse group solution, while the higher order equations are decoupled from each other and only depend on the leading order solution due to the orthogonality property of the discrete Legendre polynomials selected. This decoupling leads to computational times comparable to the coarse group calculation but provides an accurate fine group energy spectrum. A source update process is also introduced which provides improvement of integral quantities such as eigenvalue and reaction rates over the coarse group solution.

An online energy recondensation methodology is proposed to improve traditional multilevel approach in reactor core simulations. Since the discrete generalized multigroup (DGM) method produces an unfolded flux with a fine group structure, this flux can then be used to recondense the coarse group cross-sections using the obtained core level fine group DGM solution, which can be done iteratively. Computational tests on light water reactors and high temperature reactors are performed. Results indicate that flux can fully converge to the fine group solution with a computational time less than that of standard fine group calculation as long as a flat angular flux approximation is used spatially.

The recondensation concept is extended to a nonlinear energy acceleration form. The method can effectively accelerate the fine group calculation by providing a more accurate initial guess provided from a few iterations of DGM recondensation calculation. Computational results show that the computational time and number of transport sweeps of the accelerated algorithm are much less than those of corresponding standard fine group calculations.

Thesis Supervisor: Benoit Forget
Title: Assistant Professor of Nuclear Science and Engineering

Thesis Reader: Kord S. Smith
Title: KEPCO Professor of the Practice of Nuclear Science and Engineering

Acknowledgements

I would like to express my deepest gratitude to my advisor, Prof. Benoit Forget for his continuous support and constructive advices throughout my PhD study at MIT. His encouragements and help have made me really enjoy this research project over the past a few years.

I am deeply grateful to my thesis reader, Prof. Kord Smith for his incredibly helpful discussions and advices. His wide knowledge in computational reactor physics has been of great value to me.

Many thanks to Dr. Thomas Newton for his advice and funding support during my first year of study on the MIT Reactor fuel conversion project. Many thanks to the funding support from the Consortium for Advanced Simulation of Light Water Reactors (CASL) project.

I would like to thank all the professors, staffs, colleagues and friends in the Department of Nuclear Science and Engineering. Additionally, I would like to thank the department for giving me the opportunity to study here.

I would like to thank my parents for their continuous support and love throughout my life. Thanks for their encouragement for my graduate study in the US.

Lastly, I would like to give a special thank to my wife, Shanshan, for her support and love.

Table of Contents

Abstract 3

Acknowledgements 4

Table of Contents 5

List of Figures 7

List of Tables 10

Acronyms 12

Chapter 1. Introduction 14

1.1 Motivation 14
1.2 Objectives 15
1.3 Thesis organization 16

Chapter 2. Background and Review 18

2.1 Energy related discretization methods in deterministic transport 18
2.1.1 Multigroup methodology 18
2.1.2 CENTRM and submoment expansion 19
2.1.3 RAZOR continuous energy lattice code 22
2.1.4 Linear multigroup method 22
2.1.5 Wavelet energy expansion 23
2.1.6 Opacity distribution function concept 25
2.1.7 Energy expansion using continuous orthogonal polynomials 26
2.2 Current multilevel approaches in reactor simulations 28
2.2.1 General multilevel approaches 28
2.2.2 Lattice-core online iteration methods 30

Chapter 3. Discrete Generalized Multigroup Energy Expansion Theory 33

3.1 DGM method derivation 33
3.2 Comparison of discrete and continuous energy expansions 41
3.3 Computational results 45
3.3.1 One dimensional BWR assembly tests 47
3.3.2 One dimensional BWR core tests 49
3.3.3 Eigenvalue and fluxes updates 52
3.4 Summary 61

Chapter 4. Online Energy Recondensation Methodology 64

4.1 Method description 64
4.2 Computational results 70
4.2.1 One dimensional BWR core tests 70
4.2.2 One dimensional HTR core tests 81
4.2.3 Two dimensional PWR core tests 96
4.2.4 Two dimensional HTR core tests 106
4.3 More discussions on recondensation 115
4.3.1 Spatial dependence of the DGM method 115
4.3.2 Perturbation technique in collision term 123
4.3.3 Memory requirement of recondensation 127
4.4 Summary 128

Chapter 5. Nonlinear Energy Acceleration using DGM method 130

5.1 Method description 130
5.2 Computational results 130
5.3 Summary 134

Chapter 6. Summary and Future Work 135

6.1 Summary 135
6.2 Future work 139

Appendix A. Derivation of Standard Multigroup Method 140

Appendix B. Orthogonal Polynomials 148

B.1 Continuous orthogonal polynomials 148
B.2 Discrete orthogonal polynomials 150
B.3 Discussion on discrete expansions 154

Appendix C. Derivation of DGM Method on Diffusion Equation 164

Appendix D. Definition of Errors 171

Appendix E. Algorithms of Fixed Point Iterations 173

E.1 Algorithms of power iteration 173
E.2 Algorithms of external source problems 178

References 179

List of Figures

FIGURE		Page
2.1	Typical multilevel approach in Light Water Reactor calculations	29
2.2	Lattice-core online iteration	31
3.1	Expansion of a step function using continuous Legendre polynomials	43
3.2	Expansion of a step function using discrete Legendre polynomials	44
3.3	47 group cross section condensation	45
3.4	1-D BWR core and assembly configurations	46
3.5	Core 1 scalar flux comparison (fast groups)	57
3.6	Core 1 scalar flux relative error (fast groups)	57
3.7	Core 1 scalar flux comparison (thermal groups)	58
3.8	Core 1 scalar flux relative error (thermal groups)	58
3.9	Core 3 scalar flux comparison (fast groups)	59
3.10	Core 3 scalar flux relative error (fast groups)	59
3.11	Core 3 scalar flux comparison (thermal groups)	60
3.12	Core 3 scalar flux relative error (thermal groups)	60
4.1	Flow chart of the traditional multilevel procedure	66
4.2	Flow chart of the recondensation procedure	67
4.3	Scalar flux *rms* relative errors of 1-D BWR core 1	76
4.4	Eigenvalue relative errors of 1-D BWR core 1	76
4.5	Scalar flux *rms* relative errors of 1-D BWR core 3	77
4.6	Eigenvalue relative errors of 1-D BWR core 3	77

4.7 Scalar flux comparison for core 3 water region 78

4.8 Scalar flux relative error for core 3 water region 79

4.9 Scalar flux comparison for core 3 Fuel (high enrichment) region 79

4.10 Scalar flux relative error for core 3 Fuel (high enrichment) region 80

4.11 Scalar flux comparison for core 3 Fuel+Gd region 80

4.12 Scalar flux relative error for core 3 Fuel+Gd region 81

4.13 1-D HTR core configuration 82

4.14 Scalar flux *mre* errors 85

4.15 Eigenvalue relative errors 85

4.16 Average flux on the Graphite/Fuel 1 interface 86

4.17 Scalar flux 295 group solution on full space and energy mesh 87

4.18 Fission rate relative error in the first 3 DGM iterations 88

4.19 Absorption rate relative error in the first 3 DGM iterations 89

4.20 Group 1 flux spatial distribution 90

4.21 Group 2 flux spatial distribution 90

4.22 Group 50 flux spatial distribution 91

4.23 Group 150 flux spatial distribution 91

4.24 Group 275 flux spatial distribution 92

4.25 Group 295 flux spatial distribution 92

4.26 Scalar flux *mre* errors 95

4.27 Eigenvalue relative errors 95

4.28 Overview of 2-D PWR core configuration 96

4.29 Detailed 2-D PWR core configuration 97

4.30 Fuel pin approximation in Cartesian geometry 97

4.31 Scalar flux *rms* relative errors of 70 group 2-D PWR core 102

4.32 Eigenvalue relative errors of 70 group 2-D PWR core 102

4.33 Fission density relative error (%) for 1st DGM iteration 103

4.34 Fission density relative error (%) for 2nd DGM iteration 104

4.35 Fission density relative error (%) for 3rd DGM iteration 105

4.36 Fission density relative error (%) for 4th DGM iteration 105

4.37 Fission density relative error (%) for 13th DGM iteration 105

4.38 2-D HTR core configuration 106

4.39 Scalar flux *mre* relative errors of 26 group 2-D HTR core 109

4.40 Eigenvalue relative errors of 26 group 2-D HTR core 110

4.41 Fission density distribution of 26 group 2-D HTR core 111

4.42 Fission density relative error (%) for 1st DGM iteration 112

4.43 Fission density relative error (%) for 2nd DGM iteration 112

4.44 Fission density relative error (%) for 3rd DGM iteration 113

4.45 Fission density relative error (%) for 4th DGM iteration 113

4.46 Fission density relative error (%) for 5th DGM iteration 114

4.47 Fission density relative error (%) for 38th DGM iteration 114

4.48 Scalar flux *rms* relative error of 1-D BWR core 1 (SC vs. SD) 122

4.49 Eigenvalue relative error of 1-D BWR core 1 (SC vs. SD) 123

5.1 Flow chart of energy acceleration procedure 131

List of Tables

TABLE		Page
3.1	Assemblies 1 and 4 eigenvalue and computational time	48
3.2	Assembly 1 DGM result errors	48
3.3	Assembly 4 DGM result errors	48
3.4	Cores 1 and 3 eigenvalue and computational time	50
3.5	Core 1 DGM result	50
3.6	Core 3 DGM result	51
3.7	Cores 1 and 3 eigenvalue and time after the updates	54
3.8	Core 1 DGM result after the updates	54
3.9	Core 3 DGM result after the updates	55
4.1	1-D BWR Core 1 errors in fluxes	72
4.2	1-D BWR Core 1 computational results	73
4.3	1-D BWR Core 3 errors in fluxes	73
4.4	1-D BWR Core 3 computational results	74
4.5	1-D HTR core configuration	82
4.6	1D HTR errors in fluxes	84
4.7	1D HTR eigenvalue and computational time	84
4.8	1D HTR (anisotropic) errors in fluxes	94
4.9	1D HTR (anisotropic) eigenvalue and computational time	94
4.10	70 group 2-D PWR core errors in fluxes	98
4.11	70 group 2-D PWR core errors in fission density	100

4.12 70 group 2-D PWR core computational results 101

4.13 26 group 2-D HTR core errors in fluxes 108

4.14 26 group 2-D HTR core computational results 109

4.15 1-D BWR Core 1 errors in fluxes (step characteristics) 120

4.16 1-D BWR Core 1 computational results (step characteristics) 121

5.1 3 coarse group with expansions acceleration results 132

5.2 2 coarse group with expansions acceleration results 133

6.1 Recondensation result summary 137

B.1 Double precision DLOP values of N=4 156

B.2 Exact and reconstructed step functions (1) 157

B.3 Exact and reconstructed step functions (2) 158

B.4 Discrete polynomial expansion of step function (N=50) 160

B.5 Discrete polynomial expansion of step function (N=100) 161

Acronyms

BWR	Boiling Water Reactor
CENTRM	Continuous ENergy TRansport Module
CMFD	Coarse Mesh Finite Difference
DGM	Discrete Generalized Multigroup Method
DLOP	Discrete Legendre Orthogonal Polynomials
DRAGON	A collision probability transport code for cell and supercell calculations
DSA	Diffusion Synthetic Acceleration
DT	Discrete Tchebichef Polynomials
ENDF	Evaluated Nuclear Data File
Gd	Gadolinium
GS	Gauss-Seidel
HELIOS	A lattice physics code
HTR	High Temperature Reactors
IEEE	Institute of Electrical and Electronics Engineers
IGDM	Iterative Transport-Diffusion Methodology
LWR	Light Water Reactors
MCNP	Monte Carlo N-Particle
MOC	Method of Characteristics
MOX	Mixed Oxide Fuel
MRE	Mean Relative Error
NJOY	Nuclear data processing system

ODF	Opacity Distribution Function
PI	Power Iteration
PWR	Pressurized Water Reactor
RMS	Root Mean Square Relative Error
SCALE	Standardized Computer Analyses for Licensing Evaluation
SC	Step Characteristics
SD	Step Difference
Sn	Discrete Ordinates
UO_2	Uranium Dioxide Fuel

Chapter 1. Introduction

1.1 Motivation

Current core-level deterministic methods rely entirely on the multigroup energy treatment of the nuclear cross-sections [Bell 1970] [Henry 1975] [Duderstadt 1976] [Lamarsh 1983] [Hébert 2009]. In the energy condensation process, continuous energy data is condensed in a more manageable multigroup format through multiple levels of approximation to eventually produce a reduced-complexity dataset with which the core calculation can be performed efficiently. Reaction rates are conserved based on the knowledge of the exact energy spectrum. Since this quantity is unknown *a priori*, a multilevel approach is used to refine the flux spectrum approximation which is then used to condense the cross-sections into a smaller number of groups.

As the number of energy groups is reduced, spatial detail is added often going from a 1-D pin cell to a 2-D fuel assembly to an eventual full 3-D core. This multilevel approach generally assumes that strong spectral effects are local and can be approximated coarsely as the spatial size increases to reduce computational costs. As the level of heterogeneity increases in nuclear reactor core designs, this assumption breaks down and requires adjustments.

Additionally, this process leads to a considerable loss of energy resolution. In typical core level calculations, 2 groups are used in Light Water Reactors (LWR) and 20 groups are

used in Fast Reactors. While such an approach has proven sufficient for current reactors for which many experiments were performed, it is envisioned that high-fidelity core modeling will require thousands of energy groups if one desires to improve the predictive capability of the simulation. Increasing the number of energy groups allows for a better representation of the resonance region and a more accurate spectral description but comes with a substantial computational cost which is proportional to the number of energy groups.

In particle transport problems, the neutron flux is a function of space, angle, energy and time. The nuclear community has put much effort on development of different spatial and angular discretization methods and associated acceleration algorithms, while less effort has been put on the energy discretization methods. The dominant treatment of the energy dependence is the multigroup method, especially at the core level.

The goal of this dissertation is to develop an energy treatment for the neutron transport equation that reduces the computational cost needed for high-fidelity modeling of nuclear reactors.

1.2 Objectives

The main objective of this work is to develop a new energy discretization approach that reduces reliance on the multilevel approach (i.e. 1D pin cell, 2D lattice, 3D core). The goal is to embed the cross-section condensation process inside the core level calculation

and eliminate the need for pin cell or lattice level calculations. Additionally this new approach must remain computationally competitive with current few group strategy and fit in the framework of common deterministic transport methods.

1.3 Thesis organization

This thesis is organized as follows. Chapter 2 reviews existing methods and includes four subsections. Section 2.1 briefly reviews the existing energy variable discretization methodologies in deterministic transport theory. Section 2.2 reviews existing lattice-core level iterations methods.

Chapter 3 is dedicated to the Discrete Generalized Multigroup (DGM) method. Section 3.1 derives the DGM form of the transport equation. Section 3.2 compares discrete and continuous energy expansions and illustrates the advantages of discrete expansions. Section 3.3 shows computational results for 1-D BWR assemblies and cores tests. Section 3.4 summarizes important findings.

Chapter 4 develops the online recondensation methodology with computational results. Section 4.1 describes the method while Section 4.2 presents the computational results of this extension. Section 4.3 discusses limitations of DGM recondensation from the perspective of spatial discretization and accuracy of the perturbation technique used in the collision term, and briefly analyzes memory requirement of recondensation. Section 4.4 provides a brief summary of the chapter.

Chapter 5 develops an energy acceleration method based on the recondensation result as an initial guess for fine group calculation.

Chapter 6 summarizes the theories and methodologies developed in this work, followed by a discussion of possible future work and directions.

Chapter 2. Background and Review

This chapter first reviews existing energy discretization methods in deterministic radiation transport theory, followed by the multilevel approach using the multigroup energy discretization simulations and lattice-core level iteration methods. The third section reviews energy related acceleration methods, followed by a review of orthogonal polynomials.

2.1 Energy related discretization methods in deterministic transport

2.1.1 Multigroup methodology

Current core-level deterministic methods rely exclusively on the multigroup energy treatment of the nuclear cross-sections [Bell 1970] [Henry 1975] [Duderstadt 1976] [Lamarsh 1983] [Hébert 2009]. The multigroup discretization divides the energy domain into G energy intervals. Group flux is defined as an integral quantity within each group, and group cross sections are defined as an average value over each group using an approximate flux spectrum as the weighting function.

Since the discrete generalized multigroup method is closely related to the standard multigroup method, a brief derivation from continuous energy to the standard multigroup form of the transport equation is given in Appendix A. The key aspect is the definition of

the group cross sections which are averaged cross sections within a group weighted by the exact flux spectrum:

$$\sigma_g = \frac{\int_{E_g}^{E_{g-1}} \sigma(E) f(E) dE}{\int_{E_g}^{E_{g-1}} f(E) dE}. \qquad (2.1)$$

For a problem with defined geometry and composition, the only way to obtain accurate multigroup cross sections is to know the exact flux spectrum $f(E)$ within each group which should also depend on space and angle in heterogeneous problems. Unfortunately this spectrum is not known and approximation is needed. Errors in this approximation are the major cause of uncertainty associated with the multigroup method. The flux spectrum is very sensitive to the isotope concentration and spatial dependence, especially when resonances are present. A phenomenon known as self-shielding occurs, which refers to a change in resonance absorption due to spatial and spectral variations of the neutron flux. Self-shielding effects should be considered in the processing of nuclear cross section data. The following sub-sections briefly review alternative energy discretization methods in the literature.

2.1.2 CENTRM and submoment expansion

An alternate approach to the multigroup method is the use of pointwise cross section data [Ching 1976] [Liu 1981]. Williams *et al* developed the 1-D discrete ordinates code

CENTRM for nuclear data processing that treats part of the nuclear data as pointwise cross-sections [Williams 1995] [Williams 2009]. The method uses a combination of multigroup and pointwise treatments to obtain a very accurate pointwise neutron spectrum. The "submoment" expansion technique is used to accurately evaluate the scattering transfer function. CENTRM is currently used in the SCALE [Bowman 2007] package to generate resonance shielded multigroup data. The code solves a fixed source transport equation in infinite media or 1-D pin-type geometries.

The full energy range (0-20MeV) is divided into 3 intervals, i.e., Upper Multigroup Range (UMR), Pointwise Range (PW) and Lower Multigroup Range (LMR). Flux calculations in the 3 intervals are coupled through the scattering sources. The PW region is chosen to be above the thermal energy range and to include all the resolved resonances of important isotopes, i.e., 4eV-10keV. In particular, the PW region should be below the inelastic scatter threshold of all significant materials. UMR and LMR are regions where cross sections have much smoother variation where multigroup calculations are performed.

Results from CENTRM provide a pointwise energy flux spectrum on a fine energy structure (~30,000-70,000 discrete points) and thus greatly improves the energy resolution. The discrete pointwise flux is then used as weighting function for PMC [Williams 2009, 2], a module in Scale to process results from CENTRM, to generate self-shielded group cross sections used for higher spatial dimensional calculations. Computational results showed that CENTRM/PMC provides a more accurate flux

spectrum for the treatment of resolved resonances than NITAWL [Greene 2009], the prior module used for self-shielding in SCALE which uses the Nordheim Integral method [Hollenback 1998].

A special consideration in CENTRM is that in the expression of spherical harmonic moments of elastic and inelastic (if included) scattering sources, the integrand contains coupling of the initial and final energy of the scattered neutrons which make the overall algorithm very inefficient. Thus a submoment expansion method was proposed to evaluate the anisotropic scattering source efficiently under this pointwise transport framework [Williams 2000].

In order to decouple the initial and final energy dependence in the integrand of scattering source moments, this spherical harmonic scattering source moment is further expanded in a series of factored submoments. This double expansion facilitates the treatment of the scattering sources but introduces numerical instability for heavy nuclides that require high angular expansion. The total number of submoments increases rapidly with increasing order of scatter, which limits the order of anisotropic scattering.

CENTRM solves one dimensional simple geometry problems, e.g., 1D pin cell geometry with a white boundary condition. This representation is an important limitation of this approach. Moreover, due to the fine energy nature of CENTRM, it is difficult to extend to core level calculations where much more spatial details are needed. An extension was proposed for 2D pin cell geometries which showed promise [Zhong 2005] [Zhong 2006].

2.1.3 RAZOR continuous energy lattice code

The RAZOR lattice code proposes a "near-continuous" energy pointwise solution method on the lattice level calculation to generate few-group diffusion constants that account for self-shielding effect [Zerkle 1997]. This method was developed to improve the resonance energy treatment within the multigroup methodology and uses pointwise data to generate the multigroup data. RAZOR solves one and two dimensional fixed source neutron transport problems.

Continuous energy transport is used in both fast and thermal energy ranges. In the slowing down algorithm a "dual energy resolution" was developed to obtain detailed energy resolution while at the same time reducing memory requirements by a combination of fine and coarse group slowing down buffers.

Similar to CENTRM, RAZOR and these lattice level codes with detailed energy treatments are difficult to extend to core level calculations due to the high computational resource requirements.

2.1.4 Wavelet energy expansion

A wavelet function expansion method was developed for the treatment of self-shielding effect [Wu 2010]. Similar to CENTRM, the non-resonance energy ranges use standard multigroup method. In the resonance range, the energy is divided into many group

intervals. The energy dependence of angular flux is then expanded using Daubechies' wavelet scaling function [Daubechies 1992] to separate energy dependence spectrum with spatial and angular dependence coefficients of the angular flux. A set of equations can be solved for the spatial and angular dependent coefficients using the orthogonality properties of Daubechies' wavelets scaling function. Finally the flux spectrum can be unfolded after obtaining these coefficients.

A program WAVRESON was developed using this methodology with the method of characteristics (MOC). Benchmark problems with infinite homogeneous medium, single pin and cylindrical cluster geometries were tested and results showed that this method can give errors on the order of less than one percent on *k*-infinity by comparing with MCNP reference solutions.

A disadvantage of the method is the computational burden because the angular flux needs to be expanded to high orders. Within each of the resonance energy intervals, many coefficient equations need be solved. The detailed energy treatment makes it difficult to be applied to complex geometry problems.

2.1.5 Linear multigroup method

A linear multigroup method was developed [Attieh 2002] [Attieh 2004]. The standard multigroup method is assumed to have a piecewise constant spectrum within each group, i.e.,

$$f_g(E) = 1, \quad E \in [E_g, E_{g-1}]$$
$$= 0, \quad \text{else.} \tag{2.2}$$

Under this assumption, the authors proposed a generalized member function; in particular, the linear multigroup method assumes a hat basis function to give the spectrum a linear dependence within each group:

$$f_g(E) = \frac{E - E_{g+1}}{E_g - E_{g+1}}, \quad E \in [E_{g+1}, E_g]$$
$$= \frac{E_{g-1} - E}{E_{g-1} - E_g}, \quad E \in [E_g, E_{g-1}]. \tag{2.3}$$

This shape function is similar to the linear basis function used in continuous finite element method, thus the name Linear Multigroup (LMG) method. With this linear shape function, the LMG cross sections were generated by modifying NJOY modules and the resulting cross sections were used to solve for gamma ray fluxes and absorption rates in different energy groups.

The proposed LMG method was tested on two gamma ray spectrum calculations in infinite homogeneous oxygen medium, with continuous spectrum and monoenergetic sources, respectively. The results from multigroup and LMG with the same number of energy groups were compared. Results showed that errors with the LMG or a combination of LMG and multigroup were smaller than those with standard multigroup

method, given the same multigroup energy structure. With the increase of number of energy groups, the new approaches converge faster than the multigroup method.

There are a few issues with this method. Firstly, due to the overlapping of basis functions in a particular group, the total cross section has "group-to-group" dependence which is non-physical, i.e., instead of σ_{tg} in a group, $\sigma_{tg(g-1)}, \sigma_{tgg}$ and $\sigma_{tg(g+1)}$ exist in a group. The generation of these pseudo cross sections requires extra computational effort. Moreover, solving the linear system with these extra pseudo entries also require more computational effort. The scattering matrix similarly has non-physical entries for scattering from each group to the next higher group (named "fictitious upscattering") for each group, which makes the scattering matrix denser than the standard multigroup method and thus requires more computational effort to solve.

Secondly, this method is tested in the infinite homogeneous medium, and it can be applied in shielding problems, as well as the early stage of cross section processing with ultra-fine energy groups when the standard multigroup method is assumed to have a constant shape function within each energy group. The extension of the method to core level simulation would be difficult.

2.1.6 Opacity distribution function concept

Up to this point all the discussions are related to different energy treatment in particle transport and reactor simulations. This section briefly discusses an opacity distribution

function (ODF) concept in the astrophysics field [Carbon 1973] [Carbon 1974] [Querci 1974]. The calculations of opacities within a frequency interval is conceptually similar to the discrete generalized multigroup method developed in this study because both methods allow spectrum variation within each discretized interval of either frequency or energy.

The ODF concept was initially introduced by Chandrasekar in 1935 to represent a range of opacities within a frequency interval which he used to study stellar radiation, and was subsequently used in model-atmosphere calculations by Strom and Kurucz in 1966 [Carbon 1974]. The ODF method separates the frequency domain into intervals somewhat equivalent to the multigroup concept in reactor physics. The opacity in each interval is then distributed as a probability distribution function (pdf) over the opacity range covered. The pdf is most often represented by a histogram. This methodology allows for frequency variations within the interval when performing the calculations, but all the frequency dependence within an interval is lost. The approach is similar to the probability table concept adapted in nuclear reactor analysis [Hébert 2009]. The approach is also conceptually very similar to the proposed discrete generalized multigroup method; however the DGM method has the added advantage of conserving the energy dependence within each group.

2.1.7 Energy expansion using continuous orthogonal polynomials

In previous studies, a generalized multigroup method was developed [Forget 2007] [Rahnema 2008]. This was achieved by generalizing the standard condensation procedure,

assuming that the energy dependence of the neutron flux (spectrum) could be expanded in a set of orthogonal basis functions, and folding this dependence into the cross-section condensation process. It was shown that the standard condensation procedure is contained within this generalized method as a zeroth-order approximation and by implementing this method, computational time is reduced to that of standard coarse-group computations, but preserving some details usually associated with much finer-group solutions.

The validity of the method was demonstrated with a 1-D Sn transport code with a Legendre polynomial expansion of the energy variable on 1-D problems of varying heterogeneity. The results showed that a few-group solution could provide a continuous energy flux spectrum that closely matched a much finer group solution.

The main problem that arises is that the multigroup method is discrete in energy. Expansions using continuous orthogonal polynomials will introduce numerical instabilities, i.e., Gibbs effects [Gibbs 1898] near multigroup boundaries where flux discontinuity occurs. This naturally introduces negative fluxes at near-zero flux regions and cannot be eliminated regardless of expansion order.

Also due to nonphysical negative fluxes, iterative core level recondensation which uses unfolded fluxes to regenerate cross sections can be difficult. Nonphysical flux oscillations near group boundaries induce numerical issues when the flux is used as a weighting spectrum to regenerate cross section moments. Furthermore, without recondensation, integral quantities cannot be further improved.

The proposed DGM method in this study is very similar in nature but has proven more appropriate for discrete energy treatment in deterministic codes. Instead of using a continuous orthogonal expansion, this study proposes the use of a discrete orthogonal expansion. The discrete expansion is a more appropriate fit in the multigroup framework and provides enormous advantages over the previous formulation as will be shown in this thesis. A detailed comparison of the discrete and continuous expansions will be discussed in the next chapter.

2.2 Current multilevel approaches in reactor simulations

2.2.1 General multilevel approach

In nuclear reactor simulations, generally it is difficult to solve core level fine energy structure flux due to the computational burden and memory requirements. A multilevel approach is used to refine the flux spectrum approximation, as is shown in Fig. 2.1. Starting from basic nuclear database such as the Evaluated Nuclear Data File (ENDF) [Herman 2010], cross section processing codes such as NJOY [MarFarlane 2000] are generally used to generate fine group (a few hundred groups) cross sections, assuming an infinite homogeneous medium, by including resonance self-shielding and Doppler broadening information. The GROUPR module in NJOY provides a set of built-in weight functions that are representative of a few typical nuclear systems. For resonant isotopes,

the slowing down equation is solved to obtain a more representative weighting function that accounts for the self-shielding effects [MarFarlane 2000].

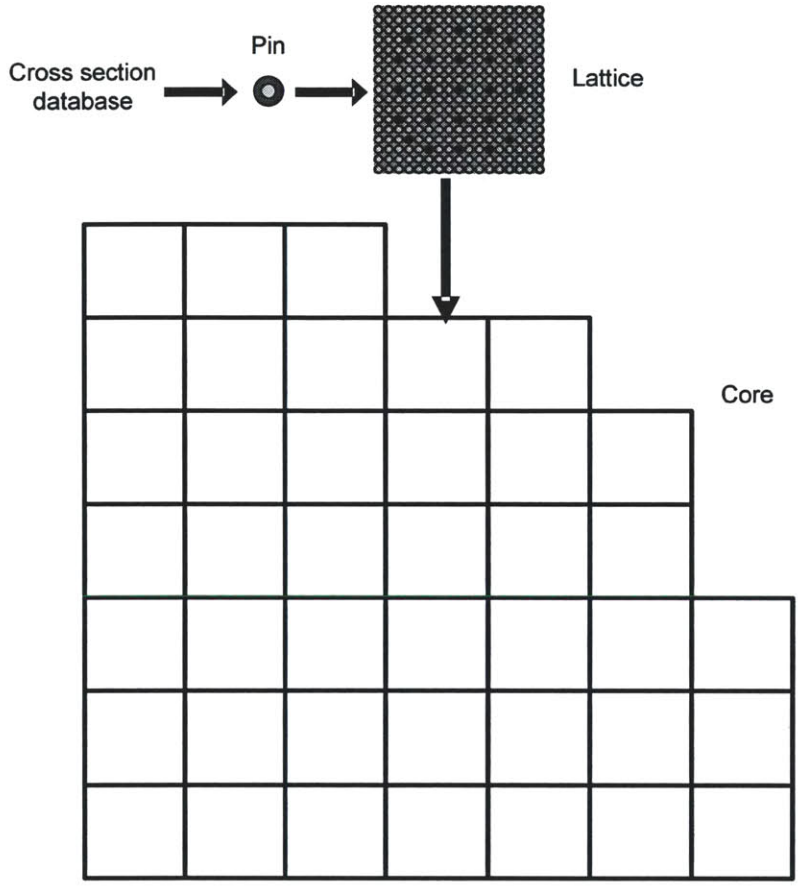

Fig. 2.1 Typical multilevel approach in Light Water Reactor calculations.

The processed data is then used to evaluate the spatial self-shielding effects either on a pin-cell or a subset of a lattice using either subgroup methods [Levitt 1972] [Cullen 1974] [Nikolaev 1976], equivalence in dilution methods [Stamm'ler 1983], or point-wise treatment [Williams 1995] [Williams 2000] [Williams 2009]. The obtained fine group cross sections are then used for lattice level calculations. Their purpose is to compute

few-group cross sections for core level calculations, in a small component of the core with local operating conditions.

The lattice level solution is then used as a weighting function for spatial homogenization and energy condensation. The obtained coarse group, spatially homogenized cross sections are then used at the core level using diffusion theory. The main idea is to preserve the reaction rates and boundary currents as one reduces the complexity of the problem.

2.2.2 Lattice-core online iteration methods

As discussed in Section 2.1.1, in the existing multilevel approach, the lattice level fine group calculation assumes an infinite lattice condition which is a major source of error when generating coarse group cross sections for core calculations. In order to provide higher fidelity calculations for advanced reactor cores, online condensation of lattice – core iteration techniques have been actively pursued [Gougar 2009] [Jung 2009] [Roberts 2010]. The general idea of these methods is to improve the infinite lattice assumption by iterating between lattice and core level calculations, as is shown in Fig. 2.2, using the boundary conditions of the core level solution. Two examples are as follows.

Iterative Transport-Diffusion Methodology (IGDM) was developed by Roberts *et al* for Light Water Reactor core analysis to improve the accuracy of the noted spectral effect [Roberts 2010]. Iterations between the lattice level and core level calculations were

performed to improve the condensation of the nuclear data by accounting for the effect of neighboring nodes. The method was tested on a set of two dimensional LWR mini-core benchmark problems and showed good improvement.

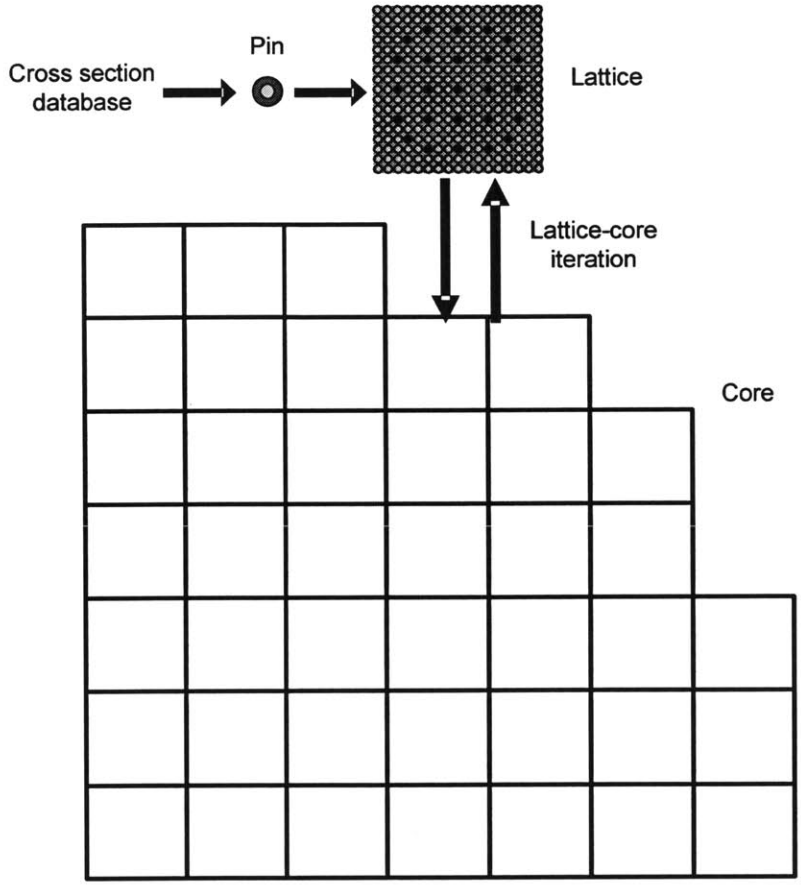

Fig. 2.2 Lattice-core online iteration.

Similarly, a combination of COMBINE unit cell calculations, one dimensional discrete ordinates transport calculations of SCAMP, and nodal diffusion calculations of PEBBED were implemented to account for the neighboring effects in core with long mean free paths [Gougar 2009]. COMBINE generates homogenized unit cell cross sections for each

1-D node which are used by SCAMP to solve for the flux distribution along the dimension. The obtained flux distribution is used to generate nodal diffusion parameters for core calculations.

These lattice-core online iteration methods improve the general once through lattice-core multilevel approach used in most existing deterministic core simulations. However, these online iteration methods are typically very time consuming as the lattice details must be computed for each iteration for each lattice in the core.

Chapter 3 Discrete Generalized Multigroup Energy Expansion Theory

This chapter derives the DGM method in which the discrete orthogonal polynomials are used [Zhu 2010]. Following the derivation is a detailed comparison between the DGM method and the continuous energy expansion method. One dimensional computational tests on a set of BWR-like assemblies and cores are performed. Accuracy of discrete expansions in limiting cases and numerical issues are discussed.

3.1 DGM method derivation

The starting point for the derivation is the time-independent integro-differential neutron transport equation with no external sources (i.e. eigenvalue problem). A similar procedure can be applied readily to a source-driven problem, time-dependent problem or other forms of the transport equation:

$$\begin{aligned}&\vec{\Omega}\cdot\nabla\psi(\vec{r},\vec{\Omega},E)+\sigma_t(\vec{r},E)\psi(\vec{r},\vec{\Omega},E)=\\&\int_0^\infty dE'\int_{4\pi}d\vec{\Omega}'\sigma_s(\vec{r},\vec{\Omega}'\to\vec{\Omega},E'\to E)\psi(\vec{r},\vec{\Omega}',E')+\\&\frac{\chi(\vec{r},E)}{4\pi k}\int_0^\infty dE'\int_{4\pi}d\vec{\Omega}'\nu\sigma_f(\vec{r},E')\psi(\vec{r},\vec{\Omega}',E').\end{aligned}\tag{3.1}$$

In Eq. (3.1), definitions of all variables can be found in Appendix A. If the energy spectrum is separated into G coarse groups, the scattering kernel can be expressed using

spherical harmonics, and assuming fission to be isotropic, Eq. (3.1) in coarse group g with energy E_g can be written as:

$$\begin{aligned}&\vec{\Omega}\cdot\nabla\psi(\vec{r},\vec{\Omega},E_g)+\sigma_t(\vec{r},E_g)\psi(\vec{r},\vec{\Omega},E_g)=\\&\sum_{g'=1}^{G}\sum_{l=0}^{\infty}\sum_{m=-l}^{l}\frac{Y_{lm}^{*}(\vec{\Omega})}{4\pi}\int_{\Delta E_{g'}}dE_{g'}\sigma_{sl}(\vec{r},E_{g'}\rightarrow E_g)\phi_{lm}(\vec{r},E_{g'})+\\&\frac{\chi(\vec{r},E_g)}{4\pi k}\sum_{g'=1}^{G}\int_{\Delta E_{g'}}dE_{g'}\nu\sigma_f(\vec{r},E_{g'})\phi(\vec{r},E_{g'}).\end{aligned}\tag{3.2}$$

Eq. (3.2) thus separates the transport equation over G coarse groups, but the energy is still continuous within each group. It is now possible to apply the multigroup methodology within each coarse group g as:

$$\begin{aligned}&\vec{\Omega}\cdot\nabla\psi(\vec{r},\vec{\Omega},K)+\sigma_t(\vec{r},K)\psi(\vec{r},\vec{\Omega},K)=\\&\sum_{g'=1}^{G}\sum_{l=0}^{\infty}\sum_{m=-l}^{l}\frac{Y_{lm}^{*}(\vec{\Omega})}{4\pi}\sum_{L=0}^{M-1}\sigma_{sl}(\vec{r},L\rightarrow K)\phi_{lm}(\vec{r},L)+\frac{\chi(\vec{r},K)}{4\pi k}\sum_{g'=1}^{G}\sum_{L=0}^{M-1}\nu\sigma_f(\vec{r},L)\phi(\vec{r},L)\end{aligned}\tag{3.3}$$

In going from Eq. (3.2) to Eq. (3.3), it is assumed that there are N fine group points within coarse group g with point index $K=0,1,2,...,N-1$, and M fine group points within coarse group g' with point index $L=0,1,2,...,M-1$. This is equivalent to having an ultra-fine multigroup equation where each coarse group has varying fine group structure.

The following step is to expand the energy dependence of the angular flux into a set of Discrete Legendre Polynomials (DLOP) or Discrete Tchebichef Polynomials (DT) moments. A review of discrete orthogonal polynomials is in Appendix B. The energy dependence of the angular flux in Eq. (3.3) can be expanded using DLOP or DT within each coarse group g as:

$$\psi(\vec{r},\vec{\Omega},K)=\sum_{i=0}^{N-1}\frac{1}{\rho(i,N-1)}P_i(K,N-1)\psi_{ig}(\vec{r},\vec{\Omega}), \tag{3.4}$$

where $\Delta E_K \in \Delta E_g$, $K=0,...,N-1$ is the index of the fine energy group point within the coarse group g, N is the total number of fine group points within the coarse group g, and $\rho(i,N-1)$ is defined in Eq.(B.13) for DLOP and in Eq. (B.20) for DT. The flux moments can be obtained from the orthogonality relation:

$$\psi_{ig}(\vec{r},\vec{\Omega})=\sum_{K=0}^{N-1}P_i(K,N-1)\psi(\vec{r},\vec{\Omega},K). \tag{3.5}$$

Substituting Eq. (3.4) into Eq. (3.3), and then multiplying and summing by $\sum_{K=0}^{N-1}P_i(K,N-1)$ to obtain:

$$\vec{\Omega}\cdot\nabla\psi_{ig}(\vec{r},\vec{\Omega})+\sigma_{t,ig}(\vec{r},\vec{\Omega})\psi_{ig}(\vec{r},\vec{\Omega})=$$
$$\sum_{K=0}^{N-1}P_i(K,N-1)\sum_{g'=1}^{G}\sum_{l=0}^{\infty}\sum_{m=-l}^{l}\frac{Y_{lm}^{*}(\vec{\Omega})}{4\pi}\sum_{L=0}^{M-1}\sigma_{sl}(\vec{r},L\rightarrow K)\phi_{lm}(\vec{r},L)+ \tag{3.6}$$
$$\frac{\chi_{ig}(\vec{r})}{4\pi k}\sum_{g'=1}^{G}\sum_{L=0}^{M-1}\nu\sigma_f(\vec{r},L)\phi(\vec{r},L)$$

where $\psi_{ig}(\vec{r},\vec{\Omega})$ is defined in Eq. (3.5) and where

$$\chi_{ig}(\vec{r})=\sum_{K=0}^{N-1}P_i(K,N-1)\chi(\vec{r},K), \tag{3.7}$$

$$\sigma_{t,ig}(\vec{r},\vec{\Omega})=\frac{\sum_{K=0}^{N-1}P_i(K,N-1)\sigma_t(\vec{r},K)\psi(\vec{r},\vec{\Omega},K)}{\sum_{K=0}^{N-1}P_i(K,N-1)\psi(\vec{r},\vec{\Omega},K)}. \tag{3.8}$$

In writing Eq. (3.1), it is assumed that χ does not depend on isotopic concentrations. If χ has isotopic dependence, it cannot be separated from the rest of the fission term since it should be weighted by the isotopic fission rates.

A multigroup equation is now obtained in which each coarse group g contains an expanded flux. The zeroth order of this expansion reverts directly to the well-known multigroup approximation and all higher orders offer information of the spectrum within each coarse group. Additionally, as was done in [Rahnema 2008], the total cross-section is defined as the mean within the coarse group g and a higher order perturbation term:

$$\sigma_t(\vec{r},K)=\sigma_{t,0g}(\vec{r})+\delta_g(\vec{r},K), \tag{3.9}$$

where

$$\sigma_{t,0g}(\vec{r})=\frac{\sum_{K=0}^{N-1}\sigma_t(\vec{r},K)\phi(\vec{r},K)}{\sum_{K=0}^{N-1}\phi(\vec{r},K)}, \tag{3.10}$$

and thus

$$\delta_{ig}(\vec{r},\vec{\Omega})=\frac{\sum_{K=0}^{N-1}P_i(K,N-1)\delta_g(\vec{r},K)\psi(\vec{r},\vec{\Omega},K)}{\sum_{K=0}^{N-1}P_0(K,N-1)\psi(\vec{r},\vec{\Omega},K)}. \tag{3.11}$$

The advantage of this δ-term approximation is that only the zeroth order flux appears in the denominators, which makes the method more stable numerically in the presence of cross-section moments that are near zero.

Another reason to define such a perturbation term is due to the angular dependence of the total cross section moments, which is not unique to the DGM method. In the derivation of multigroup equation from continuous energy transport equation, or from fine to coarse group energy condensation, or from fine to coarse mesh spatial homogenization [Smith 1980], the angular dependence of total cross section appears in the equation due to reaction rates conservation in these transport-transport processes. A similar perturbation technique in deriving the multigroup equation from continuous transport equation is described in [Bell 1970] and [Lewis 1993]. If the "pseudo" angular independent total cross section is weighted using scalar flux as in Eq. (3.10), it is called "consistent Pn"

approximation in [Bell 1970], which is also the case here. A more detailed discussion about this perturbation technique will be discussed in the next chapter. Equation (3.6) thus becomes:

$$\vec{\Omega}\cdot\nabla\psi_{ig}(\vec{r},\vec{\Omega})+\sigma_{t,0g}(\vec{r})\psi_{ig}(\vec{r},\vec{\Omega})+\delta_{ig}(\vec{r},\vec{\Omega})\psi_{0g}(\vec{r},\vec{\Omega})=$$
$$\sum_{K=0}^{N-1}P_i(K,N-1)\sum_{g'=1}^{G}\sum_{l=0}^{\infty}\sum_{m=-l}^{l}\frac{Y_{lm}^{*}(\vec{\Omega})}{4\pi}\sum_{L=0}^{M-1}\sigma_{sl}(\vec{r},L\rightarrow K)\phi_{lm}(\vec{r},L)+ \qquad (3.12)$$
$$\frac{\chi_{ig}(\vec{r})}{4\pi k}\sum_{g'=1}^{G}\sum_{L=0}^{M-1}\nu\sigma_f(\vec{r},L)\phi(\vec{r},L)$$

The next step is to treat the scattering and fission terms on the right hand side (*RHS*) by preserving the reaction rates. The reaction rates can be defined as:

$$R_f(\vec{r},L)=\nu\sigma_f(\vec{r},L)\phi(\vec{r},L) \qquad (3.13)$$

$$R_{s,lm}(\vec{r},L\rightarrow K)=\sigma_{sl}(\vec{r},L\rightarrow K)\phi_{lm}(\vec{r},L) \qquad (3.14)$$

Expanding both the reaction rates in the following way:

$$R(\vec{r},L)=\sum_{j=0}^{M-1}\frac{1}{\rho(j,M-1)}P_j(L,M-1)R_{jg}(\vec{r}), \qquad (3.15)$$

where

$$R_{jg}(\vec{r})=\sum_{L=0}^{M-1}P_j(L,M-1)R(\vec{r},L). \qquad (3.16)$$

By the treatment of orthogonal expansion in Eq. (3.15), the reaction rates are preserved. The *RHS* of Eq. (3.12) becomes:

$$
\begin{aligned}
RHS &= \sum_{K=0}^{N-1} P_i(K,N-1) \sum_{g'=1}^{G} \sum_{l=0}^{\infty} \sum_{m=-l}^{l} \frac{Y_{lm}^*(\vec{\Omega})}{4\pi} \sum_{L=0}^{M-1} \sum_{j=0}^{M-1} \frac{1}{\rho(j,M-1)} P_j(L,M-1) R_{s,lm,jg'}(\vec{r},K) + \\
&\frac{\chi_{ig}(\vec{r})}{4\pi k} \sum_{g'=1}^{G} \sum_{L=0}^{M-1} \sum_{j=0}^{M-1} \frac{1}{\rho(j,M-1)} P_j(L,M-1) R_{f,jg'}(\vec{r}) \\
&= \sum_{g'=1}^{G} \sum_{l=0}^{\infty} \sum_{m=-l}^{l} \sum_{j=0}^{M-1} \frac{Y_{lm}^*(\vec{\Omega})}{4\pi} \sum_{K=0}^{N-1} P_i(K,N-1) \frac{1}{\rho(j,M-1)} R_{s,lm,jg'}(\vec{r},K) \sum_{L=0}^{M-1} P_j(L,M-1) + \\
&\frac{\chi_{ig}(\vec{r})}{4\pi k} \sum_{g'=1}^{G} \sum_{j=0}^{M-1} \frac{1}{\rho(j,M-1)} R_{f,jg'}(\vec{r}) \sum_{L=0}^{M-1} P_j(L,M-1)
\end{aligned}
\tag{3.17}
$$

Now applying the properties of DLOP or DT stated in Eqs. (B.16) and (B.21), only the zeroth order terms ($j=0$) remain on the *RHS*. The *RHS* can thus be simplified as:

$$
\begin{aligned}
RHS &= \sum_{g'=1}^{G} \sum_{l=0}^{\infty} \sum_{m=-l}^{l} \frac{Y_{lm}^*(\vec{\Omega})}{4\pi} \sum_{K=0}^{N-1} P_i(K,N-1) R_{s,lm,0g'}(\vec{r},K) + \frac{\chi_{ig}(\vec{r})}{4\pi k} \sum_{g'=1}^{G} R_{f,0g'}(\vec{r}) \\
&= \sum_{g'=1}^{G} \sum_{l=0}^{\infty} \sum_{m=-l}^{l} \frac{Y_{lm}^*(\vec{\Omega})}{4\pi} \sum_{K=0}^{N-1} P_i(K,N-1) \sum_{L=0}^{M-1} \sigma_{sl}(\vec{r},L \to K) \phi_{lm}(\vec{r},L) + \\
&\frac{\chi_{ig}(\vec{r})}{4\pi k} \sum_{g'=1}^{G} \sum_{L=0}^{M-1} \nu\sigma_f(\vec{r},L) \phi(\vec{r},L) \\
&= \sum_{g'=1}^{G} \sum_{l=0}^{\infty} \sum_{m=-l}^{l} \frac{Y_{lm}^*(\vec{\Omega})}{4\pi} \sigma_{s,lm,i,g' \to g}(\vec{r}) \phi_{lm,g'}(\vec{r}) + \frac{\chi_{ig}(\vec{r})}{4\pi k} \sum_{g'=1}^{G} \nu\sigma_{f,g'}(\vec{r}) \phi_{g'}(\vec{r}),
\end{aligned}
\tag{3.18}
$$

where the coarse group scalar flux and the coarse group fission and scattering cross-sections are given by:

$$\phi_{g'}(\vec{r}) = \sum_{L=0}^{M-1} \phi(\vec{r}, L), \tag{3.19}$$

$$\phi_{lm,g'}(\vec{r}) = \sum_{L=0}^{M-1} \phi_{lm}(\vec{r}, L), \tag{3.20}$$

$$\nu\sigma_{f,g'}(\vec{r}) = \frac{\sum_{L=0}^{M-1} \nu\sigma_f(\vec{r}, L)\phi(\vec{r}, L)}{\sum_{L=0}^{M-1} \phi(\vec{r}, L)}, \tag{3.21}$$

$$\sigma_{s,lm,i,g'\to g}(\vec{r}) = \frac{\sum_{L=0}^{M-1} \phi_{lm}(\vec{r}, L) \sum_{K=0}^{N-1} P_i(K, N-1)\sigma_{sl}(\vec{r}, L \to K)}{\sum_{L=0}^{M-1} \phi_{lm}(\vec{r}, L)}. \tag{3.22}$$

Finally, the transport equation with discrete orthogonal polynomial expansion becomes:

$$\begin{aligned} &\vec{\Omega} \cdot \nabla \psi_{ig}(\vec{r}, \vec{\Omega}) + \sigma_{t,0g}(\vec{r})\psi_{ig}(\vec{r}, \vec{\Omega}) + \delta_{ig}(\vec{r}, \vec{\Omega})\psi_{0g}(\vec{r}, \vec{\Omega}) = \\ &\sum_{g'=1}^{G} \sum_{l=0}^{\infty} \sum_{m=-l}^{l} \frac{Y_{lm}^*(\vec{\Omega})}{4\pi} \sigma_{s,lm,i,g'\to g}(\vec{r})\phi_{lm,g'}(\vec{r}) + \frac{\chi_{ig}(\vec{r})}{4\pi k} \sum_{g'=1}^{G} \nu\sigma_{f,g'}(\vec{r})\phi_{g'}(\vec{r}). \end{aligned} \tag{3.23}$$

The zeroth order (*i=0*) calculation is equivalent to the standard coarse group calculation, and Eqs. (3.19)-(3.22) can be determined by the zeroth order calculation. From Eq. (3.23) it can be seen that the higher order equations are decoupled from each other and only depend on the zeroth order (coarse group) flux. This decoupling leads to computational

costs comparable to the common multigroup solution over G coarse groups (higher order equations are solved very quickly since their *RHS* is known) but can give a fine-group energy spectrum by the unfolding of the angular flux from all the moments:

$$\psi(\vec{r},\vec{\Omega},K)=\sum_{i=0}^{N-1}\frac{1}{\rho(i,N-1)}P_i(K,N-1)\psi_{ig}(\vec{r},\vec{\Omega}). \tag{3.24}$$

A similar derivation of the DGM method for diffusion equation is in Appendix C. Scalar flux is instead expanded and a series of scalar flux moment equations is obtained. Solving these moment equations and a fine group structure scalar flux can be obtained by unfolding the solved scalar flux moments.

3.2 Comparison of discrete and continuous energy expansions

The continuous form of the generalized multigroup theory proved very promising, but there are some obvious disadvantages compared to the discrete generalized multigroup method. Firstly, the presence of negative fluxes due to Gibbs oscillations [Rahnema 2008] limited its applications. This oscillation effect is associated with continuous expansion and is difficult to eliminate, while discrete expansion does not have such concern.

Secondly, in the continuous energy derivation of a fine group database from a multigroup library, the energy boundaries of the energy groups are needed such that a cross-section moment database can be built. Fluxes and cross sections in each energy group need be rescaled to match the definition of continuous polynomials. With discrete expansion,

group fluxes and group cross sections are counted using group numbers, and no rescaling is needed. Detailed energy structure (starting and ending energy/lethargy values of each group) is not needed.

Thirdly, evaluation of continuous moments typically includes an integral which is normally evaluated using quadratures, and discretization errors may exist in such a process. Such error is inherent in implementations of continuous domain moments and does not appear with the discrete expansion.

Thus, discrete orthogonal polynomials expansion in nature matches multigroup definition. Two examples are given below to demonstrate the above advantages of discrete expansion over continuous expansion.

The first example is a step function with 4 piecewise constant values within each domain given in Figure 3.1. Assume we know the exact step function $f(x)$. In order to reconstruct it using continuous (Legendre) polynomials, continuous moments are first generated as:

$$F_m = \int_{-1}^{1} P_m(x) f(x) dx, \tag{3.25}$$

where m is the expansion order. The reconstructed step function can be obtained as:

$$\tilde{f}(x) = \sum_{m=0}^{M} \frac{1}{\rho_m} F_m P_m(x). \tag{3.26}$$

Figure 3.1 plots $\tilde{f}(x)$ with expansion order *M=20* and *100*, respectively. The oscillation effects are very obvious with different expansion orders, especially near the discontinuities. Note that in this example the variable x varies in the domain [-1,1] and thus no extra rescaling of the function $f(x)$ is needed to generate the moments.

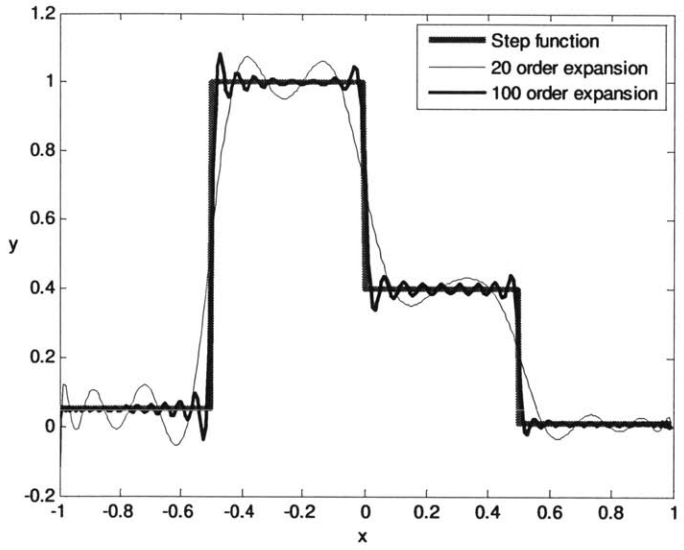

Figure 3.1. Expansion of a step function using continuous Legendre polynomials.

Approximating the step function by applying a $3^{rd}(N-1)$ order discrete expansion as follows. First generate discrete moments as:

$$F_m = \sum_{K=0}^{N-1} f_K P_m(K, N-1), \tag{3.27}$$

where K is the discrete variable index, m is the expansion order and N=4 in this case. The exact step function can be reconstructed as:

$$\tilde{f}_K = \sum_{m=0}^{N-1} \frac{1}{\rho(m, N-1)} F_m P_m(K, N-1). \tag{3.28}$$

The reconstructed step function $\tilde{f}_K$ is shown in Figure 3.2. Note that the expansion order is fixed at $N-1$ due to the definition of discrete orthogonal polynomials. The number of expansion moments (4) is much smaller than the continuous case (20 or 100) while it reconstructs the step function accurately with no oscillations. Furthermore, one only needs to know the number of discretization domains ($N=4$), while the information of where the domains start and end is not required, i.e., $x \in (-1.0,-0.5)$, $(-0.5,0.0)$, $(0.0,0.5)$, and $(0.5,1.0)$, respectively, in this example.

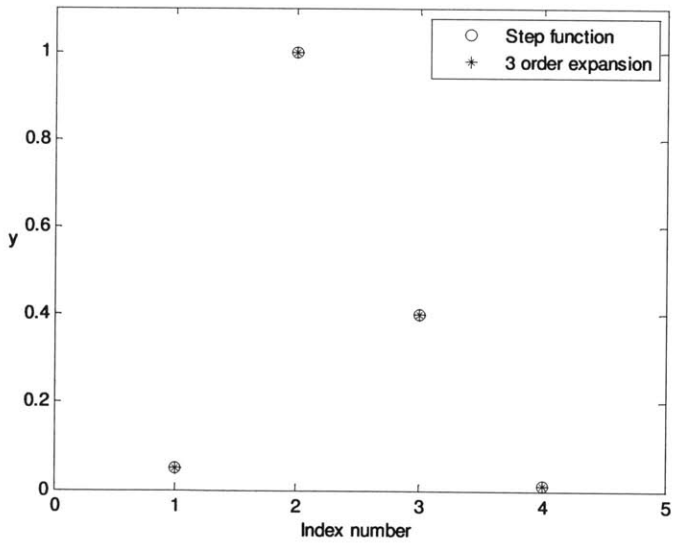

Figure 3.2. Expansion of a step function using discrete Legendre polynomials.

For sake of clarity on how this can be applied to nuclear reactor applications, a second example is in order. Assuming a fine group library of 47 groups, a coarse group library of 2 energy groups can be formed (with thermal cutoff of 0.625eV, 12 and 35 fine groups within each coarse group) that is condensed from an estimated energy spectrum, as illustrated in Fig. 3.3. The system of 2 equations (assuming only energy) would correspond to the multigroup method, but the DGM method also provides 45 (34 from group 1 and 11 from group 2) higher order equations that provide additional information about the energy spectrum, which is shown in Fig. 3.3. These additional equations are all independent of each other and only depend on the zeroth order solution.

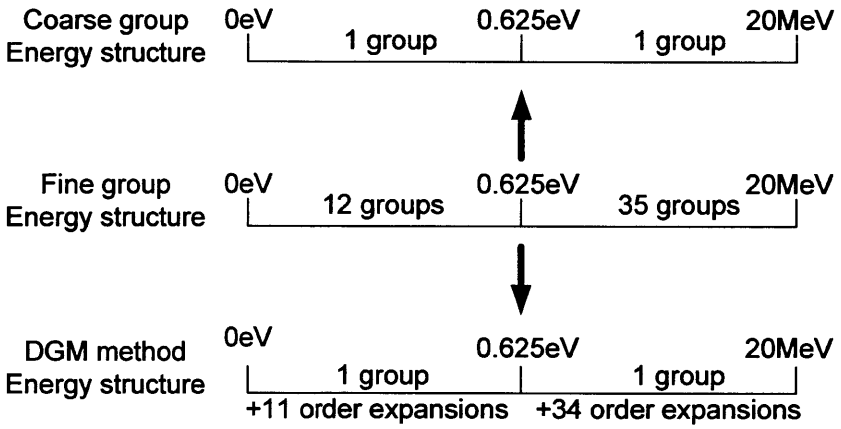

Fig. 3.3. 47 group cross section condensation.

3.3. Computational results

The purpose of this section is to verify the proposed DGM method. A 1-D discrete ordinates code is written to test the DGM method on several 1-D reactor problems typical

of boiling water reactor BWR core configurations, each composed of seven fuel assemblies. The full description of these problems, illustrated in Figure 3.4, can be found in [Rahnema 2008]. The method was tested on all four assemblies and three cores on an Intel 2.4GHz Core (TM) 2 Duo P8600 2.4 GHz PC. The current implementation is limited to discrete-ordinates, but the extension to other solution techniques of the transport equation or diffusion equation is straightforward. It should also be noted that the 1-D discrete-ordinate implementation includes no form of acceleration as this facilitates the comparison between methods. However, it should be noted that acceleration techniques would most certainly reduce the computational time disparity presented in these results.

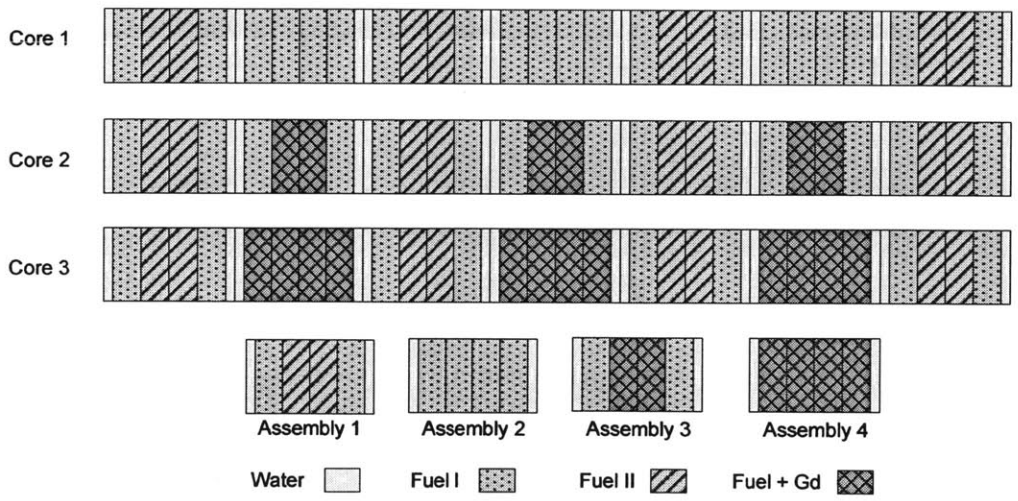

Figure 3.4. 1-D BWR core and assembly configurations.

In 1-D discrete ordinates, assuming isotropic scattering and applying transport cross-sections as a linear anisotropic scattering approximation, Eq. (3.23) can be written as:

$$\mu\frac{\partial\psi_{ig}(x,\mu)}{\partial x}+\sigma_{tr,0g}(x)\psi_{ig}(x,\mu)+\delta_{ig}(x,\mu)\psi_{0g}(x,\mu)=$$
$$\frac{1}{2}\sum_{g'=1}^{G}\sigma_{s,i,g'\to g}(x)\phi_{g'}(x)+\frac{\chi_{ig}(x)}{2k}\sum_{g'=1}^{G}\nu\sigma_{f,g'}(x)\phi_{g'}(x). \tag{3.29}$$

where the transport cross-section moments and the perturbation term are defined in the same way as Eqs. (3.8)-(3.11) by using transport cross-section data instead of total cross-section data.

3.3.1 One dimensional BWR assembly tests

The DGM method was initially tested on each of the four assemblies. It should also be noted that for this first test case, the cross-section moments were generated with the exact reference spectrum, thus the goal of this test is to verify the accuracy of the approximation made in the DGM method. In this implementation, an 8 group cross-section database serves as the "fine" group structure and is used to calculate our reference solution. The DGM method is applied to a 1 group database with 7^{th} order expansion condensed from the reference solution. Both the reference and the DGM calculations are performed using an S_{16} angular approximation and the same spatial mesh. The scalar flux is converged to 10^{-5} and the eigenvalue is converged to within 10^{-6}. Reflective boundary conditions are set on both sides. The step difference [Lewis 1993] method is applied in the spatial sweep process.

Results for assemblies 1 and 4 are given in Tables 3.1-3.3 as they give a good breath of the capabilities of the method. Assembly 4 is by far the most constraining assembly due to the high Gadolinium loading. The reported computational time for the 1 group with expansion also includes the time needed to generate the cross-section moments.

Table 3.1. Assemblies 1 and 4 eigenvalue and computational time.

	Eigenvalue k	Δk *(pcm)*	Computational time *(seconds)*
Assembly 1, 8 group	1.240588	--	0.3
Assembly 1, 1 group/exp	1.240576	1.2	0.03
Assembly 4, 8 group	0.323416	--	0.2
Assembly 4, 1 group/exp	0.323416	0.0	0.02

Table 3.2 Assembly 1 DGM result errors.

	rms (%)	*mre* (%)	err_{max} (%)
Scalar flux	0.00035	0.00015	0.0012
Absorption rate	0.00013	0.000098	0.00020

Table 3.3 Assembly 4 DGM result errors.

	rms (%)	*mre* (%)	err_{max} (%)
Scalar flux	0.052	0.00098	0.31
Absorption rate	0.017	0.015	0.034

As seen in Tables 3.1, 3.2 and 3.3, the DGM method gives an accurate flux solution while the computational time is much less than the fine group calculation. The values of the root mean square relative error, mean relative error, and maximum relative error of scalar flux and absorption rate of assembly 4 are larger than those of assembly 1 because of the strong heterogeneities of assembly 4 caused by the presence of Gadolinium. The mean relative error is an average error in which the relative errors are weighted by the flux values. For assembly 4, the mean relative error is much smaller than the root mean square error, which indicates that the larger errors occur in regions of very low flux (i.e., thermal groups in the Gd rich regions).

3.3.2 One dimensional BWR core tests

Now that the methodology has shown the ability to reproduce the reference flux solution, a tougher test is needed to illustrate the advantages of the DGM method for whole core calculations. A comparison is made between 47 group reference solutions for the three cores of Figure 3.4 with a 2 group DGM calculation with respective expansion orders of 34 and 11. The 47 group cross sections were generated from the HELIOS lattice depletion code [Rahnema 2008] [Giust 2000], in which the first 35 groups are in the fast region above the thermal cutoff of 0.625eV while groups 36-47 cover the thermal energy range. Once again, a S_{16} angular approximation is applied and the step difference method is used for the spatial sweep. The scalar flux is converged to within 10^{-5} and the eigenvalue is converged to within 10^{-6}. Vacuum boundary conditions are set on both sides.

In this calculation, the 2 group cross-sections and moments needed in the DGM method are not generated from the reference solution but from fine group assembly calculations (such as would be done in current multi-level calculations). Tables 3.4-3.6 list the flux and absorption rates, eigenvalue, and the computational time (including the calculation time needed for obtaining the cross-section moments) for cores 1 and 3. The results for core 2 were omitted from the discussion since they fall somewhere between the results of cores 1 and 3. From Table 3.4, the computational time of the DGM method is very small compare to the fine group calculation. The eigenvalues from the DGM method are equivalent to the ones from the coarse group calculations.

Table 3.4 Cores 1 and 3 eigenvalue and computational time.

	Eigenvalue k	Δk *(pcm)*	Computational time *(seconds)*
Core 1, 47 group	1.151877	--	10.2
Core 1, 2 gr/exp	1.165302	1342	0.3
Core 3, 47 group	0.722289	--	10.1
Core 3, 2 gr/exp	0.791960	6967	0.3

Table 3.5 Core 1 DGM results.

	rms (%)	*mre* (%)	err_{max} (%)
Scalar flux	4.2	1.8	42
Absorption rate	2.5	1.8	4.8

Table 3.6 Core 3 DGM results.

	rms (%)	*mre* (%)	err_{max} (%)
Scalar flux	31	9.0	640
Absorption rate	16	12	30

In core 1, the mean relative error and root mean square relative error are on the order of 1-4% for both the scalar flux and absorption rate, while they are about an order of magnitude larger in core 3, once again due to the strong heterogeneities introduced by the many instances of assembly 4 (with Gadolinium). In core 3, the maximum relative error of scalar flux seen is 640%, which happens in the 47^{th} group (most thermal) in which the flux is almost zero due to the presence of Gd. At this particular location of maximum flux error, the scalar flux from the fine group calculation is 4.6E-6 and the value from the DGM method is -2.5E-5. Both of these values are very small by comparison to the flux in other locations in the core and the unfolded flux also has an unphysical negative value which can explain the large relative error. These results will be improved on in the next section by the introduction of the source updating procedure.

The issue that was identified with the DGM method is that if a particular group flux at a particular spatial point is near zero, i.e., the 47^{th} group in the Fuel+Gd regions, it is possible that the DGM method will give a slightly negative flux at some spatial points. Section 3.4 will analyze the reason why larger errors typically exist at smaller value points with discrete expansions, especially when strong absorbers are present in the core. While this issue has been shown to happen in the results for core 3, it should be noted

that in core 1, which does not contain Gadolinium, and all single assembly cases, no negative fluxes were observed from the DGM calculation. In single assembly calculations, the cross-section moments were generated with the exact reference spectrum, while in the whole core calculations, as done in the standard multi-level approach, the cross-section moments were generated from fine group assembly calculations. Thus, the combination of inaccurate spectrum to generate cross-sections and the strong heterogeneities of the core due to the presence of Gadolinium lead to the negative fluxes and large maximum relative errors as observed in core 3. The following update procedure, which takes advantage of the discrete nature of the DGM method, can eliminate this occurrence, as well as improve the eigenvalue and flux errors.

3.3.3 Eigenvalue and fluxes updates

In the previous results, the DGM method has shown to provide accurate expanded fluxes but maintained the same coarse group eigenvalue. At this point, integral quantities, i.e., the eigenvalue and reaction rates, are not improved and are identical to those obtained from the standard coarse group calculation.

Since the expanded flux shape is more accurate than the coarse group flux shape which is piecewise flat within each coarse group, the coarse group eigenvalue can be updated by simple neutron balance, using the obtained expanded flux and the reference fine group cross-section data:

$$k_{update} = \frac{\text{Production}}{\text{Absorption+Leakage}} = \frac{\sum_{i=1}^{I}\sum_{h=1}^{H} \nu\sigma_f(i,h)\phi_{G/\exp}(i,h)\Delta_i}{\sum_{i=1}^{I}\sum_{h=1}^{H} \sigma_a(i,h)\phi_{G/\exp}(i,h)\Delta_i + \sum_{m=1}^{M}\sum_{g=1}^{G} \mu_m w_m \psi_{G,b}(m,g)}, \quad (3.30)$$

where the fission and absorption terms are calculated using the unfolded expansion scalar flux and fine group cross-sections, and the leakage term is calculated using the coarse group (leading order) angular boundary flux $\psi_{G,b}$, and where Δ_i is the spatial mesh width, μ_m and w_m are abscissas and weights of Gauss-Legendre quadrature for m=1,…,M, and h, g, and i are fine group, coarse group and spatial mesh point indices.

After updating the eigenvalue, the angular flux is updated in order to eliminate possible negative angular fluxes. On the right hand side of Eq. (3.3), for each fine group h, the fission and scattering fixed source can be calculated using the updated eigenvalue, the unfolded expansion fluxes and the fine group cross-sections.

$$Q(\vec{r},\vec{\Omega},K) = \sum_{g'=1}^{G}\sum_{l=0}^{\infty}\sum_{m=-l}^{l} \frac{Y_{lm}^{*}(\vec{\Omega})}{4\pi}\sum_{L=0}^{M-1}\sigma_{sl}(\vec{r},L\to K)\phi_{lm}(\vec{r},L) + \frac{\chi(\vec{r},K)}{4\pi k}\sum_{g'=1}^{G}\sum_{L=0}^{M-1}\nu\sigma_f(\vec{r},L)\phi(\vec{r},L), \quad (3.31)$$

where $k = k_{update}$, and $\phi_{lm}(\vec{r},L)$ and $\phi(\vec{r},L)$ are from the DGM calculation. With this new more accurate driving source, the left hand side of Eq. (3.3) can be re-evaluated as a fixed source problem.

$$\vec{\Omega}\cdot\nabla\psi_{update}(\vec{r},\vec{\Omega},K) + \sigma_t(\vec{r},K)\psi_{update}(\vec{r},\vec{\Omega},K) = Q(\vec{r},\vec{\Omega},K). \quad (3.32)$$

Each flux update is very quick since it is a fixed source problem and source iteration is not required. In the reported results with negative angular fluxes, it was observed that a single flux update was enough to eliminate all negative angular fluxes, and the errors are also improved when compared to the fine group reference solution.

Tables 3.7-3.9 list the results obtained after 1 update of the eigenvalue k and the flux. The computational time of the updates is very small compared to that of the coarse group calculation.

Table 3.7 Cores 1 and 3 eigenvalue and time after the updates.

	Eigenvalue k	Δk *(pcm)*	Computational time *(seconds)*
Core 1, 2gr/exp update	1.163845	1197	0.1
Core 3, 2gr/exp update	0.780053	5776	0.1

Table 3.8 Core 1 DGM result after the updates.

	rms (%)	*mre* (%)	err_{max} (%)
Scalar flux	3.2	1.6	14
Absorption rate	2.5	1.7	4.8

Table 3.9 Core 3 DGM result after the updates.

	rms (%)	*mre* (%)	err_{max} (%)
Scalar flux	15	8.4	32
Absorption rate	14	10	25

By comparing Tables 3.4-3.6 to Tables 3.7-3.9, for core 1, the mean relative error and root mean square error are on the order of 1-3% for both flux and absorption rate, which is marginally better than before the update. The maximum error, however, is substantially reduced from 42% to 14%. For core 3, the mean relative error and root mean square error of both flux and absorption rate are also reduced quite a bit. Of note the root mean square error dropped from 31% to 15%. The maximum relative error of scalar flux is also reduced considerably from 640% to 32% before and after the update. These errors arise from the inaccurate spectrum used to generate the cross-section moments of each assembly, but for very little added computational cost, they can provide improved results over a coarse group calculation.

By adding the computational times of the expansion calculation and the times of the eigenvalue and flux updates, the total times required to perform the DGM calculation plus the updates are about 0.5 seconds for both cores 1 and 3. In comparison, the computational times of the fine group calculations are about 10*sec*. Thus, the computational time of the DGM method plus the updates is much less than that of the standard fine group reference calculation.

Figures 3.5, 3.7, 3.9 and 3.11 plot the group fluxes in cores 1 and 3 as a function of spatial mesh point index for different energy groups. Figures 3.6, 3.8, 3.10 and 3.12 are their corresponding relative errors. Note that the expanded fluxes are the values after the update process and thus have no negative values. In these figures, only half the core is represented (symmetric core) and one in every three spatial points are plotted to avoid unnecessary clutter. In the fast energy region, the two groups with the highest total reaction rates are plotted (groups 9 and 11 for both cores), and two groups in the resonance region corresponding to the two important U^{238} resonances, i.e., 6.67eV (group 19) and 20.8eV (group 15) for both cores. In the thermal energy region, the group with the highest fission rate, i.e., group 43 for both cores, and the group with the highest group scalar flux, i.e., group 39 for both cores are plotted. As the figures show, the DGM method can reproduce very accurately the fine group solution. Even in core 3, with the presence of Gadolinium, the flux from the DGM calculation matches the fine group reference calculation. It can be observed that the fluxes in the thermal groups (plotted in Figure 3.11) are very small in the Fuel+Gd regions.

From Figs. 3.6, 3.8, 3.10 and 3.12, it can be observed that larger errors exist near the vacuum boundary. This is due to the selected weighing function generated from assembly level calculations which assumes reflective boundary condition. Thus larger errors near the boundary are observed due to the leakage in the core. From Figs. 3.10 and 3.12, it can be observed that relative errors in core 3 are very large in the regions containing Gd (Assembly 4).

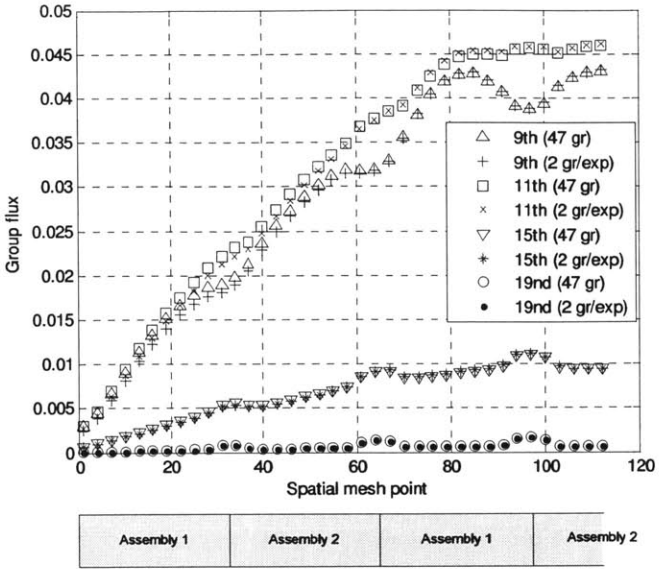

Fig. 3.5 Core 1 scalar flux comparison (fast groups).

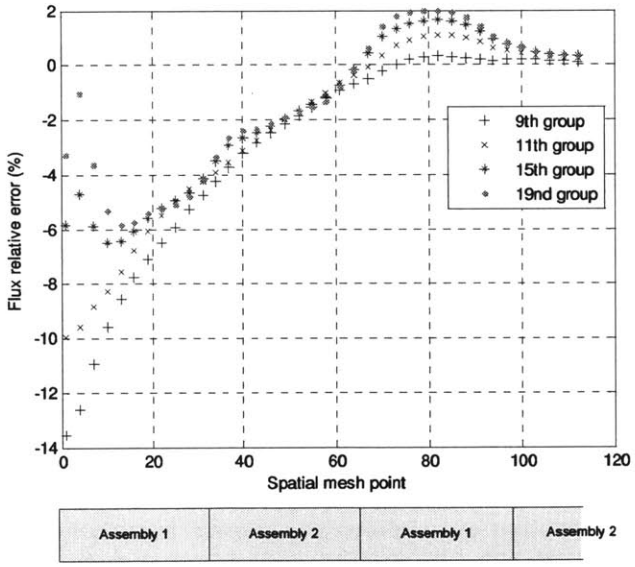

Fig. 3.6 Core 1 scalar flux relative error (fast groups).

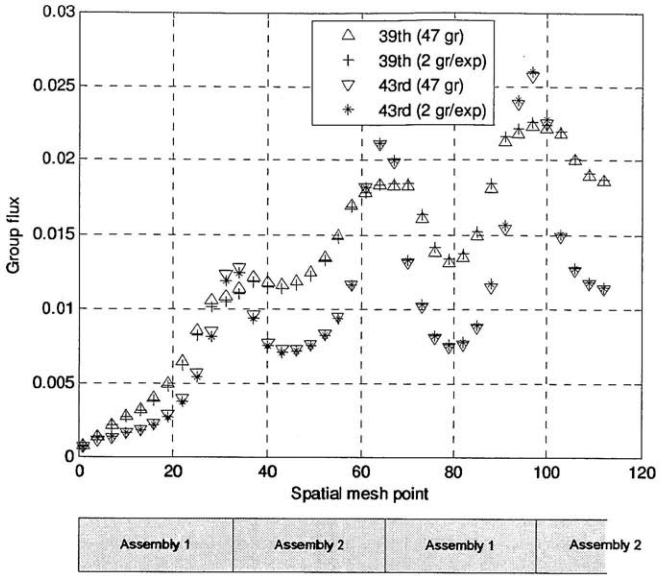

Fig. 3.7 Core 1 scalar flux comparison (thermal groups).

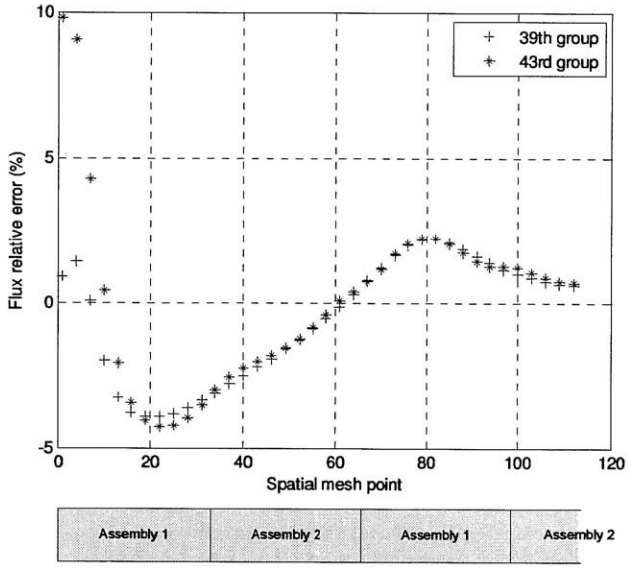

Fig. 3.8 Core 1 scalar flux relative error (thermal groups).

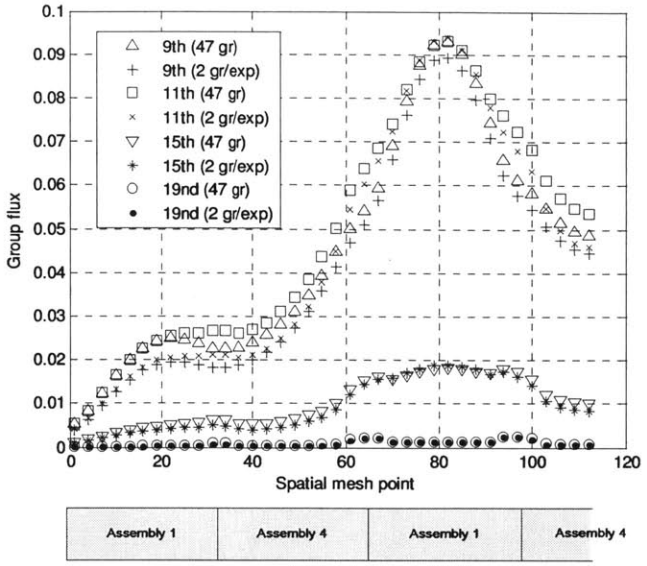

Fig. 3.9 Core 3 scalar flux comparison (fast groups).

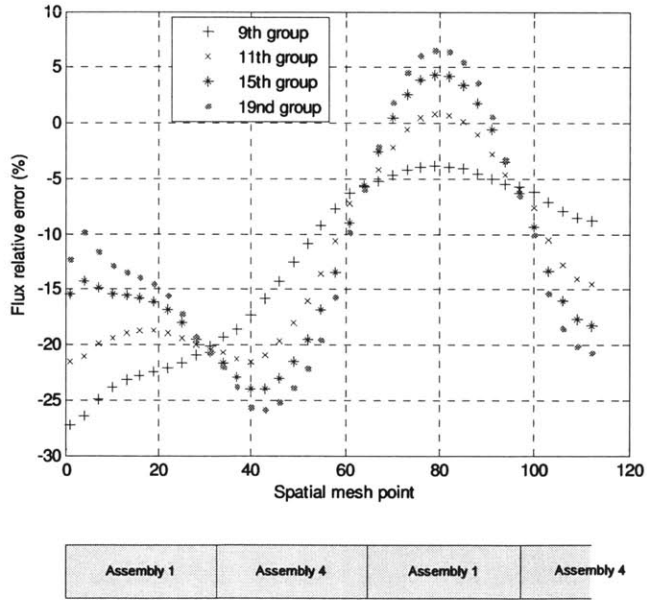

Fig. 3.10 Core 3 scalar flux relative error (fast groups).

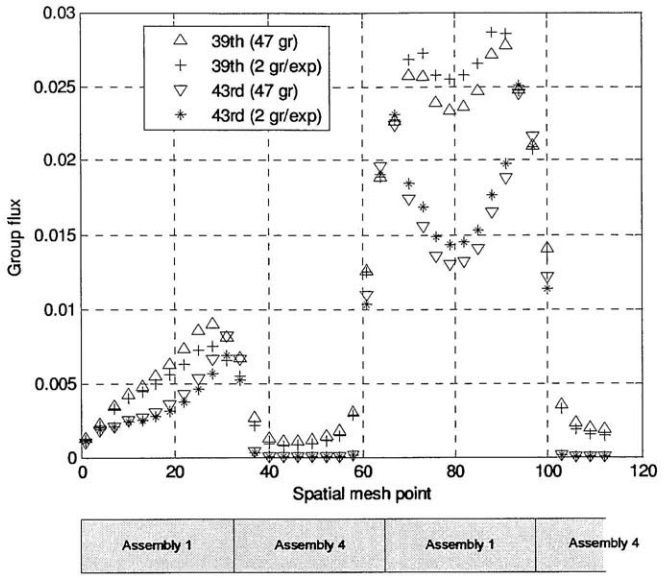

Fig. 3.11 Core 3 scalar flux comparison (thermal groups).

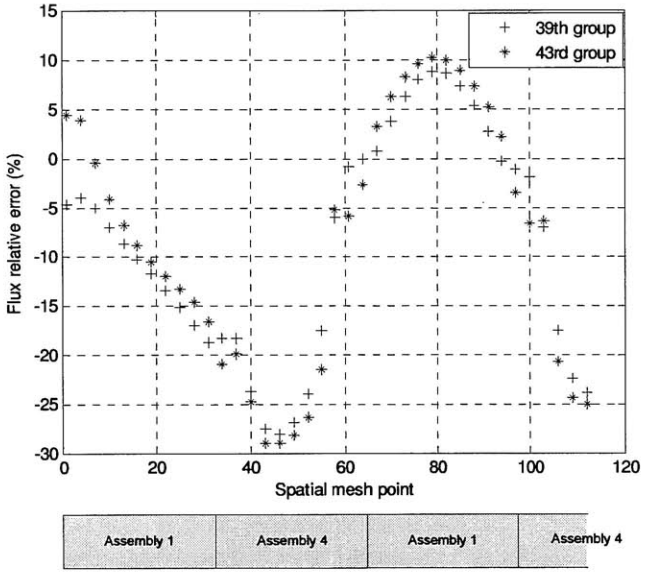

Fig. 3.12 Core 3 scalar flux relative error (thermal groups).

Up to this point the integral quantities have been improved through the above update procedures. Since more accurate flux values are obtained, further improvement is possible by repeated application of Eqs. (3.30)-(3.32) in which the scalar flux and boundary angular flux values are from the previous update calculations. Note that in Eq. (3.30), for the following eigenvalue updates, boundary angular flux has a fine group structure. Normalization to the fission source needs to be performed before each new flux update calculation. A successive update procedure thus becomes a fine group solution (the form with no within group scattering) in which the DGM solution was used as an initial guess. The DGM method could thus also be pursued as an acceleration method for the fine group calculation. Acceleration methods schemes using DGM method will be discussed in detail in Chapter 5.

3.4 Summary

In this chapter, the DGM method has been developed by expanding the energy dependence of the angular flux as a set of flux moments. An initial guessed flux (e.g. assembly level calculation) is used as the weighting function for generating the discrete cross-section moments which are used to solve the flux in the core for each expansion moments. The obtained flux moments are unfolded to construct a whole core energy spectrum. The obtained spectrum is an accurate estimate to the fine group solution.

Based on the properties of the discrete orthogonal polynomials expansion basis, the zeroth order equation is decoupled from the higher order equations. This decoupling

leads to reaction rates and eigenvalue that at first glance are no better than the equivalent coarse group calculations, but provides an accurate fine group spectrum with little computational cost. An additional advantage of the discrete expansion is the possibility of updating the integral parameters by using the expanded flux with the fine group data, thus providing more accurate eigenvalue and reaction rates. Furthermore, this additional step also eliminates all unphysical negative flux values.

The new method has been tested through a series of one dimensional BWR cores and assemblies using a 1-D discrete ordinates code. For the single assembly calculations in which the exact reference spectrum was used to generate the cross-section moments, the DGM method reproduced accurately the fine group spectrum. Larger errors were found in assembly 4 which contained Gadolinium, as well as near the core boundary where leakage is large.

For the whole core 1-D calculations in which fine group assembly spectrum was used to generate the cross-section moments, results have shown that the DGM method can provide a reasonable estimate to the fine group spectrum in the whole core. The mean relative error and root mean square error of both flux and absorption rate are on the order of a few percent in core 1, while they are on the order of 10% in core 3 which is the most heterogeneous case studied. The computational cost of the DGM method including a source update is less than 5% of that from the standard fine group reference calculation.

Since the DGM method can provide a very accurate estimate to the fine group spectrum, it brings many possibilities such as using this approach as an acceleration scheme for fine group solutions or the introduction of an energy recondensation process that could potentially eliminate the need for multilevel calculations. Online energy recondensation and energy acceleration methods will be developed in Chapter 4 and Chapter 5, respectively, with an extension to more realistic multi-dimensional geometries.

Chapter 4 Online Energy Recondensation Methodology

This chapter describes the online energy recondensation methodology that can be derived from the DGM method [Zhu 2011]. Computational tests on both1-D and 2-D light water reactor problems, as well as high temperature reactor problems, are performed. A discussion follows on the accuracy of the method in relation to the spatial discretization used.

4.1 Method description

While the DGM method provides greater energy resolution and keeps the computational time comparable to the coarse group calculation, the flux spectrum needed to generate cross section moments defined by Eqs. (3.9)-(3.11), (3.21)-(3.22) are not known *a priori.* This flux can be approximated from lattice level calculations, but this is in essence equivalent to the traditional multilevel approach. This inaccurate flux spectrum is the main source of error in both the current multilevel approach and the DGM calculation.

Despite these inaccuracies, the unfolded flux spectrum provided by the DGM calculation was shown to be a very reasonable estimate of the reference fine group solution. This puts forward the possibility that the DGM solution can be used as a weighing function to generate improved coarse group cross-sections and associated moments. This process can be repeated iteratively at the core level with each iteration taking essentially the computational time of a coarse group calculation.

The recondensation procedure provides a way to eliminate the assembly calculation from the multilevel process. Assuming a properly self-shielded fine group cross section database, the lattice flux calculations can be replaced by an appropriate initial guess to generate cross section moments. For example, the initial guess can be a combination of a Maxwellian spectrum in the thermal range, $1/E$ in the resonance range and the fission spectrum in the fast range. Another choice is to perform the core level fine group calculation for only a few outer iterations to obtain a rough estimate. The more accurate the initial guess of the flux, the fewer iterations will be required.

The flow chart of Fig.4.1 illustrates the traditional multilevel approach, while Fig. 4.2 presents the new recondensation approach. In this study, it is assumed that we start with an appropriate set of self-shielded cross-sections. The impact of the recondensation technique to provide self-shielding is left for future studies. The initial flux guess can be estimated by any means and will be used to generate the coarse group moments. A DGM calculation is then performed for both the 0^{th} order and higher order equations. Using the flux energy moments, a fine group flux is unfolded and then used to recondense the cross-sections to initiate the iterative process. The recondensation procedure stops when a convergence criterion is met, which was set as the root mean square relative error or mean relative error of the scalar flux between two consecutive iterations.

The flux update procedure proposed in Chapter 3 is performed at each iteration in order to eliminate negative values in the unfolded fluxes, which is very important when

regenerating cross section moments for the next DGM iteration. Negative flux values lead to a very unstable algorithm. Eigenvalue updates were not performed in the iteration process because of the small gain of such updates in comparison to the benefits of DGM iterations.

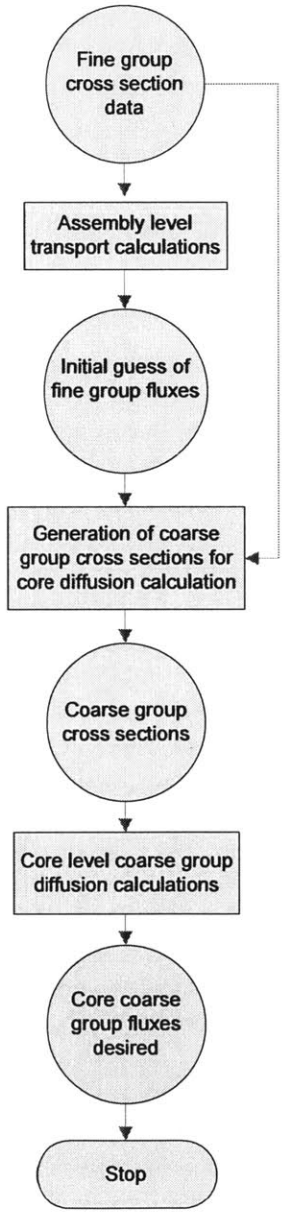

Fig. 4.1. Flow chart of the traditional multilevel procedure.

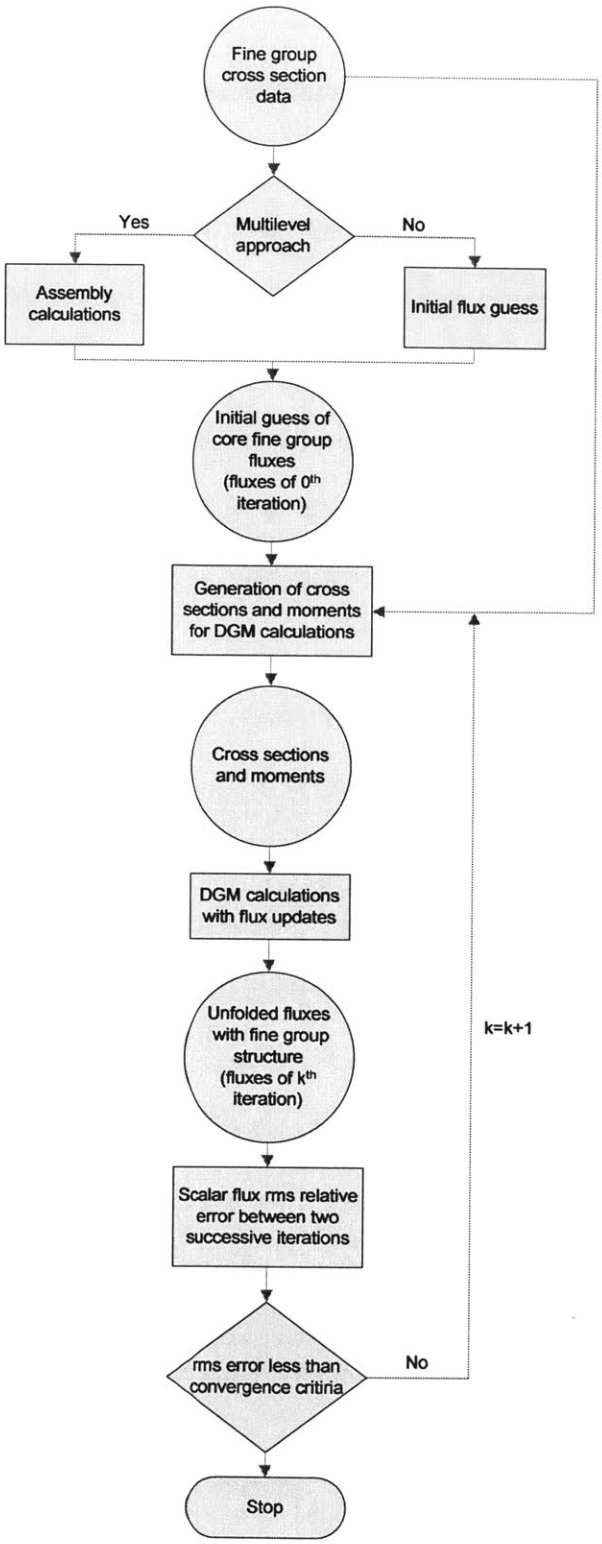

Fig. 4.2. Flow chart of the recondensation procedure.

It should also be noted that an additional simplification can be made when doing the recondensation. The collision term in the DGM method is separated into two parts, i.e. an average collision term and a perturbation term:

$$
\begin{aligned}
R_{t,ig}^{k+1}(\vec{r},\vec{\Omega}) &= \sigma_{t,0g}^{k}(\vec{r})\psi_{ig}^{k+1}(\vec{r},\vec{\Omega}) + \delta_{ig}^{k}(\vec{r},\vec{\Omega})\psi_{0g}^{k+1}(\vec{r},\vec{\Omega}) \\
&= \sigma_{t,0g}^{k}(\vec{r})\sum_{K=0}^{N-1} P_i(K,N-1)\psi^{k+1}(\vec{r},\vec{\Omega},K) \\
&+ \frac{\sum_{K=0}^{N-1} P_i(K,N-1)\delta_g^{k}(\vec{r},K)\psi^{k}(\vec{r},\vec{\Omega},K)}{\sum_{K=0}^{N-1}\psi^{k}(\vec{r},\vec{\Omega},K)} \sum_{K=0}^{N-1}\psi^{k+1}(\vec{r},\vec{\Omega},K),
\end{aligned}
\tag{4.1}
$$

where k is the index of DGM iteration. If after a certain number of DGM iterations $\psi^{k}(\vec{r},\vec{\Omega},K)$ approaches $\psi^{k+1}(\vec{r},\vec{\Omega},K)$, the total reaction rate moment within a coarse group g in Eq.(4.1) approaches the exact value in the moment equation:

$$
R_{t,ig}(\vec{r},\vec{\Omega}) = \sum_{K=0}^{N-1} P_i(K,N-1)\sigma_t(\vec{r},K)\psi(\vec{r},\vec{\Omega},K), \tag{4.2}
$$

where it is assumed that there are N fine group points within coarse group g with point index $K = 0,1,2,...,N-1$. Another way proposed here to define the collision term is:

$$
\begin{aligned}
R_{t,ig}^{k+1}(\vec{r},\vec{\Omega}) &= \sigma_{t,0g}^{k}(\vec{r})\psi_{ig}^{k+1}(\vec{r},\vec{\Omega}) + \delta_{ig}^{k}(\vec{r},\vec{\Omega})\phi_{0g}^{k+1}(\vec{r}) \\
&= \sigma_{t,0g}^{k}(\vec{r})\sum_{K=0}^{N-1} P_i(K,N-1)\psi^{k+1}(\vec{r},\vec{\Omega},K) \\
&+ \frac{\sum_{K=0}^{N-1} P_i(K,N-1)\delta_g^{k}(\vec{r},K)\psi^{k}(\vec{r},\vec{\Omega},K)}{\sum_{K=0}^{N-1}\phi^{k}(\vec{r},K)} \sum_{K=0}^{N-1}\phi^{k+1}(\vec{r},K),
\end{aligned}
\tag{4.3}
$$

where the perturbation term is:

$$
\begin{aligned}
\delta_{ig}(\vec{r},\vec{\Omega}) &= \frac{\sum_{K=0}^{N-1} P_i(K,N-1)\delta_g(\vec{r},K)\psi(\vec{r},\vec{\Omega},K)}{\sum_{K=0}^{N-1} P_0(K,N-1)\phi(\vec{r},K)} \\
&= \frac{\sum_{K=0}^{N-1} P_i(K,N-1)(\sigma_t(\vec{r},K)-\sigma_{t,0g}(\vec{r}))\psi(\vec{r},\vec{\Omega},K)}{\sum_{K=0}^{N-1} P_0(K,N-1)\phi(\vec{r},K)}.
\end{aligned}
\tag{4.4}
$$

By comparing this new perturbation term and the one in Section 3.1, the denominator is now a function of scalar flux instead of angular flux. Thus in Eq.(4.3), the corresponding term is

$$
\frac{\sum_{K=0}^{N-1} P_i(K,N-1)\delta_g^{k}(\vec{r},K)\psi^{k}(\vec{r},\vec{\Omega},K)}{\sum_{K=0}^{N-1}\phi^{k}(\vec{r},K)} \sum_{K=0}^{N-1}\phi^{k+1}(\vec{r},K) \tag{4.5}
$$

in order to remain consistent. Thus with energy recondensation, the new proposed definition of the collision term eliminate the angular flux in the denominator of the delta term. In the 1-D BWR recondensation tests, $\delta_{ig}(\vec{r},\vec{\Omega})$ is defined as in Chapter 3 to keep consistent with the DGM calculations on the same set of cores of Chapter 3. The other results in this chapter used the definitions in Eq.(4.4).

4.2. Computational Results

Sections 4.2.1 and 4.2.2 present 1-D BWR and HTR core tests, while section 4.2.3 and 4.2.4 present 2-D PWR and HTR core tests. All the tests are performed using the discrete ordinates method. It should however be noted that the methodology is general and thus not limited to this solution scheme. In this section, 1-D tests are performed on an Intel Core (TM) 2 Duo P8600 2.4 GHz PC, and 2-D tests are performed on a single core of 2.5 GHz Intel Xeon processor.

4.2.1 One dimensional BWR core tests

A detailed description of the set of 1-D BWR cores can be found in [Rahnema 2008], and an illustration of the cores and assemblies is found in Fig. 3.3. For the results presented in this section, the first iteration (DGM method) parameters are computed from assembly calculations with reflective boundary conditions as was done in Chapter 3. The main goal of the recondensation calculations is to reduce the errors associated with the coarse group representation with minimal iterations, thus improving the coarse group solution

considerably. Again a comparison is made between the 47 group reference solutions for the three 1-D cores with a 2 group DGM calculation with a thermal cutoff at 0.625 eV and respective expansion orders of 34 and 11 in each group, thus preserving exactly the 47 group dataset. A S_{16} angular approximation is applied and the step difference method is used for the spatial sweep. In the power iterations and fixed source iterations, the scalar flux is converged to 10^{-5} and the eigenvalue is converged to 10^{-6}.The maximum number of inner iteration per outer iteration is set to 20. Vacuum boundary conditions are set on both sides of the core. The recondensation calculations for all three cores with different number of iterations are performed. The root mean squared error and mean relative error will be abbreviated by *rms* and *mre*, respectively, and the definitions are in Appendix D.

Computational results are given in Tables 4.1-4.4 for cores 1 and 3, respectively. The computational time of the fine group reference calculations is roughly 10 seconds for each core with no acceleration. The numbers of transport sweeps are 22,942 and 22,888, respectively, for cores 1 and 3. Note that one transport sweep here is defined as sweeping once on the whole spatial meshes in all directions, for a single energy group (fine or coarse) or a single energy expansion moment. Thus, the count of transport sweeps can effectively compare the computational costs with different energy discretization methods.

For core 1, after 29 DGM iterations (7.4*sec*, 9,168 transport sweeps), the *rms* relative error of scalar flux between two consecutive iterations reaches the convergence criteria, i.e., 1.0^{-5} (0.001%). The *rms* and *mre* errors compared to the reference fine group solution are 0.016% and 0.012%, respectively, after 29 DGM iterations. It can be observed that

the number of transport sweeps after 29 DGM iterations (9,168) is much less than that of the fine group calculation (22,942).

For core 3, after 68 DGM iterations (17.0*sec*, 20102 transport sweeps), the *rms* relative error of scalar flux between two consecutive DGM iterations is less than 0.001%. At this point, the *rms* and *mre* errors compared to the reference fine group solution are 0.012% and 0.0061%, respectively. In core 3, a large amount of Gd is included. From Chapter 3, it is known that larger errors exist at low flux points, while these points typically have less contribution to the power distribution, and thus the *mre* errors are typically smaller than *rms* errors. Thus, an alternate convergence criterion is to stop the DGM iteration on the *mre* error. Tables 4.3 and 4.4 show that after 51 iterations, the *mre* error between two consecutive iterations drops below 0.001%. The *rms* and *mre* errors compared to the reference solution are 0.014% and 0.0063%, respectively, after 51 iterations. This indicates that the *mre* error between two consecutive iterations is a sufficient convergence criterion.

Table 4.1 1-D BWR Core 1 errors in fluxes.

	rms (%)*	*mre* (%)*	*rms (%)*	*mre (%)*
1st iteration	-	-	3.2	1.6
2nd iteration	2.9	1.5	1.0	0.62
3rd iteration	0.78	0.39	0.56	0.28
29th iteration	**0.00071**	0.00039	0.016	0.012

Note: Errors with * are between two consecutive iterations of DGM solution.
Errors without * are between DGM solution and reference solution.

Table 4.2 1-D BWR Core 1 computational results.

	Eigenvalue k	Δk *(pcm)*	Computation time *t (sec)*	Number of transport sweeps
1st iteration	1.165302	1342	0.4	1,684
2nd iteration	1.152046	17	0.8	2,561
3rd iteration	1.153073	119	1.1	3,092
29th iteration	1.151891	1	7.4	9,168
Reference solution	1.151877	-	10.2	22,942

Note: Computational time and number of transport sweeps of assembly calculations are not included. The total computational time for all the 4 assemblies is 2.2sec.

Table 4.3 1-D BWR Core 3 errors in fluxes.

	rms (%)*	*mre* (%)*	*rms (%)*	*mre (%)*
1st iteration	-	-	15	8.5
2nd iteration	17	7.1	6.3	4.3
3rd iteration	5.0	2.9	2.6	1.7
51st iteration	0.014	**0.001**	0.014	0.0063
68th iteration	**0.00073**	0.000042	0.012	0.0061

Note: Errors with * are between two consecutive iterations of DGM solution.
Errors without * are between DGM solution and reference solution.

Table 4.4 1-D BWR Core 3 computational results.

	Eigenvalue k	Δk *(pcm)*	Computation time t *(sec)*	Number of transport sweeps
1st iteration	0.791960	6867	0.5	2,197
2nd iteration	0.740797	1851	0.9	3,656
3rd iteration	0.732549	1026	1.2	4,731
51st iteration	0.722295	1	13.0	16,866
68th iteration	0.722297	1	17.0	20,102
Reference solution	0.722289	-	10.1	22,888

Note: Computational time and number of transport sweeps of assembly calculations are not included. The total computational time for all the 4 assemblies is 2.2sec.

The recondensation methodology shows that we can converge to the full fine group solution with minimal loss of accuracy in comparable time. The loss of accuracy is greater for very complex cores with strong absorbers as discussed in Chapter 3. The interesting application to keep in mind is not to use the DGM recondensation approach to solve a fine group problem, despite the slight decrease in computational time, but to perform only a few iterations to improve substantially the coarse group results. For example, looking at core 3, within 3 iterations, the eigenvalue error is reduced to 1026*pcm* and the *mre* to 1.7% when comparing to the fine group results in one-tenth of the computational time of the fine group calculation. The DGM recondensation procedure is able to correct the coarse group parameters to account for spectral shifts that cannot be captured from infinite lattice calculations. The reason for this improvement is that the

DGM calculation is performed at the core level and thus captures the neighboring effect on the fine group flux.

It can also be concluded that since the DGM calculation provides an accurate weighting function, traditional lattice level calculation in light water reactor analysis can be removed, and the initial guess can be substituted by any reasonable flux spectrum. For the 1-D and 2-D LWR core tests, assemblies are defined clearly and the initial guess of recondensation is from a lattice level calculation. For the HTR tests in Sections 4.2.2 and 4.2.4, since there are no obvious lattice geometries, the initial guess of recondensation is from a few outer iterations of fine group calculations.

Scalar flux *rms* relative errors and eigenvalue relative errors are plotted in Figs. 4.3-4.6 for cores 1 and 3. It can be observed that the *rms* errors of the scalar flux show a smoother convergence trend than the relative errors of the eigenvalue, which is the reason the *rms* error of scalar flux was selected as the convergence criterion of the recondensation.

The eigenvalue is defined as neutron production divided by the sum of absorption and leakage, and all three terms are function of the flux. In the first few DGM iterations, an oscillation of the eigenvalue is observed due to the errors associated with the flux in both the numerator and denominator of the eigenvalue definition. After a certain number of iterations, when the flux spectrum becomes more accurate, the oscillation of the eigenvalue diminishes considerably.

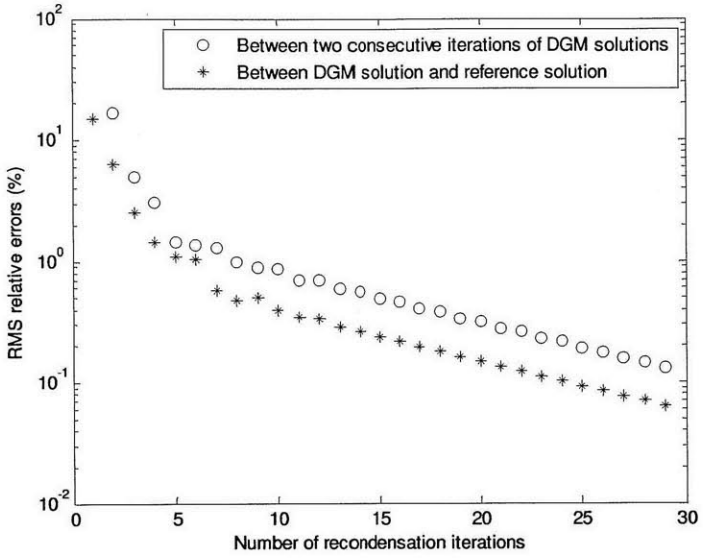

Fig. 4.3. Scalar flux *rms* relative errors of 1-D BWR core 1.

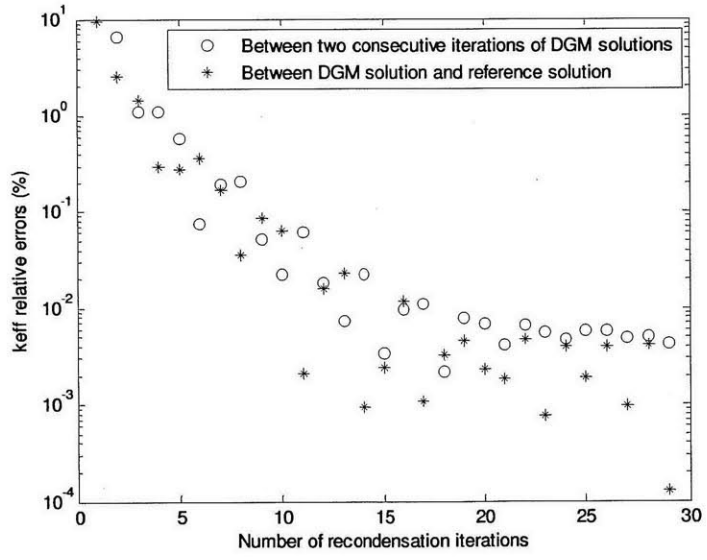

Fig. 4.4. Eigenvalue relative errors of 1-D BWR core 1.

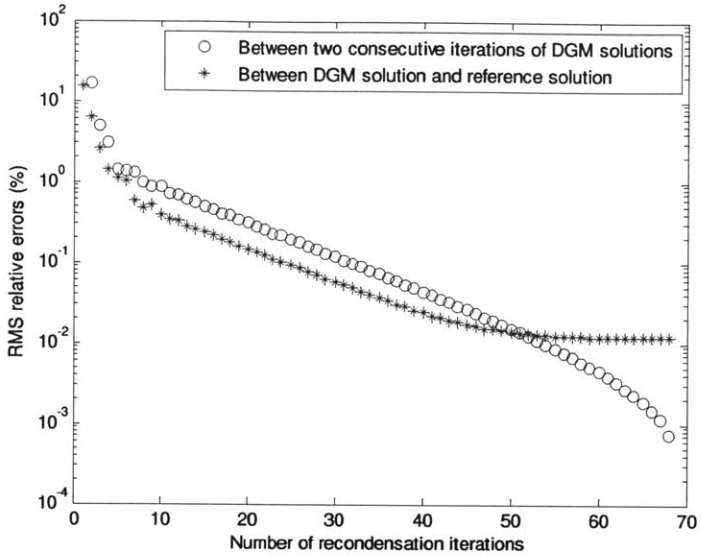

Fig. 4.5. Scalar flux *rms* relative errors of 1-D BWR core 3.

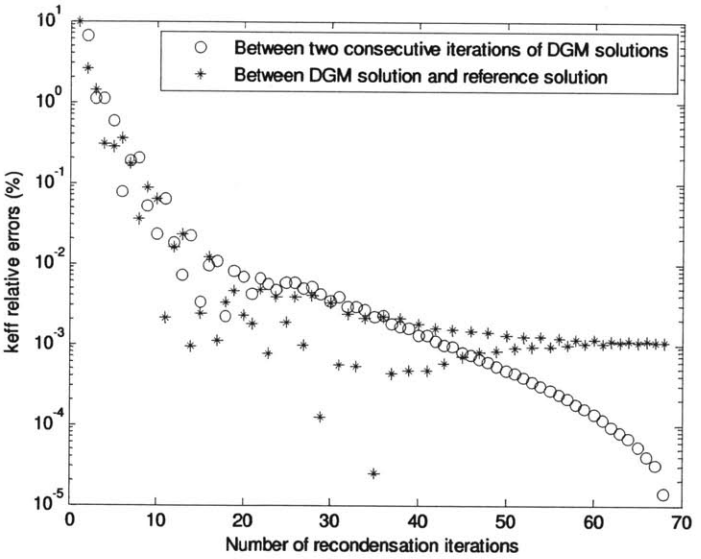

Fig. 4.6. Eigenvalue relative errors of 1-D BWR core 3.

Figs. 4.5 and 4.6 indicate that for core 3, after about 50 iterations, errors between the DGM solution and the reference solution plateaus within the accuracy of the convergence criteria, which indicates that more DGM iterations will not improve the overall accuracy. This is the main reason why the *mre** was proposed as the stopping criterion.

Figs. 4.7, 4.9 and 4.11 show the scalar flux in core 3 as a function of energy for a representative water region, fuel region, and fuel with Gd region, respectively. Figs. 4.8, 4.10 and 4.12 show the corresponding relative errors of the scalar flux. It can be observed from the first three iterations that errors are reduced and the fluxes converge to the reference spectrum with increasing number of DGM iterations.

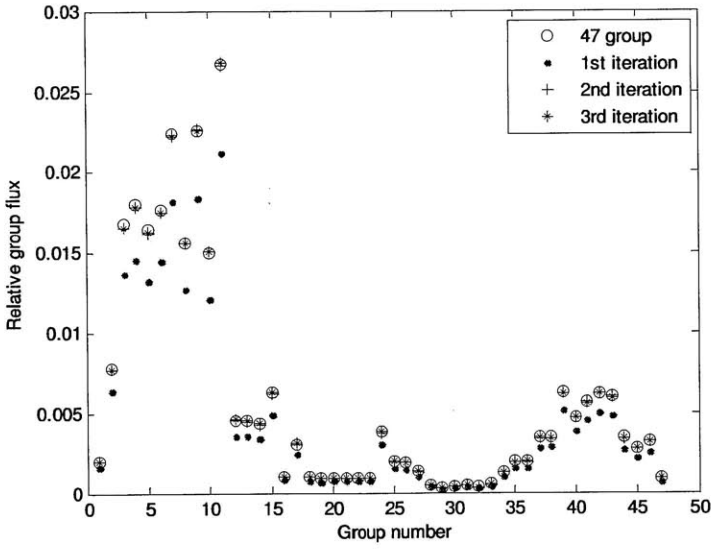

Fig. 4.7 Scalar flux comparison for core 3 water region.

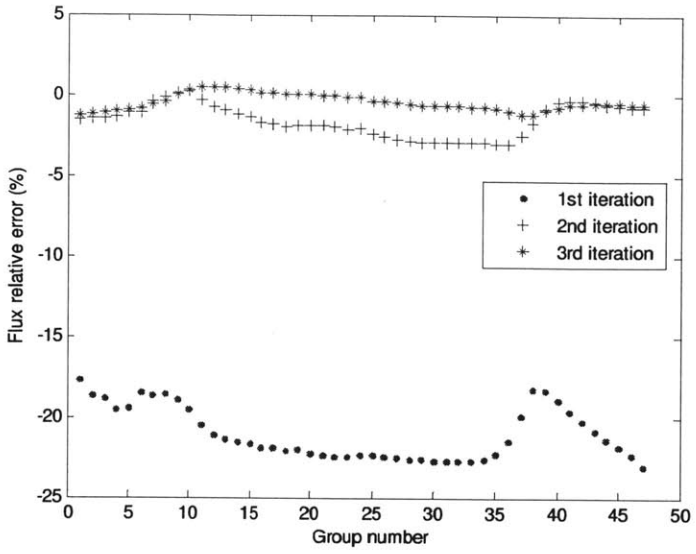

Fig. 4.8 Scalar flux relative error for core 3 water region.

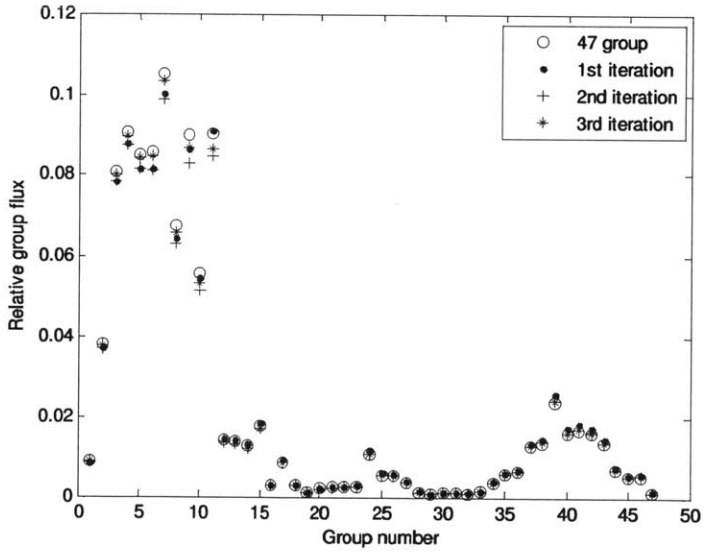

Fig. 4.9 Scalar flux comparison for core 3 Fuel (high enrichment) region.

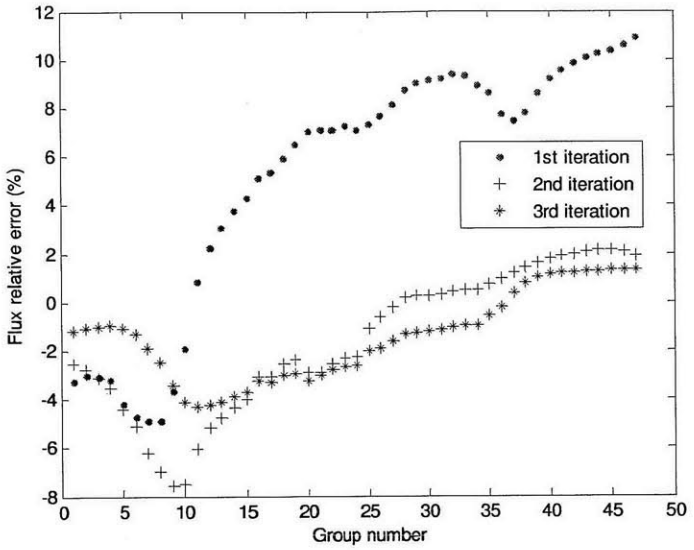

Fig. 4.10 Scalar flux relative error for core 3 Fuel (high enrichment) region.

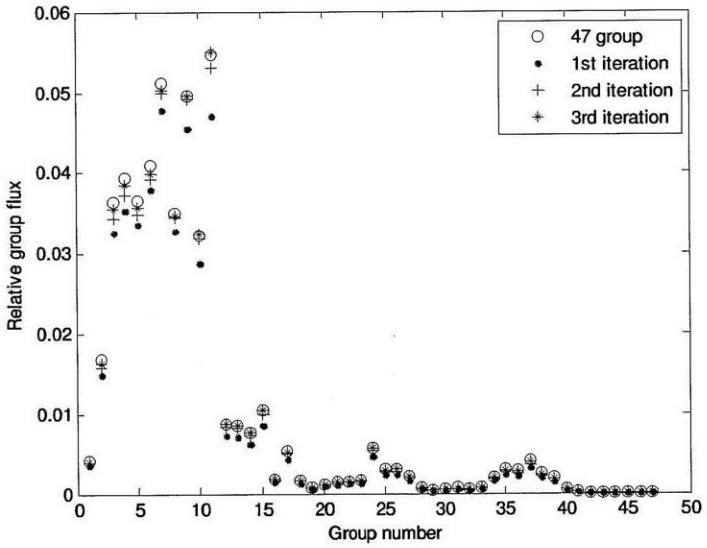

Fig. 4.11 Scalar flux comparison for core 3 Fuel+Gd region.

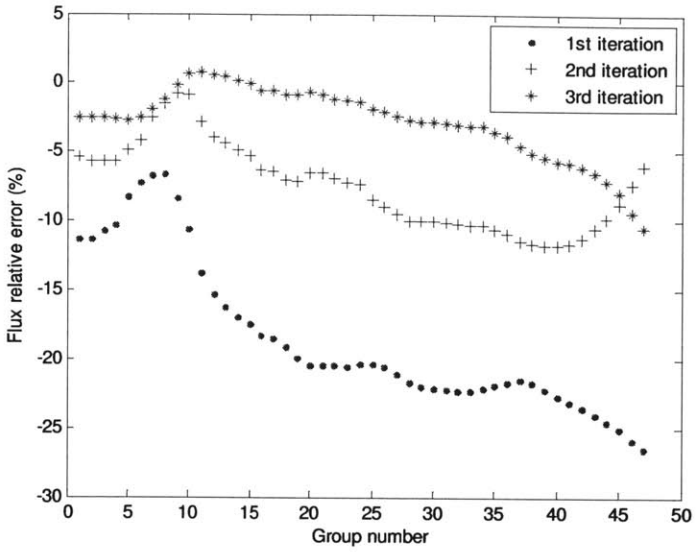

Fig. 4.12 Scalar flux relative error for core 3 Fuel+Gd region.

4.2.2 One dimensional HTR core tests

A 1-D HTR core was also used to benchmark the DGM method and is illustrated in Fig. 4.13. Graphite reactors in general usually have very strong spectral shifts for which the DGM method seems particularly well suited. The 1D core is composed of 6 regions with widths presented in Table 4.5. A reflective boundary condition is set on the left and vacuum boundary condition on the right. A 295 group cross section library with 95 upscattering groups was used [Ortensi 2010]. The 295 group macroscopic cross sections were homogenized within each region using the Dragon code.

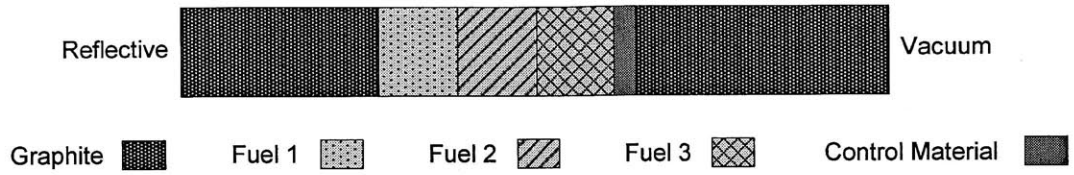

Fig. 4.13 1-D HTR core configuration.

Table 4.5 1-D HTR core configuration.

Region	1	2	3	4	5	6
Material	graphite	fuel 1	fuel 2	fuel 3	control material	graphite
Width (cm)	90	36	36	36	10	116

Although the multi-level approach dominates LWR calculations, it does not work readily for the HTR, and the initial guess of the HTR core calculation cannot be from infinite lattice calculations. Current techniques resort to mini-cores or multi-assemblies calculations to generate accurate cross-sections [Kim 2007], which can become quite cumbersome. The DGM recondensation approach can eliminate this complexity by using an arbitrary initial guess and converging on the cross-sections at the core level. In this section, the initial guess was selected as a fine group whole core power iteration with 5 outer iterations.

For this benchmark, a comparison is made between the 295 fine group reference solution and the 10 group DGM recondensation calculation. The expansion order within each coarse group is 29 for the first nine groups (30 fine groups) and 24 for the 10^{th} group (25 fine groups). A S_8 angular approximation is applied and the step difference

approximation is used spatially. In the power iterations and fixed source iterations, the scalar flux is converged to 10^{-5}. The maximum number of inner iteration for the within group solver is 20. The eigenvalue is converged to 10^{-6}. The recondensation process is terminated when the *mre* error between two consecutive DGM iterations is less than 10^{-5}. Both isotropic scattering and anisotropic scattering tests are performed.

(a) Isotropic scattering

Tables 4.6-4.7 list the computational results of this 1-D HTR test. The fine group calculation takes about 9 minutes and 1,327,128 transport sweeps to converge. The recondensation algorithm is converged after 11 DGM iterations on the *mre*. After 11 DGM iterations, the *rms* and *mre* errors of scalar flux compared to the reference are 0.18% and 0.049%, respectively, and the error of eigenvalue is 37*pcm*.

Computational time and number of transport sweeps of the recondensation calculation are much smaller than those of fine group solution. The fine group calculation takes 1,327,128 transport sweeps to converge while the DGM iteration takes only 167,208 transport sweeps after 11 DGM iterations.

Table 4.6 1D HTR errors in fluxes

	rms (%)*	*mre* (%)*	*rms (%)*	*mre (%)*
1st iteration	-	-	19	3.7
2nd iteration	6.9	2.3	5.4	1.4
3rd iteration	2.6	0.84	1.8	0.57
11th iteration	0.014	**0.00070**	0.18	0.049

Note: Errors with * are between two consecutive iterations of DGM solution.
Errors without * are between DGM solution and reference solution.

Table 4.7 1D HTR eigenvalue and computational time

	Eigenvalue *k*	*Δk (pcm)*	Computation time (min)	Number of transport sweeps
1st iteration	1.076893	1473	@1	@67,440
2nd iteration	1.087591	403	1	87,627
3rd iteration	1.090606	101	1	104,956
11th iteration	1.091250	37	1	167,208
Reference solution	1.091623	-	9	1,327,128

@ Includes the time and number of transport sweeps of 5 fine group outer iterations for the initial guess.

Figs. 4.14 and 4.15 plot the scalar flux *mre* errors and eigenvalue relative errors as a function of the number of DGM iterations. It can be observed that about 8 DGM iterations errors compared to the reference solution stop decreasing, which means that more DGM iterations do not gain accuracy.

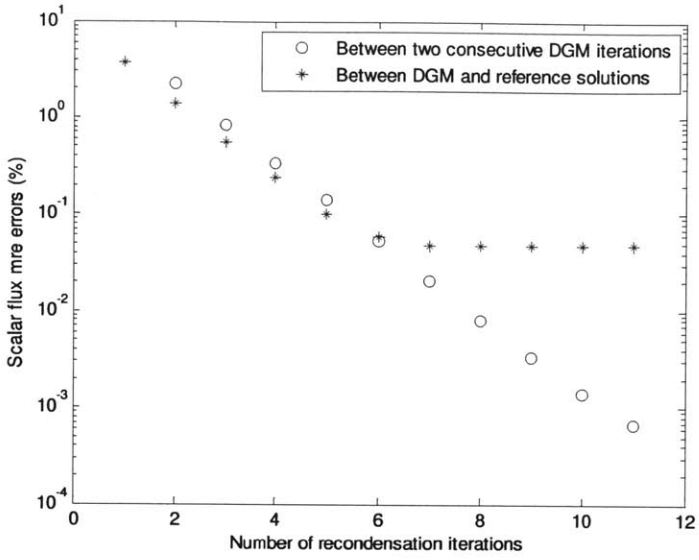

Fig. 4.14 Scalar flux *mre* errors.

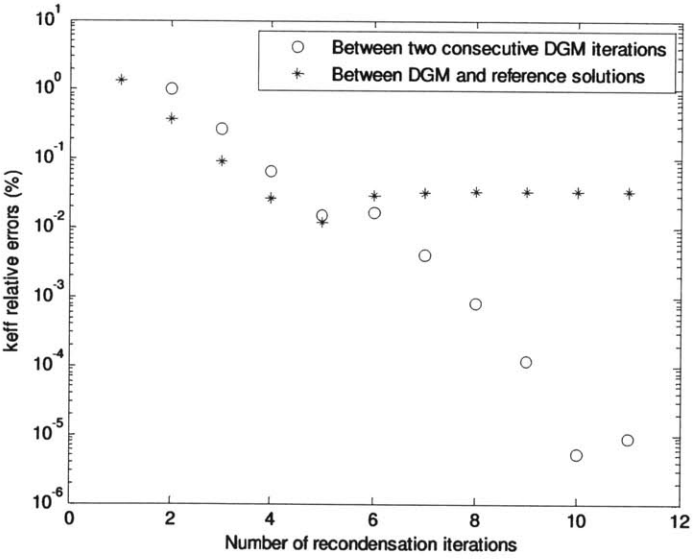

Fig. 4.15 Eigenvalue relative errors.

Fig. 4.16 plots the average scalar flux on the Graphite/Fuel 1 interface in thermal groups as a function of group numbers. This figure illustrates clearly the spectral shift at the boundary of the inner reflector.

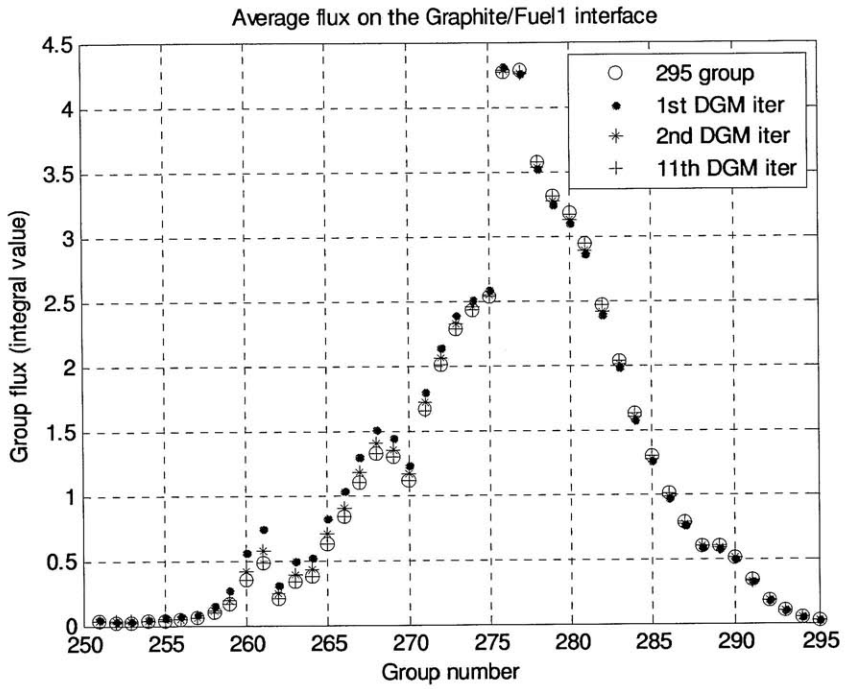

Fig. 4.16 Average flux on the Graphite/Fuel 1 interface (thermal groups).

For a better understanding of the spectral behavior of this benchmark, the flux is plotted as a function of energy and space in in Fig. 4.17. It can be observed that in Fuel 1 near the graphite region, there is a thermal flux peak. The reason is that neutrons are well thermalized in the graphite and cannot leak out the reflective boundary on the left. Thermal neutrons come back in the fuel to cause fission, creating fast neutrons that leak back to the reflector. This strong spectral effect is similar to that of a LWR near a reflector, but the long mean free paths of neutrons in graphite distributes the reflector

impact to more of the core. The DGM recondensation approach is able to "correct" the coarse group cross-sections to account for this effect.

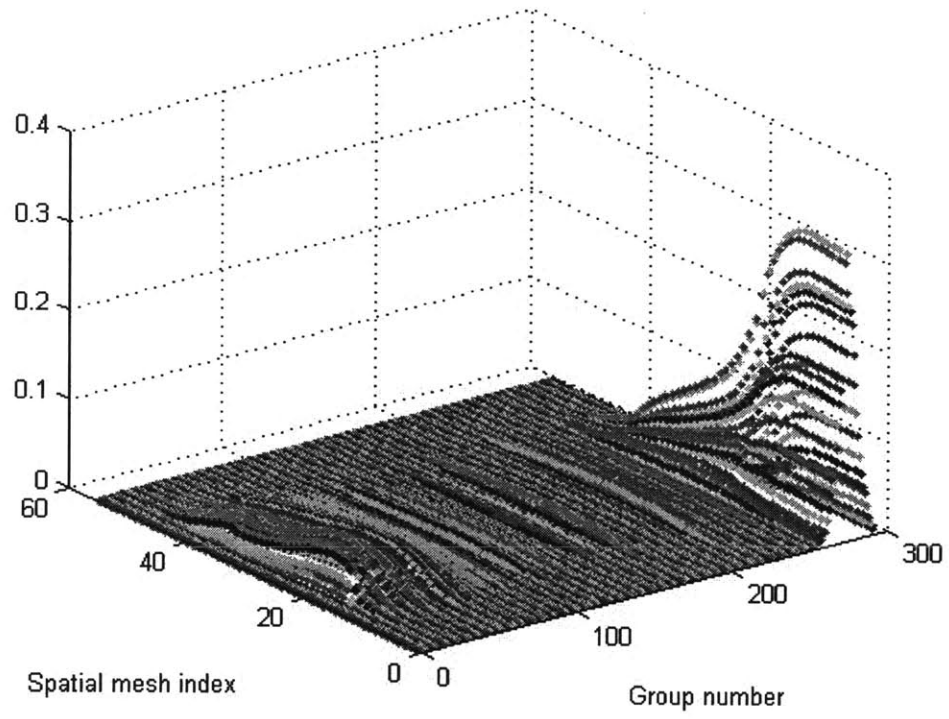

Fig. 4.17 Scalar flux 295 group solution on full space and energy mesh.

It can also be observed that there is a large region of very low flux values in the large graphite region, as well as in the control material region. These near zero fluxes are the main reason why the *rms* and *mre* errors still seem high (0.18% and 0.049%, respectively). If we only look at the fuel region, the scalar flux *rms* and *mre* errors compared to the reference are 0.051% and 0.033%, respectively. The *rms* errors in the fuel region are almost one order of magnitude smaller than that of the whole geometry.

Figs. 4.18 and 4.19 show the relative error of fission rate and absorption rate for the first 3 DGM iterations compared to the reference solution. It can be observed that the relative error of the absorption rate is very large in the outer graphite region in the first iteration. All the errors are reduced substantially with only a few DGM iterations.

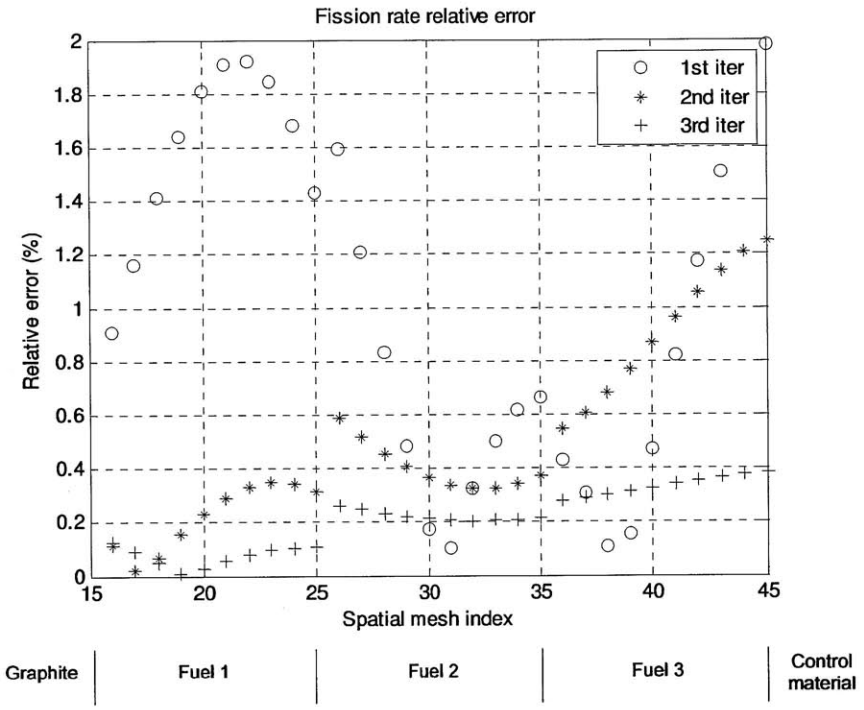

Fig. 4.18 Fission rate relative error in the first 3 DGM iterations.

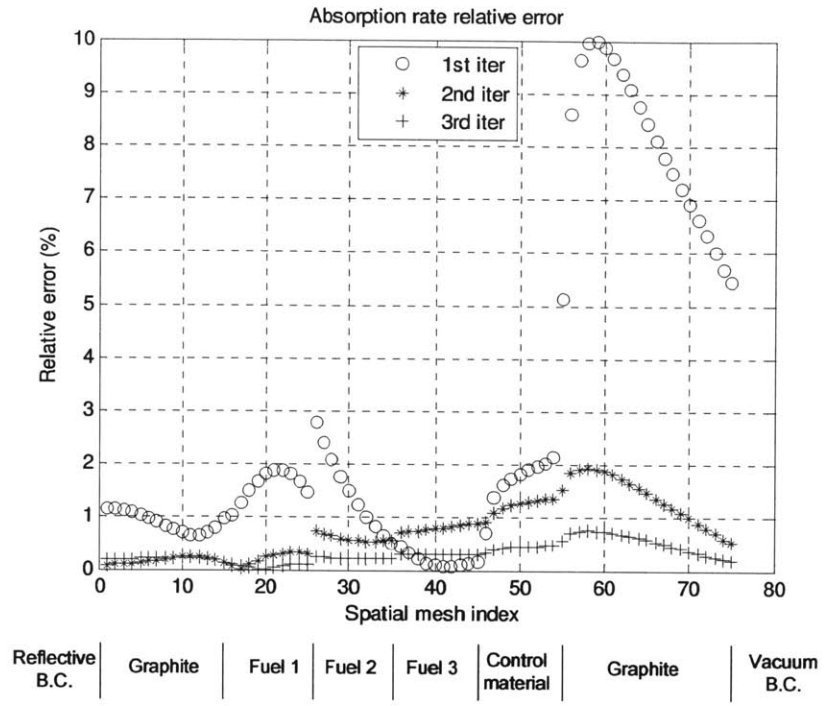

Fig. 4.19 Absorption rate relative error in the first 3 DGM iterations.

Figs. 4.20-4.25 show spatial distributions of selected group fluxes ranging from fast to thermal ranges. All these figures illustrate the substantial reduction of errors that occurs between the 1st and 2nd iteration. After 11 iterations, the fluxes converge to the fine group reference solution.

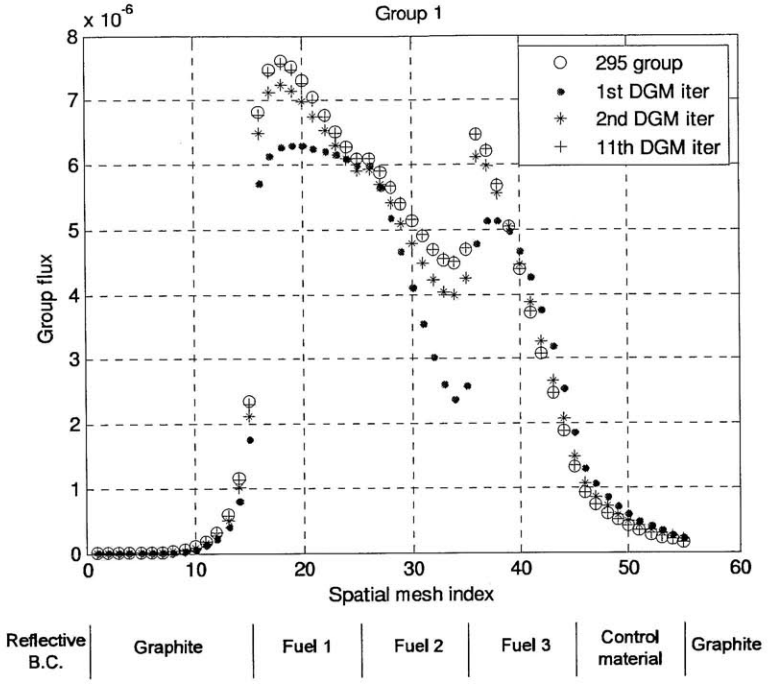

Fig. 4.20 Group 1 flux spatial distribution.

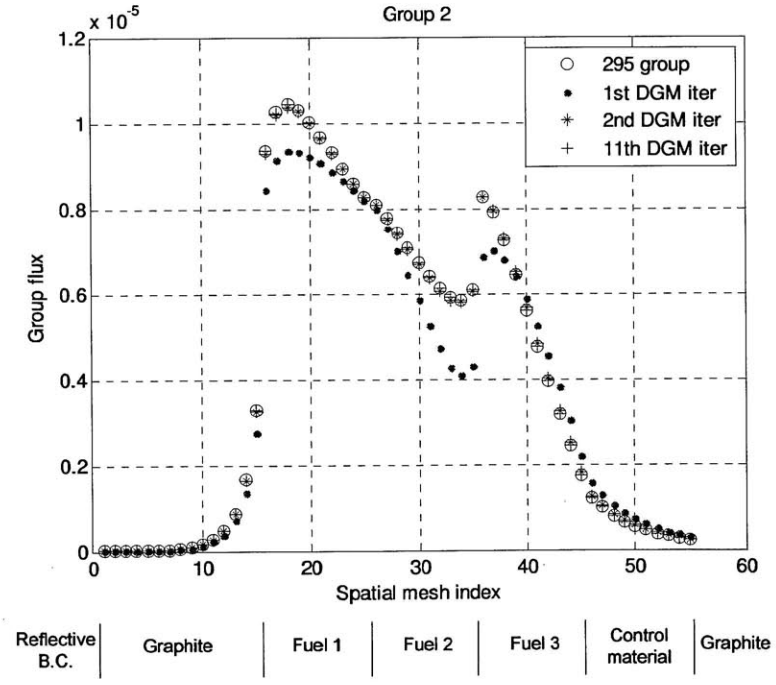

Fig. 4.21 Group 2 flux spatial distribution.

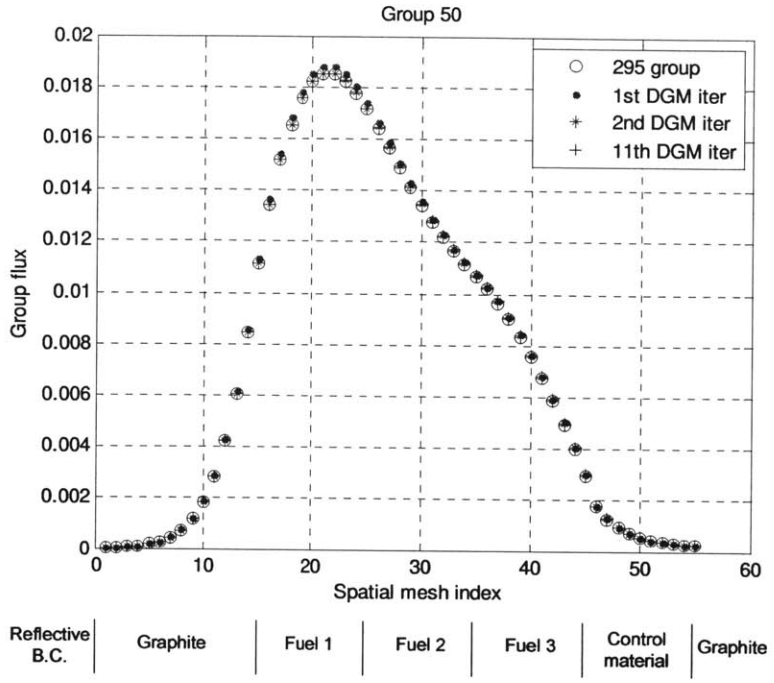

Fig. 4.22 Group 50 flux spatial distribution.

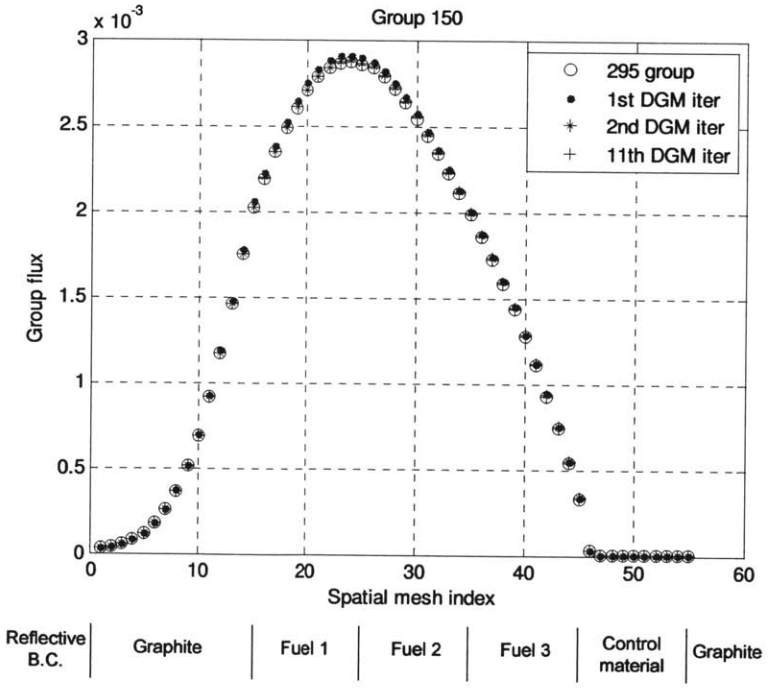

Fig. 4.23 Group 150 flux spatial distribution.

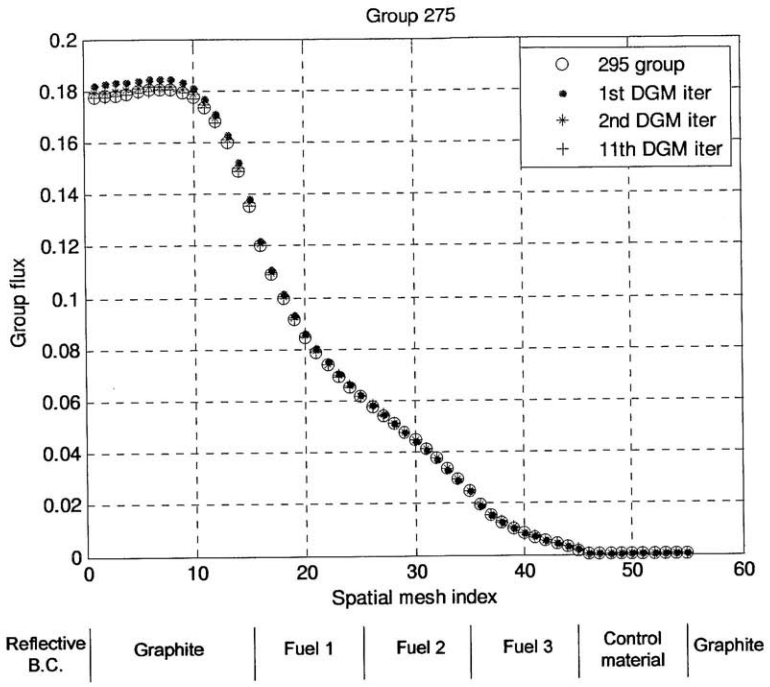

Fig. 4.24 Group 275 flux spatial distribution.

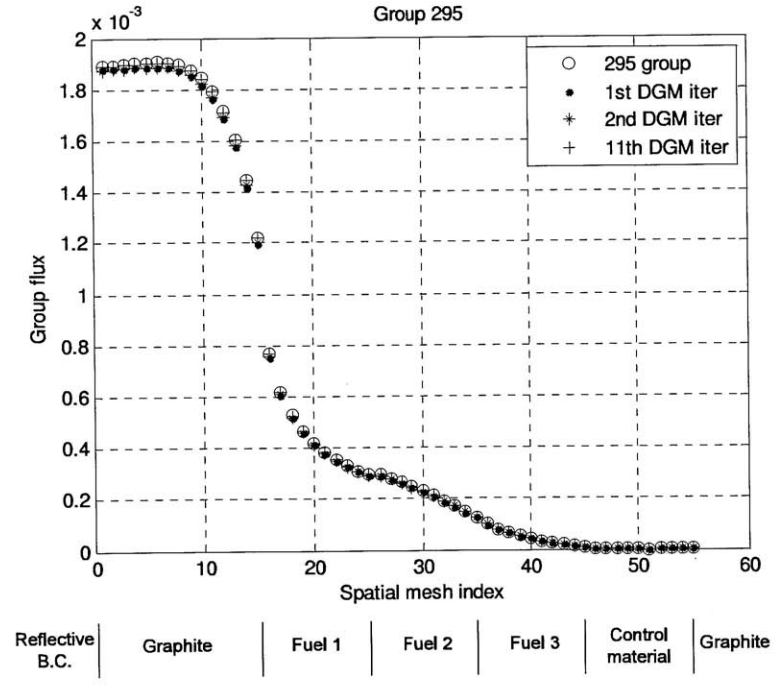

Fig. 4.25 Group 295 flux spatial distribution.

(b) Anisotropic scattering

The same benchmark was also used to illustrate the capability of handling anisotropic scattering based on the following discrete-ordinates equation:

$$\mu \frac{\partial \psi_{ig}(x,\mu)}{\partial x} + \sigma_{t,0g}(x)\psi_{ig}(x,\mu) + \delta_{ig}(x,\mu)\psi_{0g}(x,\mu) = \sum_{g'=1}^{G}\sum_{l=0}^{1} \frac{2l+1}{2}\sigma_{s,l,i,g'\to g}(x)\phi_{l,g'}(x) + \frac{\chi_{ig}(x)}{2k}\sum_{g'=1}^{G}\nu\sigma_{f,g'}(x)\phi_{g'}(x). \tag{4.6}$$

Spatial, angular and energy discretizations, initial guess and boundary conditions are the same as the isotropic scattering test. Convergence is applied to the angular flux instead of the scalar flux.

Tables 4.8-4.9 list the computational results of this 1-D HTR test. The fine group calculation takes about 59 minutes and 1,908,551 transport sweeps to converge. The recondensation process reaches the convergence criterion after 11 DGM iterations, after which the *rms* and *mre* errors of scalar flux are 0.39% and 0.14%, respectively. In the fuel regions, scalar flux *rms* and *mre* errors are 0.13% and 0.087% which are smaller than the errors over the whole geometry. Note that the errors after convergence of recondensation are all about twice as large as their counterpart in the isotropic scattering test.

Similar to the isotropic scattering test, computational time and number of transport sweeps are much smaller than those of fine group calculations, as indicated in Table 4.9.

Table 4.8 1D HTR (anisotropic) errors in fluxes.

	rms (%)*	*mre* (%)*	*rms (%)*	*mre (%)*
1st iteration	-	-	18	3.6
2nd iteration	7.2	2.8	5.2	1.4
3rd iteration	2.5	0.81	1.8	0.62
11th iteration	0.0083	**0.00077**	0.39	0.14

Note: Errors with * are between two consecutive iterations of DGM solution.
Errors without * are between DGM solution and reference solution.

Table 4.9 1D HTR (anisotropic) eigenvalue and computational time

	Eigenvalue *k*	*Δk (pcm)*	Computation time (min)	Number of transport sweeps
1st iteration	1.078179	998	@1	@64,554
2nd iteration	1.084227	393	1	70,304
3rd iteration	1.086580	158	1	82,088
11th iteration	1.087184	98	1	107,387
Reference solution	1.088164	-	59	1,908,551

@ Includes the time and number of transport sweeps of 5 fine group outer iterations for the initial guess.

Figs. 4.26 and 4.27 plot the scalar flux *rms* relative errors and eigenvalue relative errors as a function of number of DGM iterations. After 6 DGM iterations, errors compared to the reference solution stop decreasing.

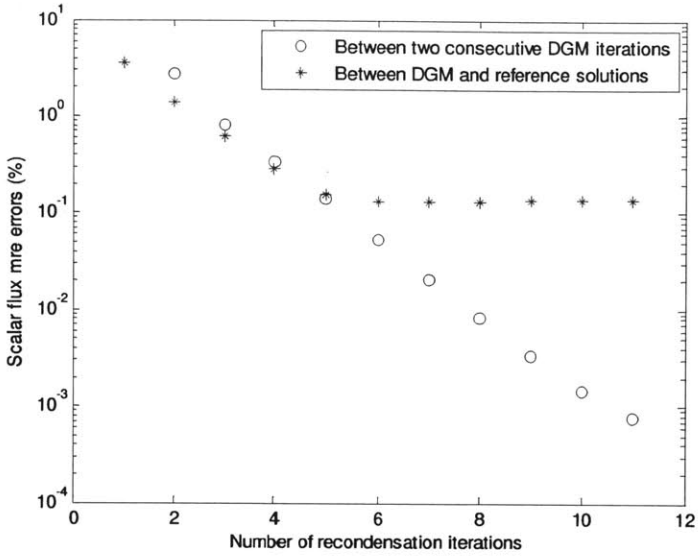

Fig. 4.26 Scalar flux *mre* errors.

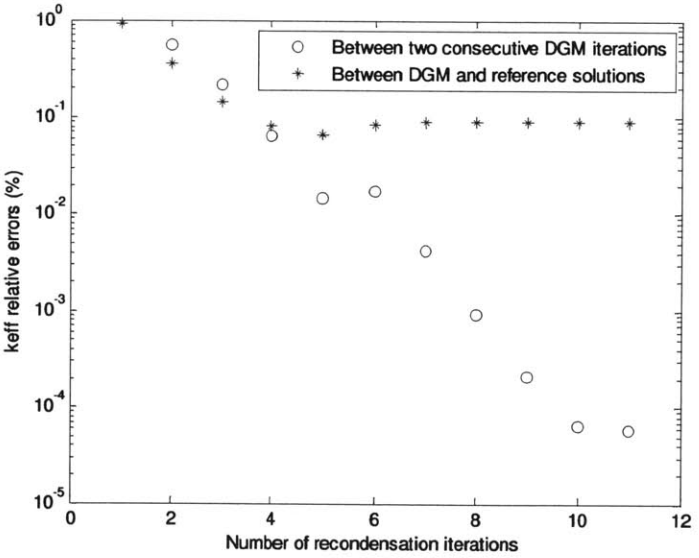

Fig. 4.27 Eigenvalue relative errors.

4.2.3 Two dimensional PWR core tests

For a better assessment of the performance of the recondensation algorithm, a more realistic 2-D PWR problem is tested in this section. The geometry and boundary conditions are similar to the C5G7 benchmark problem [Lewis 2001], and the core layouts are plotted in Figs. 4.28 and 4.29. No spatial homogenization is performed in this test. The circle fuel pin geometry is approximated in Cartesian geometry as indicated by the ORNL and GRS participants in [Lewis 2001], and is plotted in Fig. 4.30.

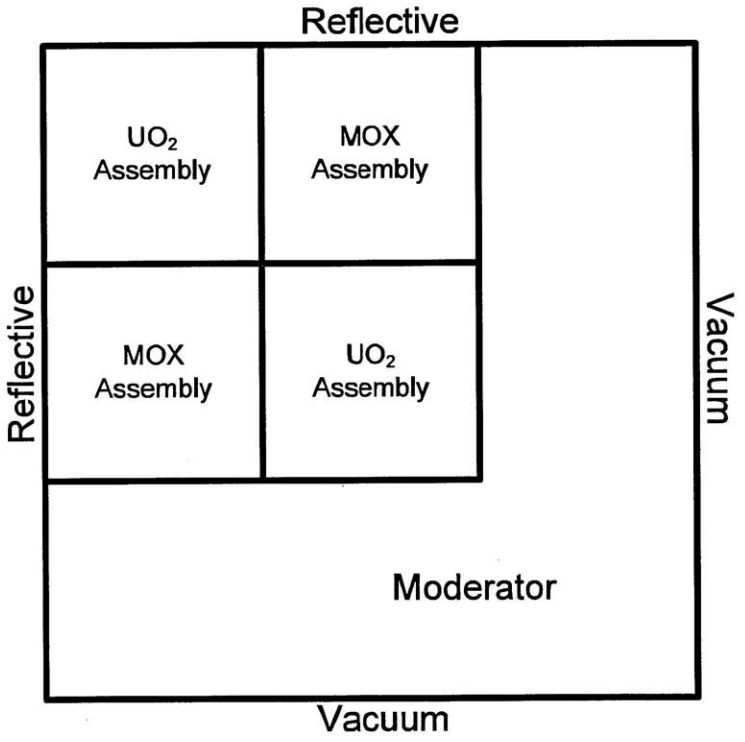

Fig. 4.28. Overview of 2-D PWR core configuration.

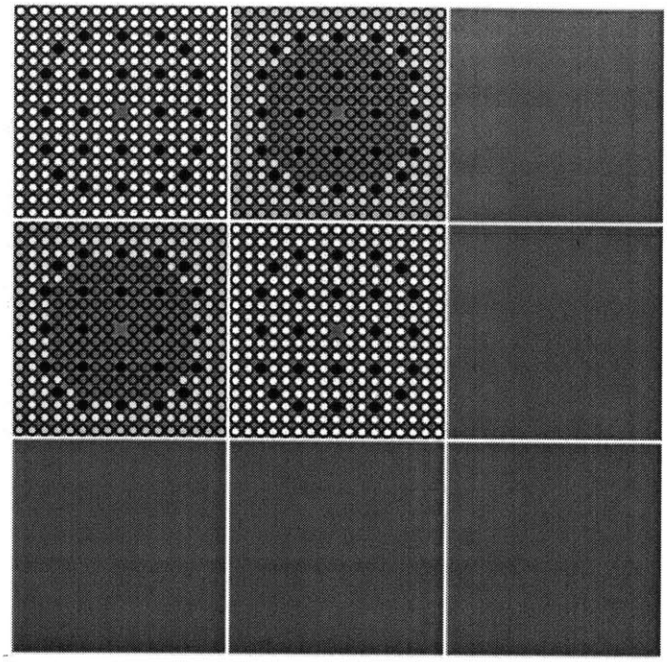

Fig. 4.29 Detailed 2-D PWR core configuration.

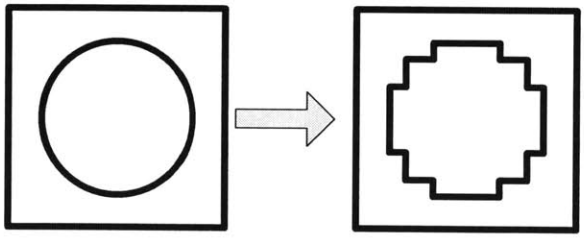

Fig. 4.30 Fuel pin approximation in Cartesian geometry.

Instead of the 7 group cross-section database, a 70 group self-shielded library was generated for both UO_2 and MOX fuels using DRAGON [Hébert 2006]. This 70 group database has 44 upscatter groups. A comparison is made between 70 group reference solutions for the 2-D cores with a 3 group DGM calculation. The numbers of fine groups within each coarse group are 26, 20, and 24, respectively.

A S_8 angular approximation is applied and the step difference method is again used for the spatial sweep. Both the reference and DGM calculations are performed using the same spatial mesh. Scalar flux is converged to within 10^{-5}, and the eigenvalue is converged to within 10^{-6} in the power iterations. Like the standard multi-level approach for LWRs, the initial flux spectrum guess is obtained from infinite assembly fine group calculations for both the UO_2 and MOX assemblies. Flux updates are performed at each iteration to eliminate all possible negative values in the unfolded fluxes, as was done in the 1-D tests.

Results are provided in Tables 4.10-4.11. Table 4.10 lists the *rms* and *mre* errors of the flux compared to the fine group solution, and the *rms** and *mre** error between two consecutive DGM iterations. The recondensation process converges after 14 and 20 iterations, respectively when *mre** and *rms** between two consecutive iterations are smaller than 10^{-5} (0.001%).

It can be observed that *rms* and *mre* errors (compared with the reference solution) decrease from 33% and 4.8% to 7.5% and 0.39%, respectively, after 3 iterations; to 0.039% and 0.0025% after 13 iterations; to 0.012% and 0.0024% after 20 iterations. *mre* errors are typically smaller than *rms* error which indicates that larger errors mainly exist in areas with near zero fluxes.

Table 4.10 70 group 2-D PWR core errors in fluxes.

	rms (%)*	*rms (%)*	*mre* (%)*	*mre (%)*
1st iteration	-	33	-	4.8
2nd iteration	45	15	5.2	0.91
3rd iteration	25	7.5	0.62	0.39
4th iteration	8.7	3.2	0.26	0.16
13th iteration	0.033	0.039	**0.00069**	0.0025
20th iteration	**0.00078**	0.012	0.000049	0.0024

Table 4.11 lists the root-mean-square error (*rms*), mean relative error (*mre*), and maximum relative error (err_{max}) of the pin fission densities compared to the fine group solution, where the pin fission densities are defined as:

$$P = \sum_{j=1}^{J_{pin}} \sum_{i=1}^{I_{pin}} \sum_{h=1}^{H} \phi(i,j,h)\sigma_f(i,j,h), \tag{4.7}$$

where I_{pin}, J_{pin} and H are number of spatial meshes in x and y directions in a pin, and number of fine groups, respectively. The definition of the *rms* error, *mre* error and relative error are the same as for the flux errors as in Appendix D except that the spatial mesh index is replaced by the fuel pin index. The err_{max} is the maximum of the relative error in absolute value of all the pins.

Errors of *rms*, *mre* and err_{max} in the first iteration are 4.9%, 3.9% and 16.0%, respectively, while they decrease to 0.65%, 0.32% and 2.2% after 3 iterations; to 0.0031%, 0.0018%

and 0.015% after 13 iterations; to 0.0035%, 0.0021% and 0.014% after 20 iterations. Once again, the *mre* error is smaller than *rms* error in each iteration, indicating that larger errors are located in pins with low fission densities.

Table 4.11 70 group 2-D PWR core errors in fission density.

	rms (%)	*mre (%)*	err_{max} *(%)*
1st iteration	4.9	3.9	16.0
2nd iteration	1.0	0.59	3.4
3rd iteration	0.65	0.32	2.2
4th iteration	0.37	0.15	0.8
13th iteration	0.0031	0.0018	0.015
20th iteration	0.0035	0.0021	0.014

Table 4.12 lists the eigenvalues, eigenvalue errors, computational time and number of transport sweeps. RE_k* is the relative error between two consecutive DGM iterations and RE_k is the relative error between DGM and fine group solutions.

The computational time of the fine group reference calculation is about 1038 minutes, while the recondensation calculation takes about 198 minutes after 13 iterations plus an additional 44 minutes for assembly calculations (initial guess). The total time after 13 iterations is much less than that of the fine group calculation and provides accuracy comparable to the convergence criteria. The number of core level transport sweeps is

145,315 with the fine group calculation and 20,503 after 13 iterations for the DGM recondensation.

Table 4.12 70 group 2-D PWR core computational results.

	Eigenvalue k	Δk *(pcm)*	Computational time (min)	Number of core transport sweeps
1st iteration	1.218178	1797	53	6,644
2nd iteration	1.198270	194	88	10,123
3rd iteration	1.200664	45	110	11,773
4th iteration	1.200311	10	127	13,229
13th iteration	1.200209	0.0	198	20,503
20th iteration	1.200212	0.3	247	23,646
Reference solution	1.200209	-	1038	145,315

Assembly calculations take an extra 44min, not included in the table.

Figs. 4.31 and 4.32 plot the errors on flux and eigenvalue as a function of the number of iterations. After about 14-15 iterations, the flux *rms* relative error stops decreasing which is consistent with Tables 4.10-4.12 that after about 13 iterations no substantial gain in accuracy is observed. Thus *mre** between to consecutive DGM iterations is a good convergence criteria.

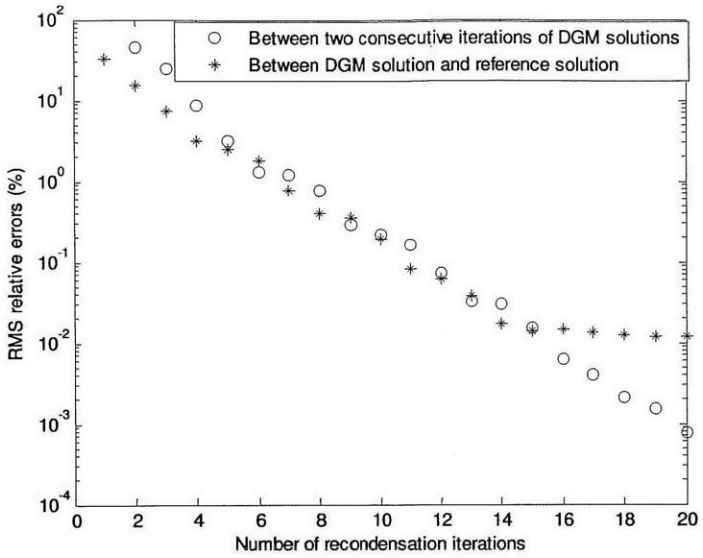

Fig. 4.31 Scalar flux *rms* relative errors of 70 group 2-D PWR core.

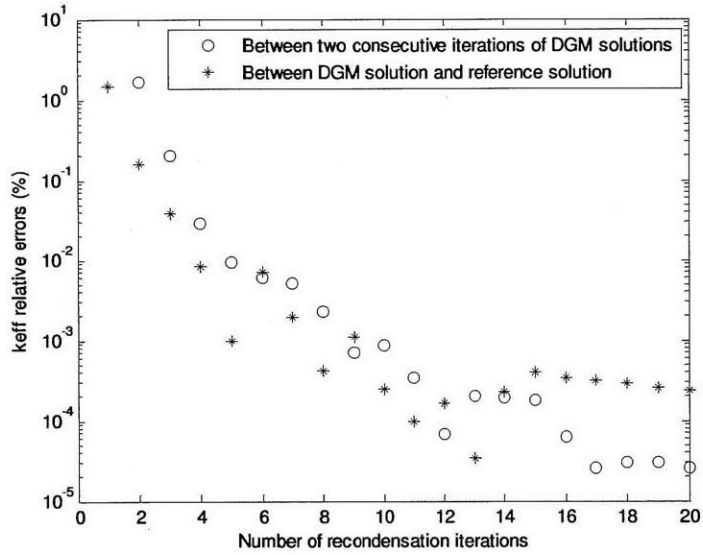

Fig. 4.32 Eigenvalue relative errors of 70 group 2-D PWR core.

Figs. 4.33-4.38 plot the relative error of fission density compared with the reference solution, for the 1st, 2nd, 3rd, 4th and 13th iterations of the DGM calculations, respectively. The data in Fig. 4.33 shows that large errors of fission density exist near the interface of fuel assemblies and moderator regions, as well as near the interface of UO_2 and MOX assemblies. This is due to the fact that the cross section moments are generated using infinite assembly fine group solutions as the weighting flux, thus neglecting the neighboring effect between different assemblies and near the reflector. Since the flux used to generate cross section moments for the 2nd iteration comes from the first iteration solution which is a core level solution, errors near assembly interfaces are reduced substantially, which is shown in Fig. 4.34. After 13 iterations, the errors become quite small throughout the core as is shown in Fig. 4.37.

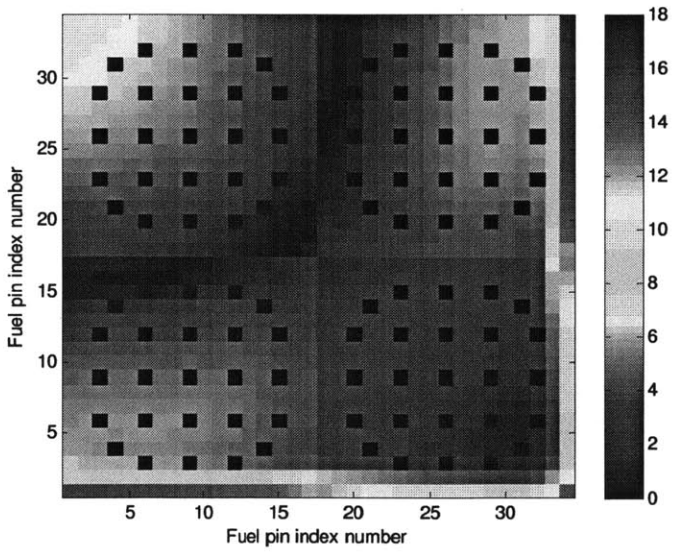

Fig. 4.33. Fission density relative error (%) for 1st DGM iteration.

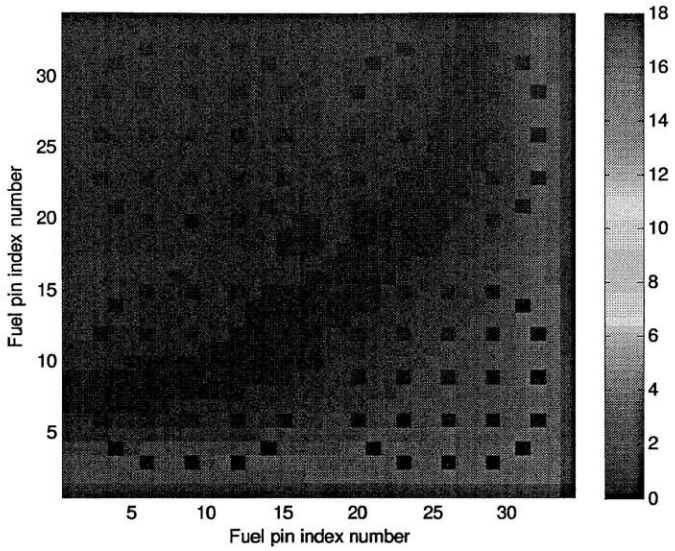

Fig. 4.34. Fission density relative error (%) for 2nd DGM iteration.

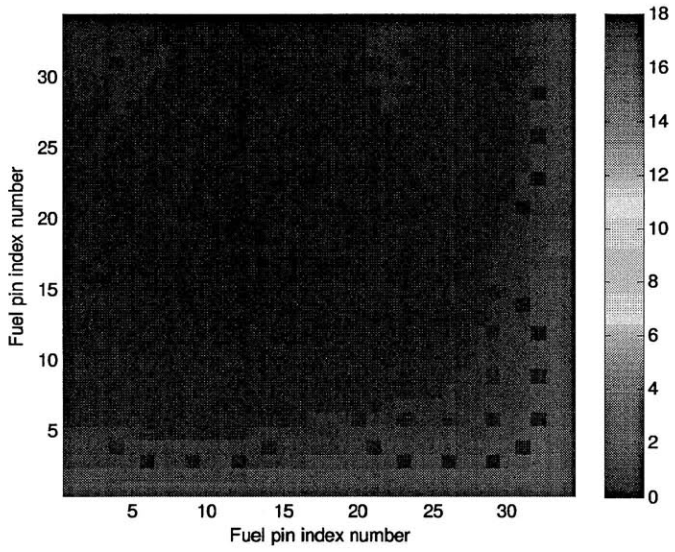

Fig. 4.35. Fission density relative error (%) for 3rd DGM iteration.

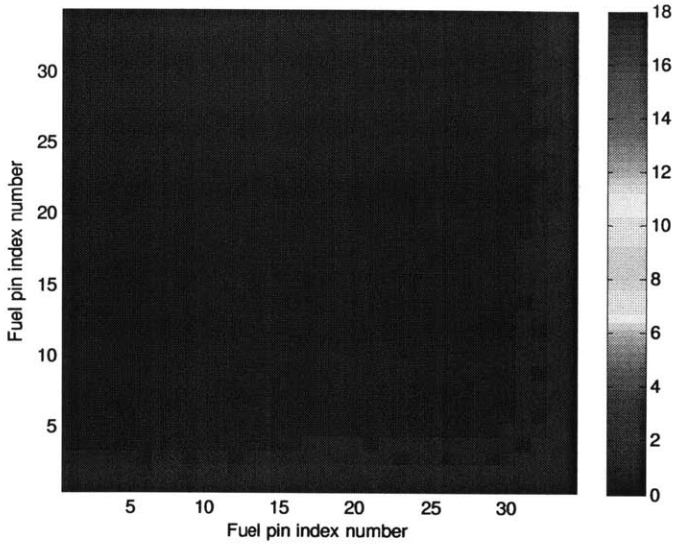

Fig. 4.36. Fission density relative error (%) for 4th DGM iteration.

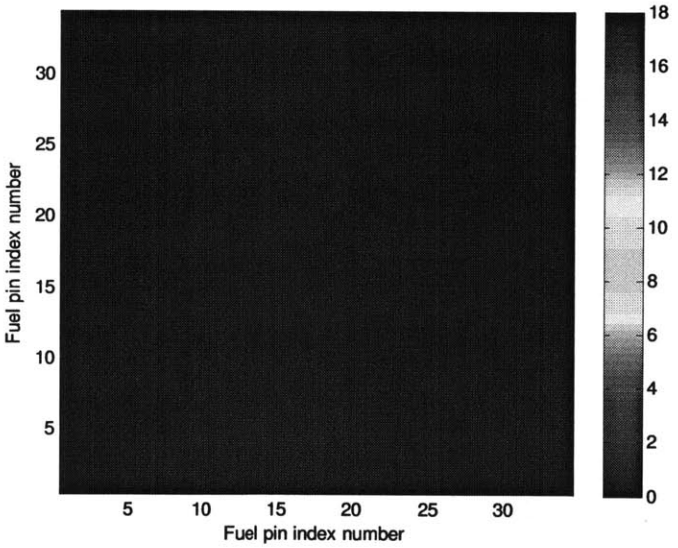

Fig. 4.37. Fission density relative error (%) for 13th DGM iteration.

From the above results, it can be concluded that the energy recondensation method has an advantage over the traditional energy condensation in core level calculations. With the traditional multilevel approach, errors in coarse group solutions are on the order of those of the 1st DGM iteration. The DGM iterations improve the coarse group parameters and provide accuracy similar to the fine group results. After only 3 iterations, *rms* and *mre* errors of fission density are reduced to 0.65% and 0.32%, respectively. Thus, energy recondensation provides a way to performed core level transport calculation with reasonable accuracy and relatively small computational cost.

4.2.4 Two dimensional HTR core tests

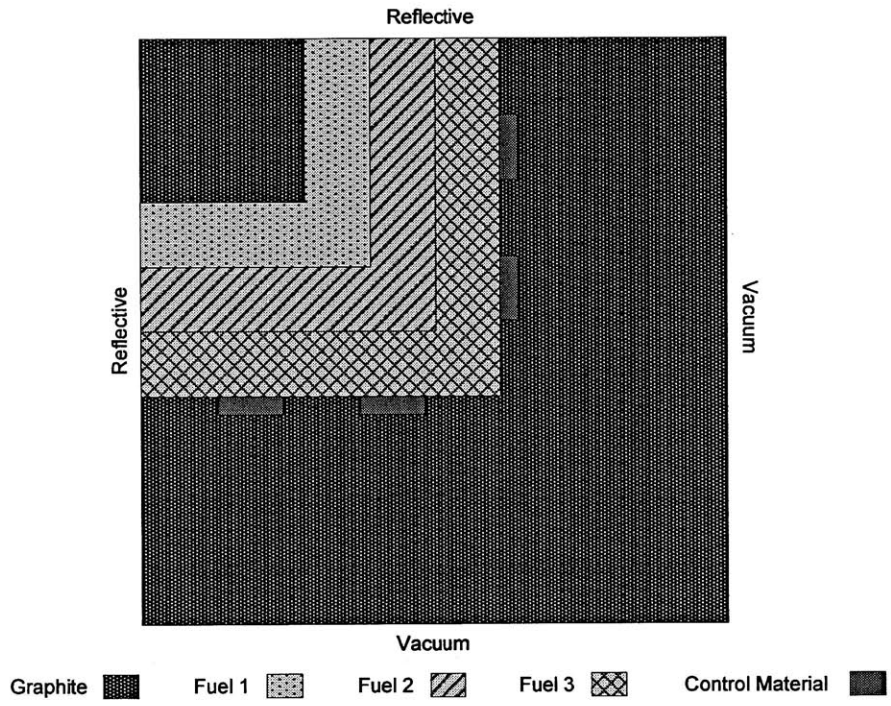

Fig. 4.38 2-D HTR core configuration.

For an additional assessment of the performance of the recondensation algorithm, a 2-D HTR core is tested in this section, which is illustrated in Fig. 4.38. The material composition for the graphite, fuel and control material are taken from the 1-D HTR core in Section 4.2.2. The top and left boundary condition is reflective and the right and bottom is vacuum. The fine group cross-section database is a 26 group library condensed from the 295 group library of the 1D HTR benchmark This 26 group library has 12 upscatter groups.

The initial flux guess is from a fine group whole core calculation with 5 outer iterations. A comparison is made between the 26 group reference solution and a 4 group DGM calculation. Within each coarse group the number of fine groups are 7, 7, 6, 6, respectively.

A S_8 angular approximation is applied and the step difference method is used for the spatial sweep. The scalar flux is converged to within 10^{-5}. The maximum number of inner iteration per outer iteration is 20. The eigenvalue is converged to within 10^{-6}. The recondensation process stops when the *mre** error between two consecutive DGM iterations is less than 10^{-5}.

Tables 4.13 and 4.14 lists the computational results of the 2-D HTR test. The solution converges after 38 DGM iterations. After the first DGM iteration, the *rms* and *mre* errors of the scalar flux and the error of the eigenvalue are 35%, 5.7% and 4140*pcm*, respectively; they decrease after 3 iterations to 19%, 3.3% and 1399*pcm*; and decrease

after 38 iterations to 0.25%, 0.029% and 19*pcm*. Similar to the 1-D HTR tests, the *mre* errors are typically one order of magnitude smaller than *rms* errors. In the fuel region, after 38 DGM iterations the *rms* and *mre* errors are 0.029% and 0.021% which are smaller than the errors on the whole core geometry (especially the *rms* error is much smaller), indicating that larger errors exist in control material and large graphite areas.

The fine group calculation takes a computational time of 191 minutes, and 266,556 core transport sweeps. For the recondensation calculation, it takes 48 minutes and 26,418 iterations after the first DGM iteration; 76 minutes and 44277 iterations after 5 DGM iterations; 114 minutes and 69,831 iterations after 38 DGM iterations.

Table 4.13 26 group 2-D HTR core errors in fluxes.

	rms (%)*	*rms (%)*	*mre* (%)*	*mre (%)*
1st iteration	-	35	-	5.7
2nd iteration	11	25	1.5	4.4
3rd iteration	6.8	19	1.2	3.3
4th iteration	5.1	15	0.85	2.4
5th iteration	4.2	12	0.65	1.8
38th iteration	0.016	0.25	**0.00085**	0.029

Table 4.14 26 group 2-D HTR core computational results.

	Eigenvalue k	Δk *(pcm)*	Computational time (min)	Number of core transport sweeps
1st iteration	1.083428	4140	48	26,418
2nd iteration	1.101021	2381	54	30,348
3rd iteration	1.110843	1399	64	36,804
4th iteration	1.115925	890	70	40,948
5th iteration	1.119024	581	76	44,277
38th iteration	1.124643	19	114	69,831
Reference solution	1.124830	-	191	266,556

Note: computational time and number of core transport sweeps for the initial guess calculation (5 outer iterations of fine group calculations) are included in the 1st iteration.

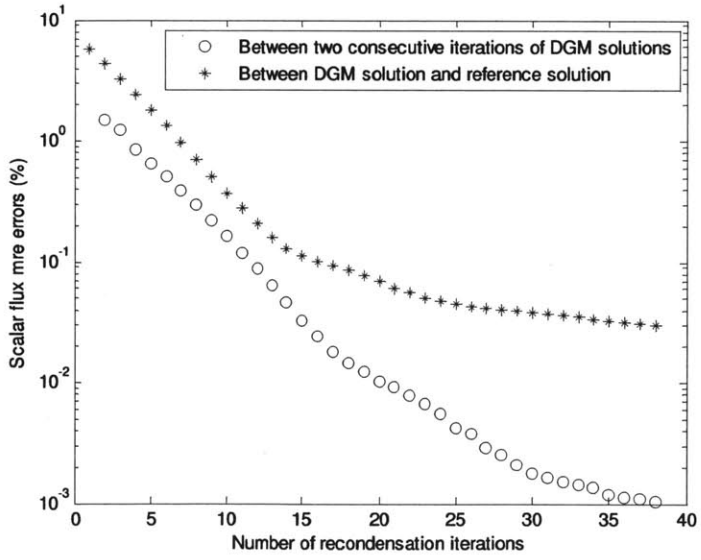

Fig. 4.39 Scalar flux *mre* relative errors of 26 group 2-D HTR core.

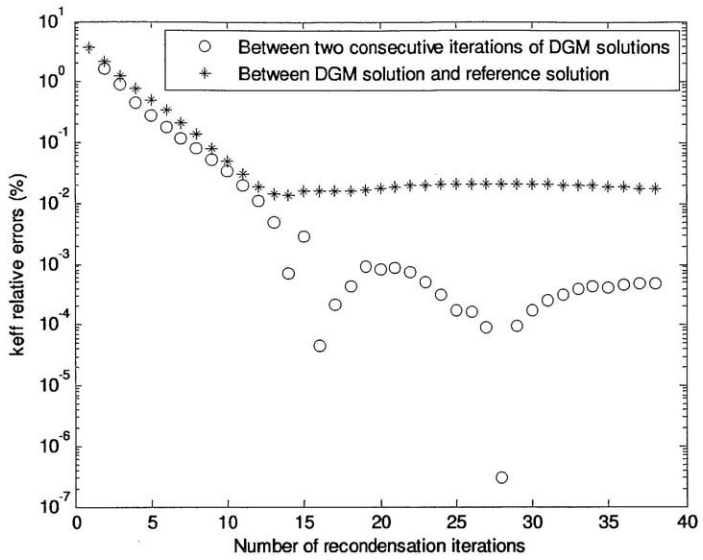

Fig. 4.40 Eigenvalue relative errors of 26 group 2-D HTR core.

Figs. 4.39 and 4.40 plot scalar flux *mre* errors and eigenvalue relative errors as a function of number of iterations. Fig. 4.41 plots the fission density on the spatial mesh from the fine group calculation. It can be observed that the fission density is highest at the interface of the inner graphite region and Fuel 1. This is once again caused by the thermalization of neutrons in the inner graphite region. The thermal neutrons cause fission at the edge of the fuel region which sends more fast neutrons to the inner reflector. At the interface of outer graphite region and Fuel 3, there is no fission density peak due to the presence of control materials.

This higher peaking factor should be suppressed by control materials in the inner graphite region in more realistic designs [Descotes 2011]. This challenging core is a true test for the DGM recondensation method.

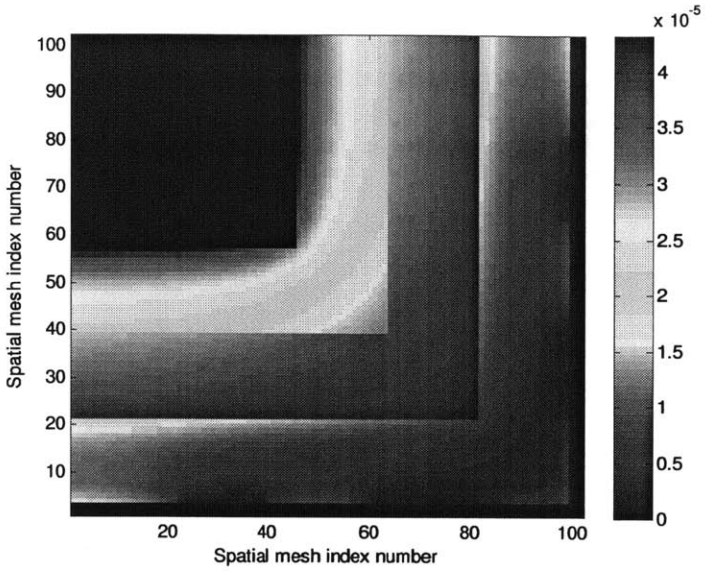

Fig. 4.41 Fission density distribution of 26 group 2-D HTR core.

Figs. 4.42-4.47 plot the fission density relative errors of the DGM calculations compared with the reference solution for the 1st, 2nd, 3rd, 4th, 5th, and 36th iterations. In the first iteration, the largest errors exist near the control material regions, which is also the region with the lowest fission density. The control material removes many of the thermal neutrons which creates a flux depression in the thermal range. After a few DGM iterations, the coarse group cross-sections are "corrected" to account for this spectral change. The inner reflector region shows very minimal error, which indicates that the initial guess was sufficient to represent that spectral effect.

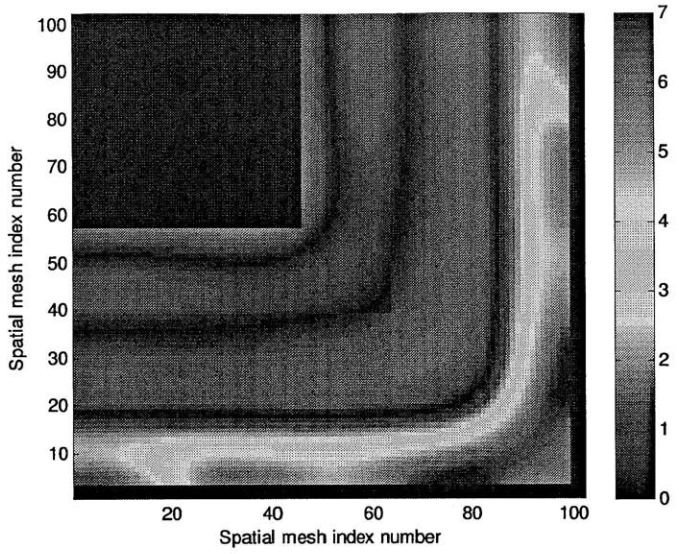

Fig. 4.42 Fission density relative error (%) for 1st DGM iteration.

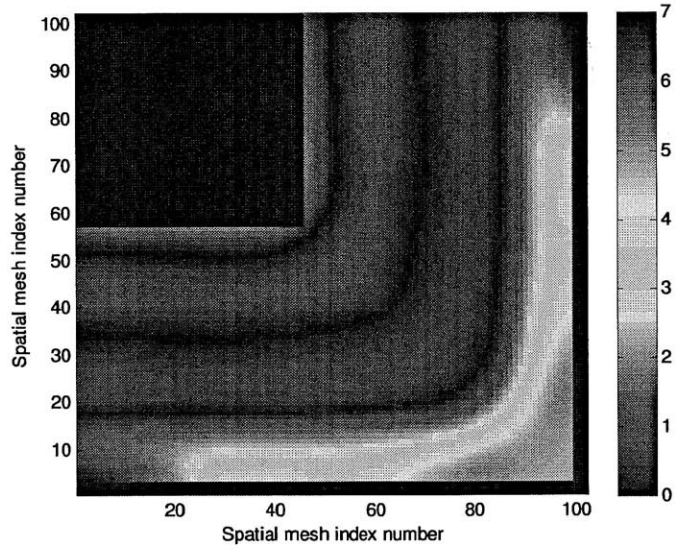

Fig. 4.43 Fission density relative error (%) for 2nd DGM iteration.

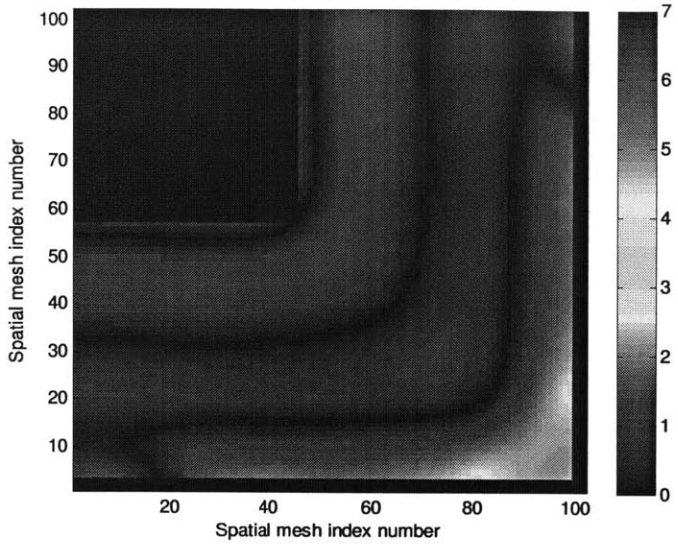

Fig. 4.44 Fission density relative error (%) for 3rd DGM iteration.

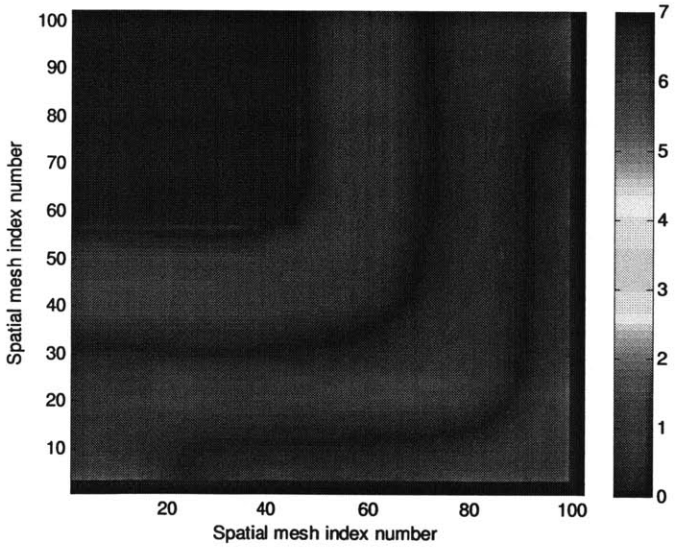

Fig. 4.45 Fission density relative error (%) for 4th DGM iteration.

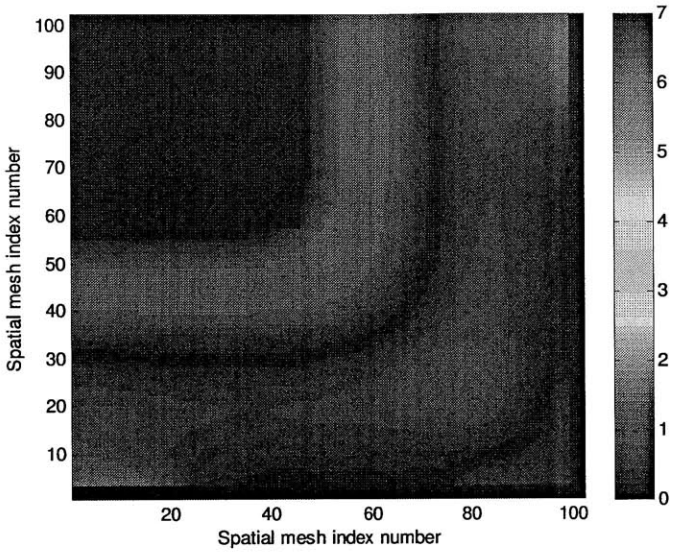

Fig. 4.46 Fission density relative error (%) for 5th DGM iteration.

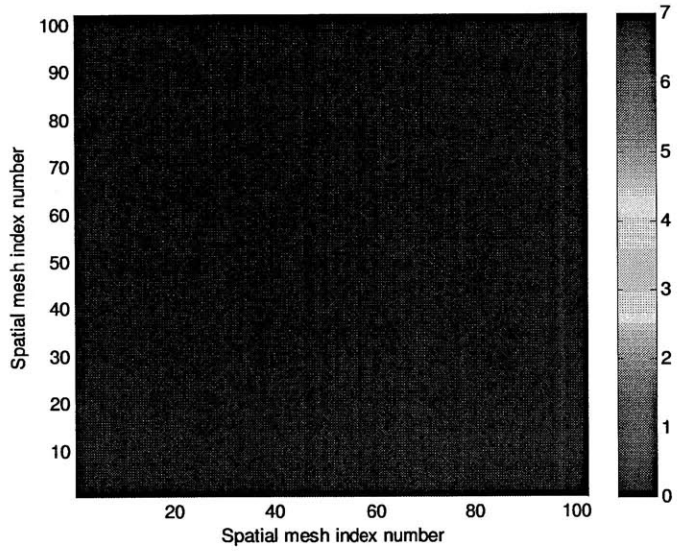

Fig. 4.47 Fission density relative error (%) for 38th DGM iteration.

HTR type reactors are not well-suited for infinite lattice calculation because of the long mean free path of neutrons in graphite. Errors induced by neighboring effect can propagate much longer than in light water reactors. Mini-cores or multiple assemblies set are typically used to define the coarse group cross-sections which are cumbersome. Energy recondensation provides a way to correct the strong spectral shift observed in the core and eliminates the need for complex multilevel processes. Moreover, the above results show that the DGM recondensation method can provide a reasonable approximation compared to the fine group solution for a minimal computational cost.

4.3. More discussions on recondensation

4.3.1 Spatial dependence of the DGM method

All the previous calculations are based on the step difference spatial discretization which assumes a piecewise constant flux over each spatial cell. These results show that the flux can converge to the fine group solution after a certain number of iterations, but unfortunately this is not the case for all spatial discretizations. This section analyzes the spatial consistency of the DGM method and discusses some of its limitations.

The cross sections and moments used in the $(k+1)^{th}$ recondensation iteration calculation are generated using fluxes from the k^{th} iteration. For a fully consistent derivation, the reaction rates from the fine group calculation and the 0^{th} order coarse group solution should be equivalent after the recondensation calculation converges. In Chapter 3, the

DGM method is derived without dependence of a particular spatial discretization. The purpose of the following analysis is to study the effect of spatial discretization on the consistency of the DGM model. An analysis of the fission term follows and similar conclusion can be derived for other terms in the transport equation. The coarse group fission cross section given in Eq. (3.21) can be written as:

$$\nu\sigma_{f,g'}^{k+1}(x)=\frac{\sum_{L=0}^{M-1}\nu\sigma_f(x,L)\phi^k(x,L)}{\sum_{L=0}^{M-1}\phi^k(x,L)}, \tag{4.8}$$

which is the fission cross section energy condensation weighted by the scalar flux. It is assumed that there are M fine group points within coarse group g' with point index $L=0,1,2,...,M-1$. Without loss of generality, spatial dependence is represented in a 1-D Cartesian formalism.

The continuous energy transport equation in Eq. (3.1) is separated into equations within each coarse energy groups. Within a coarse energy group g', if a fine group calculation is performed, the fission rate (neutron production rate) can be expressed as:

$$R_{f,g'}(x)=\sum_{L=0}^{M-1}\nu\sigma_f(x,L)\phi(x,L) \tag{4.9}$$

If a coarse group (or 0^{th} order of DGM) calculation is performed, the fission rate expressed in the coarse group equation is:

$$R_{f,g'}^{k+1}(x) = \nu\sigma_{f,g'}^{k}(x)\phi_{g'}^{k+1}(x) \tag{4.10}$$

where $\phi_{g'}^{k+1}(x)$ is the unknown to be solved in the $(k+1)^{th}$ iteration in the coarse group (0^{th} order) equation. The key point is to verify that the reaction rates in Eqs. (4.9) and (4.10) are equivalent after convergence of the recondensation process, which can be expressed by:

$$\phi^{k}(x,L) = \phi^{k+1}(x,L), \tag{4.11}$$

where $\phi^{k}(x,L)$ is the unfolded scalar flux from the kth iteration of the DGM calculation.

a) Flat-flux approximation

If the spatial dependence is expressed explicitly, it can be observed that the equivalence exists only when the step difference spatial discretization is used. In general, cross sections and moments are collapsed using the cell-averaged flux, e.g., Eq. (4.8) can be written as:

$$\nu\sigma_{f,I,g'}^{k+1} = \frac{\sum_{L=0}^{M-1}\nu\sigma_{f,I}(L)\phi_{I}^{k}(L)}{\sum_{L=0}^{M-1}\phi_{I}^{k}(L)}, \tag{4.12}$$

where I is the spatial cell index, and ϕ_I is the cell-averaged flux. In the step difference method, fluxes are piecewise constant within each spatial cell, e.g., $\phi(x,L)=\phi_I(L)$ in cell I. Thus, Eq. (4.9) can be written as:

$$R_{f,g'}=\sum_{L=0}^{M-1}\nu\sigma_{f,I}(L)\phi_I(L). \tag{4.13}$$

Eq. (4.10) can be written as:

$$R_{f,g'}^{k+1}=\frac{\sum_{L=0}^{M-1}\nu\sigma_{f,I}(L)\phi_I^k(L)}{\sum_{L=0}^{M-1}\phi_I^k(L)}\phi_{g',I}^{k+1}. \tag{4.14}$$

where the coarse group flux can be expressed using fine group fluxes as:

$$\phi_{g',I}^{k+1}=\sum_{L=0}^{M-1}\phi_I^{k+1}(L). \tag{4.15}$$

Eqs. (4.13) and (4.14) should be equivalent which indicates that the reaction rate is conserved, if Eq. (4.11) is satisfied, i.e.,

$$\phi_I^k(L)=\phi_I^{k+1}(L). \tag{4.16}$$

b) Linear-flux approximation

For higher order spatial discretization schemes, e.g., the first order method, the spatial dependence of Eq. (4.9) within a spatial mesh can be written as:

$$R_{f,g'}(x) = \sum_{L=0}^{M-1} \nu\sigma_{f,l}(L)\phi(x,L), \tag{4.17}$$

while the spatial dependence of Eq. (4.10) within a spatial mesh is:

$$R_{f,g'}^{k+1}(x) = \frac{\sum_{L=0}^{M-1} \nu\sigma_{f,l}(L)\phi_l^k(L)}{\sum_{L=0}^{M-1} \phi_l^k(L)} \phi_{g'}^{k+1}(x), \tag{4.18}$$

where the cross section is generated using cell-averaged flux. In this case, the coarse group flux with spatial details within a spatial mesh $\phi_{g'}(x)$ cannot be expressed using fine group fluxes within that coarse group, i.e., an equivalent form of Eq. (4.15) does not exist. By comparing Eqs. (4.17) and (4.18), it can be observed that they will have a different form no matter whether an equivalence of Eq. (4.15) is satisfied, which means that the reaction rate will converge in a different way.

With spatial details within a spatial mesh, other terms have similar inconsistency and thus the recondensation model will generate a solution with a systematic error compared to the fine group solution. Despite this error, the DGM recondensation will still improve the

coarse group results by correcting for local spectral effects, but it will not reproduce the fine group results exactly.

As an example, the 1D BWR (core 1) recondensation test is performed here with the step characteristic spatial discretization method (SC) [Lathrop 1969]. All other conditions of the test are identical to those stated previously.

Results of the DGM recondensation process are given in Tables 4.15 and 4.16. The computational time of the fine group reference calculation is 14 seconds with a total number of transport sweeps of 24,785. The results indicate a reduction in the flux errors over the first few DGM iterations. Convergence on the flux *rms* (10^{-5}) is reached after 29 DGM iterations (8.5*sec*, 9,483 transport sweeps). The *rms* and *mre* errors compared to the reference fine group solution are 0.092% and 0.055%, respectively.

Table 4.15 1-D BWR Core 1 errors in fluxes (step characteristics).

	rms (%)*	*mre* (%)*	*rms (%)*	*mre (%)*
1st iteration	-	-	3.5	1.8
2nd iteration	3.2	1.6	1.1	0.57
3rd iteration	0.8	0.39	0.56	0.27
29th iteration	**0.00074**	0.00022	0.092	0.055

Note: Errors with * are between two consecutive iterations of DGM solution.
Errors without * are between DGM solution and reference solution.

Table 4.16 1-D BWR Core 1 computational results (step characteristics).

	Eigenvalue k	Δk *(pcm)*	Computation time *t (sec)*	Number of transport sweeps
1st iteration	1.167267	1325	0.6	1,835
2nd iteration	1.153637	38	1.0	2,768
3rd iteration	1.154787	77	1.4	3,092
29th iteration	1.153762	26	8.5	9,483
Reference solution	1.154021	-	13.8	24,785

Note: Computational time and number of transport sweeps of assembly calculations are not included. The total computational time for all the 4 assemblies is 3.0sec.

By comparing Tables 4.15-4.16 (SC) to Tables 4.1-4.2 (SD), it can be observed that in the first 3 DGM iterations, errors of the flux and eigenvalue are on the same order when comparing to their respective reference solutions. After 3 DGM iterations, the *rms* and *mre* errors of scalar flux and error in eigenvalue are 0.56%, 0.27% and 77*pcm* with SC; the corresponding errors are 0.56%, 0.28 and 119pcm with SD.

With both SD and SC, it takes 29 DGM iterations to fully converge the flux with the *rms* convergence criterion. However, with SC, the *rms* and *mre* errors of scalar flux and error in eigenvalue are 0.092%, 0.055% and 26*pcm* in the final converged solution, larger than the corresponding values with SD, i.e., 0.016%, 0.012% and 1*pcm*. SD is fully consistent with the DGM method due to the piecewise constant flux within each spatial mesh, as analyzed in this section.

Scalar flux *rms* relative errors and eigenvalue relative errors are plotted in Figs. 4.48 and 4.49 for both SC and SD. It can be observed that the *rms* errors of the scalar flux show a smoother convergence trend than the relative errors of the eigenvalue. For SC, after about 13 iterations errors in recondensation result stop decreasing.

Although the SC is not fully consistent with the DGM method, it can be observed that the recondensation methodology still provides a substantial improvement in the coarse group parameters with only a few DGM iterations.

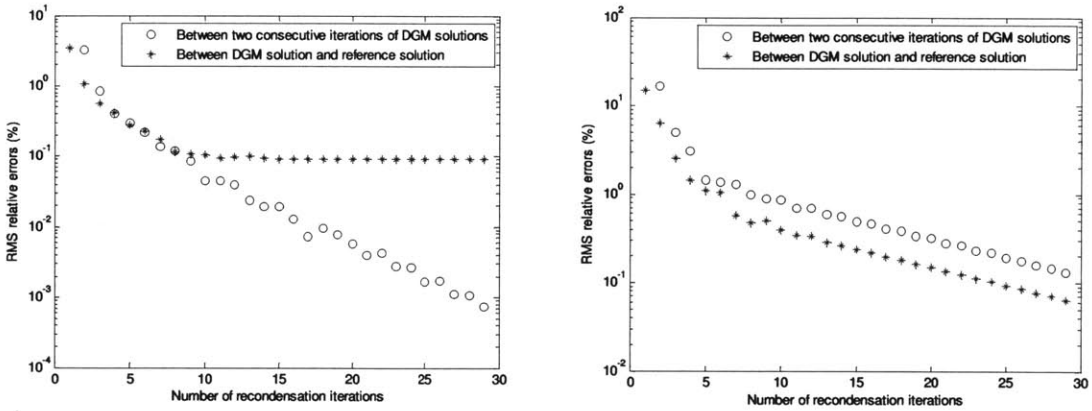

Fig. 4.48 Scalar flux *rms* relative errors of 1-D BWR core 1 (SC vs. SD).

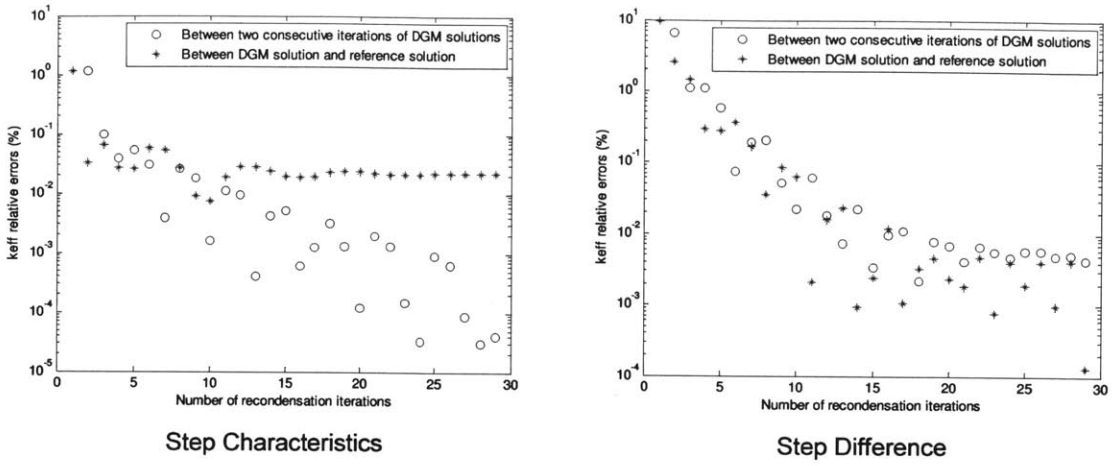

Fig. 4.49 Eigenvalue relative errors of 1-D BWR core 1 (SC vs. SD).

4.3.2 Perturbation technique in collision term

The collision term is treated differently due to the fact that a perturbation technique is applied in the derivation of the DGM method to increase stability, which is similar to the treatment of angular dependence of the collision term in the multigroup discrete ordinates equations proposed in [Bell 1970] [Lewis 1993]. The purpose of this section is to study the consistency of this approximation with the recondensation procedure. Continuous spatial dependence is used in the derivation in this section, but as stated in Section 4.3.1, consistency is only obtained when using a flat-flux approximation. If the continuous energy transport equation is separated into coarse energy group equations, the Legendre moments of collision term within a coarse group g is:

$$R_{t,ig}(\vec{r},\vec{\Omega}) = \sum_{K=0}^{N-1} P_i(K,N-1)\sigma_t(\vec{r},K)\psi(\vec{r},\vec{\Omega},K), \tag{4.19}$$

where it is assumed that there are N fine group points within coarse group g with point index $K = 0,1,2,...,N-1$. This term can be condensed as:

$$R_{t,ig}^{k+1}(\vec{r},\vec{\Omega}) = \sigma_{t,ig}^{k}(\vec{r},\vec{\Omega})\psi_{ig}^{k+1}(\vec{r},\vec{\Omega}), \tag{4.20}$$

where the angular flux moment is defined in Eq. (3.5) and the total cross section moment is defined as:

$$\sigma_{t,ig}^{k}(\vec{r},\vec{\Omega}) = \frac{\sum_{K=0}^{N-1} P_i(K,N-1)\sigma_t(\vec{r},K)\psi^k(\vec{r},\vec{\Omega},K)}{\sum_{K=0}^{N-1} P_i(K,N-1)\psi^k(\vec{r},\vec{\Omega},K)} \tag{4.21}$$

With $i = 0$, Eq. (4.20) is the total reaction rate condensed from fine group to coarse group using angular flux as the weighting function. However, there are two disadvantages with definitions in Eqs. (4.20) and (4.21). Firstly, the discrete orthogonal polynomials appear in the denominator of the definition, which may lead to large round-off error and instability when generating $\sigma_{t,ig}^{k}(\vec{r},\vec{\Omega})$ moments. Secondly, the total cross section moment in Eq. (4.21) has angular dependence, which is typical in standard energy condensation from fine to coarse groups. One way proposed in Chapter 3 is to use an averaged collision term together with a perturbation term such that:

$$R_{t,ig}^{k+1}(\vec{r},\vec{\Omega}) = \sigma_{t,0g}^{k}(\vec{r})\psi_{ig}^{k+1}(\vec{r},\vec{\Omega}) + \delta_{ig}^{k}(\vec{r},\vec{\Omega})\psi_{0g}^{k+1}(\vec{r},\vec{\Omega})$$
$$= \sigma_{t,0g}^{k}(\vec{r})\sum_{K=0}^{N-1} P_i(K,N-1)\psi^{k+1}(\vec{r},\vec{\Omega},K) \qquad (4.22)$$
$$+ \frac{\sum_{K=0}^{N-1} P_i(K,N-1)\delta_g^k(\vec{r},K)\psi^k(\vec{r},\vec{\Omega},K)}{\sum_{K=0}^{N-1}\psi^k(\vec{r},\vec{\Omega},K)} \sum_{K=0}^{N-1}\psi^{k+1}(\vec{r},\vec{\Omega},K).$$

If after many recondensation iterations, the flux converges such that:

$$\psi^k(\vec{r},\vec{\Omega},K) = \psi^{k+1}(\vec{r},\vec{\Omega},K), \qquad (4.23)$$

it can be observed that Eq. (4.22) can be simplified to Eq. (4.19), which shows consistency of the derivation. If written explicitly, the spatial dependence within a spatial mesh is satisfied only when a flat flux approximation is used. Thus, the perturbation term approximation of the collision term does not induce any extra error in the recondensation iterations for 0^{th} order spatial schemes.

To close this subsection, two 1-D examples with simple analytical solutions demonstrate why the discrete polynomials in the denominator in Eq. (4.21) induce numerical instabilities, and need be treated with the perturbation technique proposed. Let us define a 1-D slab geometry with reflective boundary conditions on both sides, S_2 angular approximation, two energy groups. The DGM method will use one group with order one expansion. To simplify the problem, also assume no scattering, no fission and an external source.

Example 1: $\sigma_{t1}=1.0,\sigma_{t2}=3.0,Q_1=1.0,Q_2=5.0$. The analytical solution of this problem is $\psi_1=\frac{Q_1}{2\sigma_{t1}}=\frac{1}{2},\psi_2=\frac{Q_2}{2\sigma_{t2}}=\frac{5}{6}$. Using this exact solution to generate cross section and source moments with both the exact approach in Eq. (4.21) and the delta term approximation approach of the collision term, both can produce the exact solution ψ_1 and ψ_2.

Example 2: $\sigma_{t1}=1.0,\sigma_{t2}=5.0,Q_1=1.0,Q_2=5.0$. The analytical solution of this problem is $\psi_1=\frac{Q_1}{2\sigma_{t1}}=\frac{1}{2},\psi_2=\frac{Q_2}{2\sigma_{t2}}=\frac{1}{2}$. Using this exact solution to generate cross section and source moments with the exact approach in Eq. (4.21) of the collision term, the denominator of the first order total cross section moment is exactly 0, i.e.,

$$\psi_1 P_1(0,1)+\psi_2 P_1(1,1)=\frac{1}{2}\cdot 1.0+\frac{1}{2}\cdot(-1.0)=0.0 \tag{4.24}$$

So even in this simple problem the exact approach in Eq. (4.21) can fail. But with the delta term definition the exact solution of ψ_1 and ψ_2 can be reproduced.

4.3.3 Memory requirement of recondensation

While the energy recondensation provides a way to improve the coarse group solution efficiently with minimal computational cost, it comes at the expense of the memory requirement.

The first issue is that in each energy condensation process, the collision term is angular dependent in order to preserve the directional reaction rate. This angular dependence is folded into the perturbation term and this term has to be kept fully to maintain overall accuracy of the algorithm. This means that the angular flux needs be stored which defers from the conventional multigroup process that only stores the scalar flux and a few moments. In the 2D PWR core with S_8 quadrature the total number of directions is 40. Thus, the angular flux is 40 times the size of the scalar flux. It should also be noted that the angular flux in the perturbation term has a fine group structure (Eq. (3.11)) and thus requires a large memory to store it.

A second issue is the spatial mesh dependence of cross section moments. In traditional multigroup calculations, cross sections can be stored for each material (either heterogeneous or homogenized), but not for each spatial mesh. However, in the recondensation process presented above, cross section moments are generated using the flux as weight function for each spatial mesh. Thus all the cross sections and moments have a different value at each spatial mesh.

The results presented earlier were able to deal with the large memory requirements because of the small benchmark problems at hand. The purpose of these results is to demonstrate the level of accucary that one can obtain with the DGM recondensation method in its most accurate form. However, approximations can be made to reduce the large storage requirements.

One way to solve the first issue is to expand the angular dependence of angular flux in the perturbation term using flux moments, as indicated in [Bell 1970]. In the definition of $\delta_{ig}(\vec{r},\vec{\Omega})$ in Eq.(4.4), the angular flux in the denominator is eliminated and exists only in the numerator, and this angular flux can be expanded using angular flux moment as in Eq. (A.18). This approach is consistent with traditional multigroup calculations which store angular flux moments instead of angular flux directly. To address the second issue, a technique similar to spatial homogenization [Smith 1980] can be used in which the cross section moments for representative regions are homogenized.

4.4. Summary

In this chapter, an energy recondensation methodology is developed based on the DGM energy expansion theory. Cross sections and moments are regenerated using the obtained DGM flux spectrum as a weighting function at the beginning of each iteration. Computational tests are performed on one dimensional BWR cores with and without Gadolinium, two dimensional PWR cores with both UO_2 and MOX fuels, 1-D and 2-D HTR cores with control materials.

In both the 1-D and 2-D tests, fluxes in the coarse group solution improve considerably with only a few iterations and are shown to converge to the core fine group solutions after multiple iterations. Full convergence of the recondensation process was shown to be fully consistent with the multigroup methodology for a spatially flat flux approximation, but is

by no means a substitute. The purpose of the recondensation technique is to substantially improve the coarse group solution with a minimal number of iterations. Step difference spatial discretization is used in this study since it is consistent with the collapsing of the cross section moments which uses cell-averaged fluxes. A brief discussion is provided that explains the consistency of flat-flux approximation and the nature of the inconsistency for higher order spatial schemes. It was shown that with the step characteristic spatial discretization, the recondensation methodology can still effectively improve the coarse group solution with minimal computational cost.

While traditional multilevel approach is sufficient for current light water reactor simulations, it is not enough for advanced light water reactors, high temperature reactors and generation IV reactors [DOE 2002] which have more heterogeneous core designs. The energy recondensation method provides a way to provide a very accurate estimate of core level fine group solution with only a few DGM iterations.

HTR reactors are difficult to model with traditional multilevel approach because of the long mean free path of neutrons in the core. This leads to strong neighboring effects that are difficult to capture by multilevel approaches. The energy recondensation methodology developed in this dissertation is particularly well-suited for HTR reactors, as was shown in the 1D and 2D HTR tests. The strong spectral shift in the core can be effectively captured at the core level, which provides improved coarse group parameters.

Chapter 5 Nonlinear Energy Acceleration Using DGM Method

5.1 Method description

In the previous chapter, a new energy recondensation method was developed using the DGM method [Zhu 2011, 2]. This section extends the previous recondensation method to an acceleration form, in which the flux obtained from a few iterations of DGM calculation serves as an initial guess for the fine group calculation. Since the DGM method can produce a very accurate estimate of the fine group solution with much less computational time, it is expected that a few iterations of the DGM calculation can provide a better initial guess and accelerate the overall fine group calculation. This section analyzes the number of DGM iterations needed to provide the greatest time savings.

Fig. 5.1 is the flow chart of this energy acceleration scheme. The flux and eigenvalue solution from the recondensation process are used as the initial guess for the standard fine group calculation.

5.2 Computational results

The core tested in this section is the 2-D PWR core described in Section 4.2.3. The same 2-D S_N code platform is used. The angular discretizaiton is S_4 in this section. In the energy acceleration algorithm, a few iterations of the DGM calculation are performed

first and the obtained flux is used as the initial guess for the following fine group calculation.

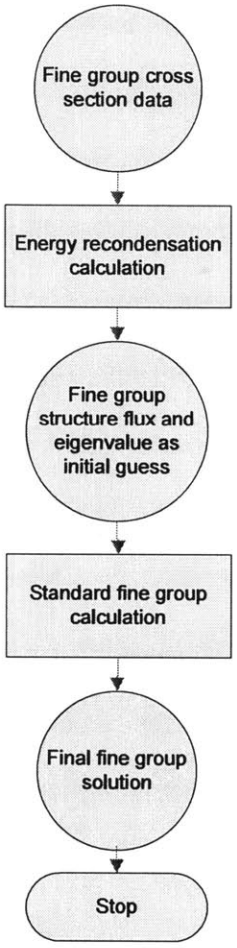

Fig. 5.1 Flow chart of energy acceleration procedure.

In the first group of tests, a 3 group DGM calculation is performed. The number of fine groups in each coarse group is 26, 20, and 24, respectively and the number of DGM iterations in the recondensation process is varied from 3 to 20. With 20 DGM iterations, the *rms** error between two consecutive iterations is less than the convergence criterion, i.e., 10^{-5}.

From Table 5.1, the 70 group reference calculation takes 517 minutes, with 146,121 core level transport sweeps. It can be observed that the DGM calculation reduces the overall computational time and total number of core level transport sweeps. With 20 DGM iterations followed by fine group calculations, the total computational time is 80 minutes, about 1/6 of the fine group computational time. The total number of core level transport sweeps is 23,865, about 1/6 of that of fine group calculations. It can also be observed that with a smaller number of DGM iterations, the computational times required are longer than with 20 iterations, but still accelerate the fine group solution effectively. With 3 DGM iterations followed by fine group calculation, the time is about 196 minutes which is less than half of that of fine group calculation.

Table 5.1 also lists final errors in eigenvalue. It can be observed that with different number of DGM iterations followed by fine group calculations, eigenvalue converge to the fine group solution to the order of $0.1pcm$, which consistent with the convergence tolerance and indicate that the solutions converges to the fine group solution.

Table 5.1 3 coarse group with expansions acceleration results.

	Eigenvalue	Time (min)	# transport sweeps
3 DGM iterations	1.198994	196	51,726
6 DGM iterations	1..198998	127	37,830
13 DGM iterations	1.198998	71	24,475
20 DGM iterations	1.198998	65	23,865
Reference solution	1.198995	517	146,121

Note: Assembly calculations take 15 minutes, not included.

The test is repeated with a 2 group DGM calculation. The numbers of fine groups within each coarse group are 26 and 44, respectively where the second coarse group includes all the 44 upscattering groups. The number of DGM iterations in the recondensation are 3, 6, 13 and 20, respectively. With 20 DGM iterations, the *rms** errors between two consecutive iterations are less than the convergence criteria, i.e., 10^{-5}.

Table 5.2 lists the computational results. The results of the 2 group expansions are similar to those of 3 group expansions. With 20 iterations, followed with the fine group solver, the total computational times and number of total core level transport sweeps are about 1/7 of those of the fine group calculation. Eigenvalues converge to the fine group solution. With fewer DGM iterations, the acceleration scheme still improves the overall performance.

Table 5.2 2 coarse groups with expansions acceleration results.

	Eigenvalue	Time (min)	# transport sweeps
3 DGM iterations	1.199002	169	47,499
6 DGM iterations	1.198998	134	36,082
13 DGM iterations	1.198996	66	22,270
20 DGM iterations	1.198996	62	21,614
Reference solution	1.198995	517	146,121

Note: Assembly calculations take 15 minutes, not included.

This new nonlinear energy acceleration scheme is totally compatible with other existing acceleration schemes including coarse mesh finite difference (CMFD) [Smith 2002] [Yamamoto 2004] and diffusion synthetic acceleration (DSA) [Alcouffe 1977] [Adams 2002] methods. In each DGM iteration, the leading order calculation is equivalent to the standard coarse group calculation and thus can be accelerated with DSA and CMFD. However, because the angular dependence is kept in the collision term, current acceleration techniques would require some adaptation. The recondensation process can be accelerated using Newton's method [Kelley 2003] [Deuflhard 2004] to further improve the overall efficiency.

5.3 Summary

This chapter developed an energy acceleration scheme which is a natural extension of the energy recondensation method developed in Chapter 4. If the fine group solution is desired, solution from the recondensation calculation can be used as an initial guess for the standard fine group calculation. This methodology was tested on a 2D PWR core with a 70 group cross section database. Recondensation calculations are 2 or 3 coarse group with expansions with different number of DGM iterations. Results showed that the new algorithm can effectively accelerate the standard fine group calculation.

Chapter 6 Summary and Future Work

6.1 Summary

In this study, a fundamentally new discrete generalized multigroup energy expansion theory was developed to bridge the broad energy range in nuclear reactor simulations. The new theory offers an innovative way of discretizing the energy variable. In the standard multigroup equations, the group angular flux is expressed using discrete energy moments. Moment equations are solved so that the multigroup angular flux can be unfolded from the solved energy moments of the flux.

The new DGM energy discretization theory provides a way to reduce the reliance on the traditional multilevel approach by proposing an online energy recondensation procedure that eliminates the dependency on approximate boundary conditions. Cross sections and moments can be regenerated using the obtained DGM core-level flux spectrum as a weighting function at the beginning of each DGM iteration. The cross-section condensation process is thus embedded inside the core level calculation and the need for pin cell or lattice level calculations can be eliminated.

A demonstration was performed on a simplified two dimensional PWR core. A straightforward infinite lattice condensation from 70 groups to 3 groups produced, at the core-level, fission density mean relative errors on the order of 3.9% after the first DGM iteration, and reduced to 0.32% after only 3 DGM iterations, and further reduced to

0.0020% after 13 DGM iterations when the solution was fully condensed to the fine group solution. Note that with the traditional multilevel approach, errors in coarse group solutions are on the order of those of the 1st DGM iteration. Additionally, due to the use of discrete orthogonal polynomials, this new approach remains computationally competitive compared to the fine group calculation. The total number of transport sweeps of obtaining the fully condensed flux calculation was about 1/6 the total of the standard fine group power iteration. Thus, the recondensation scheme provides both efficiency and accuracy for core level calculations. It is also expected that the time benefit of the DGM method will increase when tested on much larger cores.

A representative HTR benchmark was also tested. Infinite lattice calculations are ill-suited for this type of reactor because of the strong neighboring effect caused by the long neutron mean free path. The energy recondensation methodology developed in this dissertation is well-suited in capturing the spectral effects at the core-level, thus improving the coarse group results. Instead of resorting to mini-cores or color-sets, the DGM was seeded with 5 fine group outer iterations as an initial guess for the coarse group solution. In a 2D HTR core test, comparison was made between 26 group calculation and 4 coarse group recondensation calculations. Mean relative error of scalar flux was 5.7% after the first DGM iteration and after 5 DGM iterations was reduced to 1.8%, and was further reduced to 0.029% after 38 DGM iterations.

Table 6.1 list the recondensation results for a few cores tested in this study, i.e., 1D BWR core 3, 1D HTR, 2D PWR, and 2D HTR. *rms* relative error, mean relative error (*mre*),

and error in eigenvalue for the first 3 DGM iterations are listed. It can be observed from the table that in all the tests, recondensation calculations can substantially improve the coarse group solution.

Table 6.1 Recondensation result summary.

		rms (%)	*mre* (%)	Δk *(pcm)*
1D BWR core 1 (47 group vs. 2gr/exp)	1st iteration	3.2	1.6	1342
	2nd iteration	1.0	0.62	17
	3rd iteration	0.56	0.28	119
1D BWR core 3 (47 group vs. 2 gr/exp)	1st iteration	15	8.5	6867
	2nd iteration	6.3	4.3	1851
	3rd iteration	2.6	1.7	1026
1D HTR core (295 group vs. 10 gr/exp)	1st iteration	19	3.7	1473
	2nd iteration	5.4	1.4	403
	3rd iteration	1.8	0.57	101
1D HTR core (P1 anisotropic scattering)	1st iteration	18	3.6	998
	2nd iteration	5.2	1.4	393
	3rd iteration	1.8	0.62	158
2D PWR core (70 group vs. 3 gr/exp)	1st iteration	33	4.8	1797
	2nd iteration	15	0.91	194
	3rd iteration	7.5	0.39	45
2D HTR core (26 group vs. 4 gr/exp)	1st iteration	35	5.7	4140
	2nd iteration	25	4.4	2381
	3rd iteration	19	3.3	1399

The energy recondensation procedure has shown to substantially improve the coarse group solution with a minimal number of iterations. Furthermore, if the fine group solution is still desired, an energy acceleration scheme becomes a natural extension of the process. The flux from the recondensation calculations can be used as an initial guess for standard fine group calculation. Computational results showed that the scheme can effectively accelerate the fine group calculation by improving the initial guess of flux and eigenvalue. In a 2D PWR core test, a 70 group calculation was accelerated with 2 or 3 coarse group recondensation calculations with different number of recondensation iterations. With the 3 DGM recondensation calculation, the total number of transport sweeps was about 1/3 of that of the unaccelerated calculation. With fully condensed results, the number of transport sweeps was to 1/6 of that of the unaccelerated calculation.

Despite the very promising DGM results, a few important caveats were identified. The accuracy of the converged recondensation procedure towards the fine group results depends on the spatial discretization scheme used. Analysis regarding the dependency of spatial discretization methods was performed and indicated that the step difference spatial discretization which assumes piecewise constant flux within each spatial mesh is fully consistent with the recondensation methodology. When generating cross section moments, only the cell-averaged flux value is used. In higher order methods, information is lost, i.e., slope of flux with linear discretization method (i.e., linear discontinuous Galerkin), or the exponential information in step characteristics method. Even though not fully consistent for step characteristic spatial discretization, computational results show that

the DGM recondensation method can still effectively improve the coarse group solution with minimal computational cost.

6.2 Future work

In all the algorithms developed in this dissertation, energy discretizations throughout the entire spatial domain is the same. A mixed energy method [Forget 2010] was proposed to link the coarse and fine group spectrums. At the interface of coarse group and DGM regions, fluxes are connected by coarse group energy structure. At the interface of fine group and DGM regions, fluxes are connected by fine group energy structure because the unfolded flux in the DGM region does have a fine group structure. This methodology makes it possible to have different energy structures in different regions in the same core so that a fine group representation can be used in more important regions and coarse group representation can be used in less important regions in order to reduce the overall computational cost.

In Chapter 2, different energy self-shielding methods in nuclear data processing are reviewed. If calculation can be performed on ultra-fine energy group structure, self-shielding models become unnecessary. In traditional multigroup methods this is very computationally expensive. This situation can be improved by using the DGM method developed in this study. Recondensation calculation on a fine group structure can be performed and the condensed fluxes and moments can be unfolded to the ultra-fine group structure to capture the self-shielding effects.

Appendix A. Derivation of multigroup form of transport equation

The definition and derivation of the multigroup form of the Boltzmann transport equation can be found in many references, i.e., [Bell 1970] [Lewis 1993]. Because the new discrete generalized multigroup method is closely related to the standard multigroup method, a brief derivation is discussed here. Without loss of generality, the starting point of the discussion in this section is the steady state *k*-eigenvalue problem of the linear Boltzmann transport equation for neutron distribution with fission and scattering sources:

$$\begin{aligned}&\vec{\Omega}\cdot\nabla\psi(\vec{r},\vec{\Omega},E)+\sigma_t(\vec{r},E)\psi(\vec{r},\vec{\Omega},E)=\\&\int_0^\infty dE'\int_{4\pi}d\vec{\Omega}'\sigma_s(\vec{r},\vec{\Omega}'\to\vec{\Omega},E'\to E)\psi(\vec{r},\vec{\Omega}',E')+\\&\frac{\chi(\vec{r},E)}{4\pi k}\int_0^\infty dE'\int_{4\pi}d\vec{\Omega}'\nu\sigma_f(\vec{r},E')\psi(\vec{r},\vec{\Omega}',E'),\end{aligned}\tag{A.1}$$

where $\psi(\vec{r},\vec{\Omega},E)$ is the neutron angular flux, $\sigma_t(\vec{r},E)$ is the total cross section, $\sigma_f(\vec{r},E')$ is the fission cross section, $\nu(\vec{r},E')$ is the number of neutrons produced per fission reaction, $\chi(\vec{r},E)$ is the fast fission spectrum, and $\sigma_s(\vec{r},\vec{\Omega}'\to\vec{\Omega},E'\to E)$ is the double differential scattering kernel. The scalar flux is defined as:

$$\phi(\vec{r},E)=\int_{4\pi}\psi(\vec{r},\vec{\Omega},E)d\vec{\Omega}.\tag{A.2}$$

Group flux is defined as an integral quantity within each group; in particular, the group angular and scalar fluxes are defined within group g as:

$$\psi_g(\vec{r},\vec{\Omega}) = \int_{E_g}^{E_{g-1}} \psi(\vec{r},\vec{\Omega},E)dE, \tag{A.3}$$

$$\begin{aligned}\phi_g(\vec{r}) &= \int_{E_g}^{E_{g-1}} \phi(\vec{r},E)dE \\ &= \int_{E_g}^{E_{g-1}} \int_{4\pi} \psi(\vec{r},\vec{\Omega},E)d\Omega dE\end{aligned} \tag{A.4}$$

To derive multigroup equation, integrate the continuous energy transport equation over each energy interval. In particular, if the first group starts from the highest energy (and thus lowest lethargy), in order to obtain the group fluxes defined in Eqs. (A.3) and (A.4), integrate Eq. (A.1) within group g $(g=1,\ldots,G)$:

$$\begin{aligned}&\vec{\Omega}\cdot\nabla\int_{E_g}^{E_{g-1}} \psi(\vec{r},\vec{\Omega},E)dE + \int_{E_g}^{E_{g-1}} \sigma_t(\vec{r},E)\psi(\vec{r},\vec{\Omega},E)dE = \\ &\int_{E_g}^{E_{g-1}} dE\sum_{g'=1}^{G}\int_{E_{g'}}^{E_{g'-1}} dE'\int_{4\pi} d\vec{\Omega}'\sigma_s(\vec{r},\vec{\Omega}'\to\vec{\Omega},E'\to E)\psi(\vec{r},\vec{\Omega}',E') + \\ &\int_{E_g}^{E_{g-1}} \frac{\chi(\vec{r},E)}{4\pi k}dE\sum_{g'=1}^{G}\int_{E_{g'}}^{E_{g'-1}} dE'\int_{4\pi} d\vec{\Omega}'\nu\sigma_f(\vec{r},E')\psi(\vec{r},\vec{\Omega}',E'),\end{aligned} \tag{A.5}$$

where E_0 is the highest possible energy and E_G is the lowest possible energy. In reactor simulations, E_0 is on the order of 20MeV and E_G is on the order of 10^{-5}eV. In order to

obtain group cross sections in Eq. (A.5), the important idea is to preserve reaction rates of each term within each group. Thus, the multigroup form of the transport equation in terms of group fluxes and group cross sections is:

$$\vec{\Omega}\cdot\nabla\psi_g(\vec{r},\vec{\Omega})+\sigma_{tg}(\vec{r},\vec{\Omega})\psi_g(\vec{r},\vec{\Omega})= \sum_{g'=1}^{G}\int_{4\pi}\sigma_{s,gg'}(\vec{r},\vec{\Omega}'\rightarrow\vec{\Omega})\psi_{g'}(\vec{r},\vec{\Omega}')d\Omega'+\frac{\chi_g(\vec{r})}{4\pi k}\sum_{g'=1}^{G}\nu\sigma_{fg'}(\vec{r})\phi_{g'}(\vec{r}), \tag{A.6}$$

where the group cross sections are defined by preserving reaction rates for each term as:

$$\sigma_{tg}(\vec{r},\vec{\Omega})=\frac{\int_{E_g}^{E_{g-1}}\sigma_t(\vec{r},E)\psi(\vec{r},\vec{\Omega},E)dE}{\int_{E_g}^{E_{g-1}}\psi(\vec{r},\vec{\Omega},E)dE}, \tag{A.7}$$

$$\sigma_{s,gg'}(\vec{r},\vec{\Omega}'\rightarrow\vec{\Omega})=\frac{\int_{E_{g'}}^{E_{g'-1}}\int_{E_g}^{E_{g-1}}dE'dE\sigma_s(\vec{r},\vec{\Omega}'\rightarrow\vec{\Omega},E'\rightarrow E)\psi(\vec{r},\vec{\Omega}',E')}{\int_{E_g}^{E_{g-1}}\psi(\vec{r},\vec{\Omega},E)dE}, \tag{A.8}$$

$$\nu\sigma_{fg}(\vec{r})=\frac{\int_{E_g}^{E_{g-1}}\nu\sigma_f(\vec{r},E)\phi(\vec{r},E)dE}{\int_{E_g}^{E_{g-1}}\phi(\vec{r},E)dE}, \tag{A.9}$$

$$\chi_g(\vec{r}) = \int_{E_g}^{E_{g-1}} \chi_g(\vec{r}, E)dE. \tag{A.10}$$

All these multigroup cross sections can be obtained only after the exact fluxes solution is known, which is typically not known *a priori*. Note that in Eqs. (A.7), angular flux is used as a weighting function so that the generated total cross section has angular dependence. One common way to get rid of this angular dependency is to assume that the angular flux can be separated as a product of the energy spectrum within the group and the group angular flux as [Bell 1970] [Lewis 1993]:

$$\psi(\vec{r}, \vec{\Omega}, E) = \psi_g(\vec{r}, \vec{\Omega}) f(E), \tag{A.11}$$

and integrate over angle to obtain:

$$\phi(\vec{r}, E) = \phi_g(\vec{r}) f(E). \tag{A.12}$$

Substitute this approximation into Eqs. (A.7)-(A.9) to obtain the group cross sections as:

$$\sigma_{tg}(\vec{r}) = \frac{\int_{E_g}^{E_{g-1}} \sigma_t(\vec{r}, E) f(E)dE}{\int_{E_g}^{E_{g-1}} f(E)dE}, \tag{A.13}$$

$$\sigma_{s,gg'}(\vec{r},\vec{\Omega}' \to \vec{\Omega}) = \frac{\int_{E_{g'}}^{E_{g'-1}} \int_{E_g}^{E_{g-1}} dE' dE \sigma_s(\vec{r},\vec{\Omega}' \to \vec{\Omega}, E' \to E) f(E')}{\int_{E_g}^{E_{g-1}} f(E) dE}, \tag{A.14}$$

$$\nu\sigma_{fg}(\vec{r}) = \frac{\int_{E_g}^{E_{g-1}} \nu\sigma_f(\vec{r},E) f(E) dE}{\int_{E_g}^{E_{g-1}} f(E) dE}. \tag{A.15}$$

Note that the energy spectrum $f(E)$ has region and group dependence. The accuracy of the multigroup depends on how $f(E)$ is obtained. The approximation made in Eq. (A.11) is not always satisfied, especially when the system is complex and very heterogeneous, and typically requires fine enough spatial and energy grids.

A second way to treat the angular dependence of the total cross section when deriving the multigroup equations is proposed in [Bell 1970] and [Lewis 1993]. It is called "Consistent P_n" approximation if the total group cross section is assumed to be weighted using the scalar flux as:

$$\sigma_{tg}(\vec{r}) = \frac{\int_{E_g}^{E_{g-1}} \sigma_t(\vec{r},E) \phi(\vec{r},E) dE}{\int_{E_g}^{E_{g-1}} \phi(\vec{r},E) dE}. \tag{A.16}$$

By comparing Eqs. (A.7) and (A.16), the error in group g in the collision term induced from this approximation is:

$$\left(\frac{\int_{E_g}^{E_{g-1}} \sigma_t(\vec{r},E)\phi(\vec{r},E)dE}{\int_{E_g}^{E_{g-1}} \phi(\vec{r},E)dE} - \frac{\int_{E_g}^{E_{g-1}} \sigma_t(\vec{r},E)\psi(\vec{r},\vec{\Omega},E)dE}{\int_{E_g}^{E_{g-1}} \psi(\vec{r},\vec{\Omega},E)dE}\right) \bullet \psi_g(\vec{r},\vec{\Omega}). \qquad \text{(A.17)}$$

The idea is to first move this error term to the right hand side of the transport equation, and expand the angular flux using Legendre polynomials (in 1-D slab geometry). Thus Eq. (A.17) can be expressed using group angular flux Legendre moments and is further combined into the scattering kernel which is also expressed using Legendre expansion (in 1-D slab geometry).

This idea is very similar to the delta term approximation derived in the DGM method and a detailed derivation of the delta term can be found in Chapter 3. The reason of this similarity is that from continuous energy to multigroup equation, and from fine group to coarse group energy condensation, the total group cross section becomes angular dependent.

Up to this point the multigroup fluxes and cross sections have been defined and the multigroup equation is given in Eq. (A.6). The next step is to treat the angular dependence of the scattering kernel. In the scattering kernel, the group angular flux is typically expanded using spherical harmonics [Hobson 1955] [Courant 1962] [Müller

1966] and group angular flux moments. The group scattering matrix is expanded using Legendre polynomials and group scattering moment matrices. In particular,

$$\psi_g(\vec{r},\vec{\Omega}) = \frac{1}{4\pi}\sum_{l=0}^{\infty}\sum_{m=-l}^{l}\phi_{lm,g}(\vec{r})Y_{lm}(\vec{\Omega}), \tag{A.18}$$

where

$$\phi_{lm,g}(\vec{r}) = \int_{4\pi} Y_{lm}^{*}(\vec{\Omega})\psi_g(\vec{r},\vec{\Omega})d\Omega, \tag{A.19}$$

where $Y_{lm}^{*}(\vec{\Omega})$ is the complex conjugate of the spherical harmonics. The scattering kernel is:

$$\sigma_{s,gg'}(\vec{r},\vec{\Omega}'\rightarrow\vec{\Omega}) = \frac{1}{2\pi}\sigma_{s,gg'}(\vec{r},\mu_0) = \sum_{l=0}^{L}\frac{2l+1}{4\pi}\sigma_{sl,gg'}(\vec{r})P_l(\mu_0), \tag{A.20}$$

where

$$\sigma_{sl,gg'}(\vec{r}) = \int_{-1}^{1}\sigma_{s,gg'}(\vec{r},\mu_0)P_l(\mu_0)d\mu_0. \tag{A.21}$$

The orthogonality of spherical harmonics and the Legendre addition theorem are also used in deriving the scattering term:

$$\int_{4\pi} Y_{lm}^{*}(\vec{\Omega})Y_{l'm'}(\vec{\Omega})d\Omega = 4\pi\delta_{ll'}\delta_{mm'}. \tag{A.22}$$

$$P_l(\mu_0) = \frac{1}{2l+1}\sum_{m=-l}^{l} Y_{lm}(\vec{\Omega})Y_{lm}^{*}(\vec{\Omega}'). \tag{A.23}$$

Substituting these expansions and using the orthogonality properties, the transport equation with scattering moments is:

$$\begin{aligned}&\vec{\Omega}\cdot\nabla\psi_g(\vec{r},\vec{\Omega}) + \sigma_{tg}(\vec{r})\psi_g(\vec{r},\vec{\Omega}) = \\ &\sum_{g'=1}^{G}\sum_{l=0}^{L}\sum_{m=-l}^{l}\frac{Y_{lm}^{*}(\vec{\Omega})}{4\pi}\sigma_{sl,gg'}(\vec{r})\phi_{lm,g'}(\vec{r}) + \frac{\chi_g(\vec{r})}{4\pi k}\sum_{g'=1}^{G}\nu\sigma_{fg'}(\vec{r})\phi_{g'}(\vec{r}).\end{aligned} \tag{A.24}$$

Eq. (A.24) is the standard multigroup form of the transport equation used in most deterministic transport calculations.

Appendix B. Orthogonal polynomials

Orthogonal polynomials [Nikiforov 1988] [Nikiforov 1991] [Gautschi 2004] are widely used in many science and engineering fields. In nuclear engineering field, the scattering cross section matrix is typically expanded using Legendre polynomials and scattering matrix moments are stored for calculations. An important reason is that the Legendre polynomials are defined on the interval [-1,1] which matches the cosine range of the polar angle. In this section, definitions and properties of continuous and discrete polynomials are reviewed.

B.1 Continuous orthogonal polynomials

Classical polynomials are defined as a solution of equations of hypergeometric type [Nikiforov 1991]:

$$\sigma(x)y''+\tau(x)y'+\lambda y=0, \tag{B.1}$$

where $\sigma(x)$ is a polynomial of at most second degree, $\tau(x)$ is a polynomial of at most first degree, and λ is a constant. Two examples are Legendre differential equations and Tchebichef differential equations (for the polynomials of the first kind) which are defined respectively as:

$$(1-x^2)P_n''(x)-2xP_n'(x)+n(n+1)P_n(x)=0, \tag{B.2}$$

$$(1-x^2)T_n''(x)-2xT_n'(x)+n^2T_n(x)=0. \tag{B.3}$$

While explicit solutions can be expressed by Rodrigues formula, polynomials are typically generated through a three term recurrence relation:

$$xP_n(x)=\alpha_n P_{n+1}(x)+\beta_n P_n(x)+\gamma_n P_{n-1}(x) \tag{B.4}$$

All orthogonal polynomials satisfy this three term recurrence relation with different constants α_n, β_n, and γ_n [Nikiforov 1991]. Legendre polynomials can be generated through this relation:

$$\begin{aligned} &P_0(x)=1, \\ &P_1(x)=x, \\ &(n+1)P_{n+1}(x)-(2n+1)xP_n(x)+nP_{n-1}(x)=0, \quad n\geq 2. \end{aligned} \tag{B.5}$$

Tchebichef polynomials of the first kind can be generated through this relation:

$$\begin{aligned} &T_0(x)=1, \\ &T_1(x)=x, \\ &T_{n+1}(x)-2xT_n(x)+T_{n-1}(x)=0, \quad n\geq 2. \end{aligned} \tag{B.6}$$

Orthogonality properties are defined:

$$\int_{-1}^{1} P_l(x)P_m(x)dx = \frac{2}{2l+1}\delta_{lm} \tag{B.7}$$

$$\int_{-1}^{1} T_l(x)T_m(x)\frac{dx}{\sqrt{1-x^2}} = \begin{cases} 0, l \neq m \\ \pi, l = m = 0 \\ \pi/2, l = m \neq 0. \end{cases} \tag{B.8}$$

Both Legendre and Tchebichef polynomials are special cases of Jacobi polynomials [Nikiforov 1991].

B.2 Discrete orthogonal polynomials

In some mathematics and physics applications, the quantities are determined on a discrete set of argument values. An example is the multigroup form of transport equation where the group flux and group cross sections are considered piecewise constant within each energy group. In such problems, a set of orthogonal polynomials of a discrete independent variable which assume only a finite number of values in the interval can be used. The difference equation has the form [Nikiforov 1991]:

$$\sigma(K)\Delta\nabla P_n(K,N-1) + \tau(K)\Delta P_n(K,N-1) + \lambda P_n(K,N-1) = 0, \tag{B.9}$$

where the forward and backward finite difference operators are:

$$\Delta P_n(K,N-1) = P_n(K+1,N-1) - P_n(K,N-1), \tag{B.10}$$

$$\nabla P_n(K,N-1) = P_n(K,N-1) - P_n(K-1,N-1). \tag{B.11}$$

where $n = 0,1,...,N-1$; $K = 0,1,...,N-1$. The three term recurrence relation is similar to that of the continuous case in Eq. (B.4) except that the continuous variable x is replaced by the discrete variable K. From a computational point of view, the recurrence relation to generate discrete orthogonal polynomials is more important than an explicit expression which is typically expressed with Rodrigues formula.

Definition and properties of the discrete Legendre orthogonal polynomials (DLOP) are shown in [Neuman 1974]. Mathematically, the DLOP $P_n(K,N-1)$ are defined over the discrete interval $K = 0,1,2,...,N-1$ and $n = 0,1,2,...,N-1$ is the degree of the polynomial where the total number of discrete points is N. Their orthogonality relation can be expressed as:

$$\sum_{K=0}^{N-1} P_m(K,N-1)P_l(K,N-1) = \rho(m,N-1)\delta_{ml}, \tag{B.12}$$

where δ_{ml} is the Kronecker Delta and the squared norm of the m^{th} order polynomial set $\rho(m,N-1)$ is:

$$\rho(m,N-1) = \sum_{K=0}^{N-1} P_m^2(K,N-1) = \frac{(N+m)^{(m+1)}}{(2m+1)(N-1)^{(m)}}, \tag{B.13}$$

where $N^{(m)}$ is the m^{th} fading factorial of N defined as:

$$N^{(m)} = \begin{cases} N(N-1)(N-2)...(N-m+1), & m>0 \\ 1, & m=0 \end{cases}. \tag{B.14}$$

The normalization relation is:

$$P_m(0,N-1)=1 \quad \text{for all } m. \tag{B.15}$$

One of the most important properties of the DLOP to be used in the DGM method derivation comes from the othogonality relation in (B.12) by setting $m=0$ to obtain:

$$\sum_{K=0}^{N-1} P_l(K,N-1)=\rho(0,N-1)\delta_{0l}, \tag{B.16}$$

in which the following fact is used:

$$P_0(K,N-1)=1 \quad \text{for all } K. \tag{B.17}$$

The DLOP can be generated using the following recurrence relation (in m) [Neuman 1974]

$$
\begin{aligned}
&P_0(K,N-1)=1,\\
&P_1(K,N-1)=(N-1-2K)/(N-1),\\
&(m+1)(N-1-m)P_{m+1}(K,N-1)-(2m+1)(N-1-2K)P_m(K,N-1)\\
&\qquad +m(N+m)P_{m-1}(K,N-1)=0, \qquad m=1,2,...,(N-2).
\end{aligned}
\tag{B.18}
$$

Orthogonality relation of discrete Tchebichef (DT) polynomials is [Mukundan 2000] [Mukundan 2001]:

$$
\sum_{K=0}^{N-1} T_m(K,N-1)T_l(K,N-1)=\rho(m,N-1)\delta_{ml}, \tag{B.19}
$$

where

$$
\rho(m,N-1)=\sum_{K=0}^{N-1} T_m^2(K,N-1)=\frac{N(1-\frac{1^2}{N^2})(1-\frac{2^2}{N^2})...(1-\frac{m^2}{N^2})}{(2m+1)}. \tag{B.20}
$$

In Eq. (B.19), if m=0, the following obtained result is obtained:

$$
\sum_{K=0}^{N-1} T_l(K,N-1)=\rho(0,N-1)\delta_{0l}, \tag{B.21}
$$

in which the following fact is used:

$$
T_0(K,N-1)=1 \quad \text{for all } K. \tag{B.22}
$$

The DT can be generated using the following recurrence relation (in m):

$$
\begin{aligned}
&T_0(K,N-1)=1,\\
&T_1(K,N-1)=(2K+1-N)/N,\\
&mT_m(K,N-1)-(2m-1)\frac{(2K+1-N)}{N}T_{m-1}(K,N-1) \qquad \text{(B.23)}\\
&\quad +(m-1)(1-\frac{(m-1)^2}{N^2})T_{m-2}(K,N-1)=0, \qquad m=2,3,...,(N-1).
\end{aligned}
$$

In this dissertation, both DLOP and DT are used and tested in the DGM method.

B.3 Discussions on discrete expansion

This section addresses known issues associated with discrete polynomial expansions.

(a) Numerical precision of floating point numbers.

In this study, double precision is used in all the implementations of the algorithms for floating point numbers. Based on the *IEEE 754 standard* [IEEE 1985] definition, a double precision floating point number is stored in 8 bytes, 64 bits. The sign, exponent and significand occupy 1, 11 and 53 bits, respectively.

For the exponent part which occupies 11 bits, the range is from $10^{-308}-10^{308}$ where 308 is approximately from $1023\times\log_{10}2$. Beyond 10^{308} or below 10^{-308} is named *overflow/underflow*.

For the significand part, the integer resolution is on the order of $\mu = 2^{53} \approx 10^{16}$. Thus, any two double precision real numbers with a significand difference smaller than $\mu^{-1} = 2^{-53} \approx 10^{-16}$ and having the same exponent and sign are considered the same number thus causing a *roundoff error.*

The way a real number is stored limits some computational features if the range of numbers varies many orders of magnitudes. An extreme example is when summing two numbers 1.0 and 1.0E20, the result is 1.0E20 and information of the first number 1.0 is totally lost. In order to have accurate summation of the two, quadruple or arbitrary precision numbers can be defined. This will increase requirement of both memory and computational effort. With double precision, this kind of phenomenon will have an impact on the discrete expansion if values of a step function have large variations.

(b) Step function with values of large difference in magnitude.

In Section 3.2, a step function is expanded and reconstructed using both continuous and discrete orthogonal polynomials. Discrete expansion gives a very accurate reconstructed result. Here a more challenging step function is expanded. The 4 step values of function $f(K)$ are $1, \frac{1}{700}, \frac{1}{700^2}$, and $\frac{1}{700^3}$ for $K = 0,1,2,3$. The DLOP values (double precision) of $N=4$ is given in Table B.1 with order m and point number K.

Table B.1 Double precision DLOP values of $N=4$.

	m=0	1	2	3
K=0	1.00000000000000	1.00000000000000	1.00000000000000	1.0000000000000
1	1.00000000000000	0.333333333333333	-1.00000000000000	-3.00000000000000
2	1.00000000000000	-0.333333333333333	-1.00000000000000	3.00000000000000
3	1.00000000000000	-1.00000000000000	1.00000000000000	-1.00000000000000
ρ_m	4.00000000000000	2.22222222222222	4.00000000000000	20.0000000000000

Exact and reconstructed step functions are given in Table B.2. It can be observed that the largest value 1.0 at K=0 is reconstructed accurately on all the digits. For K=1 where the step value is on the order of 10^{-3}, the last 2 or 3 digits are not accurate and the relative error is on the order of 10^{-12}%. For K=2 where the step value is on the order of 10^{-6}, the last 5 digits are not accurate and the relative error is on the order of 10^{-10}%. For K=3 where the step value is on the order of 10^{-9}, the last 8 or 9 digits are not accurate and the relative error is on the order of 10^{-7}%.

Table B.2 Exact and reconstructed step functions (1).

	K=0	1	2	3
$f(K)$	1.00000000000000	1.428571428571429 E-3	2.040816326530612 E-6	2.915451895043732 E-9
$\tilde{f}(K)$	1.00000000000000	1.428571428571390 E-3	2.040816326542849 E-6	2.915451921547962 E-9
Relative error (%)	0.0	2.7E-12	7.6E-10	9.1E-7

Thus, the reconstructed function will poorly represent very small values. When generating discrete moments using Eq.(3.27), the moment F_m is stored as a double precision value. Similarly, when reconstructing the function using Eq. (3.28), the reconstructed function is also stored as a double precision value. When summing a smaller number (i.e., on the order of 10^{-3}) and a larger number (i.e., on the order of 1) in both Eqs. (3.27) and (3.28), information on the last a few digits of the smaller number will be lost.

In Section 3.2 it has been claimed that a four values step function can be reconstructed using DLOP accurately. Table B.3 shows the detailed double precision values of the exact and reconstructed values. It can be observed that although the step function in Section 3.2 is much smoother than the step function in Table B.2, small errors can still be observed in the last a few digits of low step values, as is shown in Table B.3.

Table B.3 Exact and reconstructed step functions (2).

	K=0	1	2	3
$f(K)$	5.00000000000000 E-2	1.00000000000000	0.400000000000000	1.00000000000000 E-2
$\tilde{f}(K)$	5.00000000000002 E-2	1.00000000000000	0.400000000000000	1.00000000000004 E-2

(c) High order expansions

If the number of discrete points of a step function is large, this leads to a high order expansion. Since these polynomials are generated using a three term recurrence relation, numerical errors can propagate and grow exponentially, which can deteriorate the overall performance and lead to the loss of orthogonality [Mukundan 2004]. By using the following recurrence relation:

$$\begin{aligned} P_{n+1,\varepsilon}(K) &= (\alpha_n K + \beta_n)(P_n(K) + \varepsilon_n) + \gamma_n (P_{n-1}(K) + \varepsilon_{n-1}) \\ &= (\alpha_n K + \beta_n) P_n(K) + \gamma_n P_{n-1}(K) + (\alpha_n K + \beta_n)\varepsilon_n + \gamma_n \varepsilon_{n-1} \\ &= P_{n+1}(K) + \varepsilon_{n+1}, \end{aligned} \tag{B.24}$$

where ε_n and ε_{n-1} are errors in the n^{th} and $(n\text{-}1)^{\text{th}}$ order polynomials. Note that

$$\varepsilon_{n+1} = (\alpha_n K + \beta_n)\varepsilon_n + \gamma_n \varepsilon_{n-1} \tag{B.25}$$

Eq. (B.25) has a nonlinear term (K dependence) which leads the error to propagate along the energy variable.

The value of the squared norm of discrete orthogonal polynomials (defined in Eqs. (B.13) for DLOP and (B.20) for DT) varies many orders of magnitude with high order expansions. This will lead to numerical instabilities [Mukundan 2004].

In order to remedy the issues associated with high order expansions, Mukundan [Mukundan 2004] proposed an algorithm to generate orthonormal discrete Tchebichef polynomials. Firstly, the squared norm is normalized to 1 so that the discrete orthogonal Tchebichef polynomials become orthonormal polynomials. This remedies the issue of large variation of the squared norm.

Secondly, a new recurrence relation in K was proposed to generate orthonormal Tchebichef polynomials, instead of using the recurrence relation in order m. The new recurrence relation in K was shown to be more robust [Mukundan 2004].

Thus, discrete Tchebichef polynomials in this study are generated using the algorithm in [Mukundan 2004]. A simple step function reconstruction is tested for both the DLOP and the orthonormal DT generated using the K recurrence relation.

The first test is the reconstruction of a step function with 50 step values, and thus a 50 order expansion is needed. These values uniformly equal to 1.0. Table B.4 shows the

results of the reconstructed function using both DLOP and orthnormal DT. Only the first 25 values are shown due to symmetry. It can be observed that DT gives a better solution than DLOP. The reconstructed function with DT is accurate up to the last digit, while with DLOP, a few points have 9~10 digits inaccuracies.

Table B.4 Discrete polynomial expansion of step function (*N=50*).

K+1	$f(x)$	$\tilde{f}_{DLOP}(x)$	$\tilde{f}_{DT}(x)$
1	1.00000000000000	1.00000000000000	1.00000000000000
2	1.00000000000000	1.00000000000399	1.00000000000000
3	1.00000000000000	1.00000000000165	1.00000000000000
4	1.00000000000000	0.999999999999990	1.00000000000000
5	1.00000000000000	1.00000000000017	1.00000000000000
6	1.00000000000000	0.999999999998952	1.00000000000000
7	1.00000000000000	1.00000000000584	1.00000000000000
8	1.00000000000000	0.999999999971401	1.00000000000000
9	1.00000000000000	1.00000000012329	1.00000000000000
10	1.00000000000000	0.999999999529458	0.999999999999999
11	1.00000000000000	1.00000000159881	0.999999999999999
12	1.00000000000000	0.999999995139274	0.999999999999998
13	1.00000000000000	1.00000001327880	0.999999999999998
14	1.00000000000000	0.999999967291025	0.999999999999998
15	1.00000000000000	1.00000007283855	0.999999999999998
16	1.00000000000000	0.999999853107712	0.999999999999998

17	1.00000000000000	1.00000026848282	0.999999999999998
18	1.00000000000000	0.999999555428817	0.999999999999998
19	1.00000000000000	1.00000066561060	0.999999999999998
20	1.00000000000000	0.999999102811553	0.999999999999998
21	1.00000000000000	1.00000107981626	0.999999999999999
22	1.00000000000000	0.999998857853821	0.999999999999999
23	1.00000000000000	1.00000102659385	0.999999999999999
24	1.00000000000000	0.999999282321613	0.999999999999999
25	1.00000000000000	1.00000025819740	0.999999999999999

The second test is similar to the first one except there are 100 step values of 1.0. Thus, a 100 order expansion is required. With DLOP expansion, the results are completely wrong and the detailed numbers will not be listed. With normalized DT, the results are still very accurate as indicated in Table B.5.

Table B.5 Discrete polynomial expansion of step function (*N=100*).

K+1	$\tilde{f}_{DT}(x)$	*K*+1	$\tilde{f}_{DT}(x)$
1	0.999999999999988	26	0.999999999999999
2	0.999999999999992	27	0.999999999999999
3	0.999999999999994	28	0.999999999999999
4	0.999999999999995	29	0.999999999999999
5	0.999999999999997	30	0.999999999999999
6	0.999999999999997	31	0.999999999999999

7	0.999999999999997	32	0.999999999999999
8	0.999999999999997	33	0.999999999999999
9	0.999999999999996	34	0.999999999999999
10	0.999999999999996	35	0.999999999999999
11	0.999999999999996	36	0.999999999999999
12	0.999999999999997	37	1.00000000000000
13	0.999999999999996	38	0.999999999999999
14	0.999999999999996	39	0.999999999999999
15	0.999999999999997	40	1.00000000000000
16	0.999999999999997	41	0.999999999999999
17	0.999999999999997	42	0.999999999999999
18	0.999999999999997	43	1.00000000000000
19	0.999999999999997	44	1.00000000000000
20	0.999999999999997	45	1.00000000000000
21	0.999999999999998	46	1.00000000000000
22	0.999999999999998	47	1.00000000000000
23	0.999999999999998	48	1.00000000000000
24	0.999999999999999	49	1.00000000000000
25	0.999999999999999	50	1.00000000000000

It should be noted that the step functions tested in this section have a constant value of 1.0. If the range of values is large, a similar effect illustrated in Section 3.4.2 due to double precision representation can be observed.

With the definition of orthonormal DT, the 0^{th} order values are defined as

$$T_0(K, N-1) = \frac{1}{\sqrt{N}} \tag{B.26}$$

so that the squared norm is 1.0. However, with this definition the leading order equation of the DGM method is not equivalent to the standard coarse group equation. This can be alleviated by first generating the orthonormal DT and then re-normalizing in order to satisfy:

$$T_0(K, N-1) = 1. \tag{B.27}$$

With Eq. (B.27), the leading order of the DGM method is equivalent to the coarse group equations.

In the computational tests of the 1-D BWR assemblies and cores in Section 3.3, DLOP are used as the discrete polynomials. All the tests in Section 3.3 are repeated using the developed DT. Computational results with DT are identical to the DLOP results given in Tables 3.1, 3.2 and 3.3 (with the same convergence tolerance). The reason being that the expansion order is not high enough and that our convergence criteria is insufficiently small to expose the inaccuracies discussed previously.

Appendix C. Derivation of DGM method on diffusion equation

The DGM version of the diffusion equation can be derived in a similar way as that of the transport equation. The unknown is now the scalar flux instead of the angular flux. The time-independent diffusion equation eigenvalue problem is:

$$-\nabla D(\vec{r},E)\cdot\nabla\phi(\vec{r},E)+\sigma_t(\vec{r},E)\phi(\vec{r},E)= \int_0^\infty dE'\sigma_s(\vec{r},E'\rightarrow E)\phi(\vec{r},E')+\frac{\chi(\vec{r},E)}{k}\int_0^\infty dE'\nu\sigma_f(\vec{r},E')\phi(\vec{r},E'). \quad (C.1)$$

In Eq.(C.1), the scalar flux ϕ is function of r for all three spatial components and E for the energy. D is the diffusion coefficient. The total and fission macroscopic cross-sections are represented respectively by σ_t and σ_f. The fission energy spectrum is represented by χ and the scattering transfer function is denoted by σ_s. If the energy spectrum is separated into G coarse groups, Eq. (C.1) in coarse group g with energy E_g can be written as:

$$-\nabla D(\vec{r},E_g)\cdot\nabla\phi(\vec{r},E_g)+\sigma_t(\vec{r},E_g)\phi(\vec{r},E_g)= \sum_{g'=1}^{G}\int_{\Delta E_{g'}} dE'\sigma_s(\vec{r},E_{g'}\rightarrow E_g)\phi(\vec{r},E_{g'})+\frac{\chi(\vec{r},E_g)}{k}\sum_{g'=1}^{G}\int_{\Delta E_{g'}} dE'\nu\sigma_f(\vec{r},E_{g'})\phi(\vec{r},E_{g'}). \quad (C.2)$$

Thus, the diffusion equation is separated into G coarse groups, but the energy is still continuous within each group. It is now possible to apply the multigroup methodology within each coarse group g as:

$$-\nabla D(\vec{r},K)\cdot\nabla\phi(\vec{r},K)+\sigma_t(\vec{r},K)\phi(\vec{r},K)=$$
$$\sum_{g'=1}^{G}\sum_{L=0}^{M-1}\sigma_s(\vec{r},L\rightarrow K)\phi(\vec{r},L)+\frac{\chi(\vec{r},K)}{k}\sum_{g'=1}^{G}\sum_{L=0}^{M-1}\nu\sigma_f(\vec{r},L)\phi(\vec{r},L). \tag{C.3}$$

In going from Eq. (C.2) to Eq. (C.3), it is assumed that there are N fine group points within coarse group g with point index $K=0,1,2,...,N-1$, and M fine group points within coarse group g' with point index $L=0,1,2,...,M-1$.

The following step is to expand the energy dependence of the scalar flux into a set of orthogonal moments. The energy dependence of the scalar flux in Eq. (C.3) can be expanded using DLOP or DT within each coarse group g as:

$$\phi(\vec{r},K)=\sum_{i=0}^{N-1}\frac{1}{\rho(i,N-1)}P_i(K,N-1)\phi_{ig}(\vec{r}), \tag{C.4}$$

where $\Delta E_K \in \Delta E_g$, $K=0,...,N-1$ is the index of the fine energy group point within the coarse group g, N is the total number of fine group points within the coarse group g. The flux moments can be obtained from the orthogonality relation:

$$\phi_{ig}(\vec{r})=\sum_{K=0}^{N-1}P_i(K,N-1)\phi(\vec{r},K). \tag{C.5}$$

Substituting Eq. (C.4) into Eq.(C.3), and then multiplying and summing by $\sum_{K=0}^{N-1} P_i(K,N-1)$ to obtain:

$$-\nabla D_{ig}(\vec{r})\cdot\nabla\phi_{ig}(\vec{r})+\sigma_{t,ig}(\vec{r})\phi_{ig}(\vec{r})=$$
$$\sum_{K=0}^{N-1} P_i(K,N-1)\sum_{g'=1}^{G}\sum_{L=0}^{M-1}\sigma_s(\vec{r},L\rightarrow K)\phi(\vec{r},L)+\frac{\chi_{ig}(\vec{r})}{k}\sum_{g'=1}^{G}\sum_{L=0}^{M-1}\nu\sigma_f(\vec{r},L)\phi(\vec{r},L). \quad \text{(C.6)}$$

where $\phi_{ig}(\vec{r})$ is defined in Eq. (C.5) and where

$$\chi_{ig}(\vec{r})=\sum_{K=0}^{N-1} P_i(K,N-1)\chi(\vec{r},K), \quad \text{(C.7)}$$

$$\sigma_{t,ig}(\vec{r})=\frac{\sum_{K=0}^{N-1} P_i(K,N-1)\sigma_t(\vec{r},K)\phi(\vec{r},K)}{\sum_{K=0}^{N-1} P_i(K,N-1)\phi(\vec{r},K)}, \quad \text{(C.8)}$$

$$D_{ig}(\vec{r})=\frac{\sum_{K=0}^{N-1} P_i(K,N-1)D(\vec{r},K)\nabla\phi(\vec{r},K)}{\sum_{K=0}^{N-1} P_i(K,N-1)\nabla\phi(\vec{r},K)}. \quad \text{(C.9)}$$

To avoid the flux gradient in the denominator in Eq. (C.9), some approximations can be made. One way is to define the diffusion coefficient moment in a similar way as in [Henry 1975]:

$$D_{ig}(\vec{r}) = \frac{\sum_{K=0}^{N-1} P_i(K, N-1) D(\vec{r}, K) \phi(\vec{r}, K)}{\sum_{K=0}^{N-1} P_i(K, N-1) \phi(\vec{r}, K)}. \tag{C.10}$$

Note that in Eqs. (C.8) and (C.10), the DLOP or DT appear in the denominators of the expressions. To increase stability of the method, similar to the perturbation technique in the derivation of DGM method for transport equation in Section 3.1, perturbation techniques can be defined for the total cross section moments and diffusion coefficient moments.

We now have a multigroup equation in which each coarse group g contains an expanded flux. The zeroth order of this expansion reverts directly to the well-known multigroup approximation and all higher orders offer information of the spectrum within each coarse group.

The next step is to treat the scattering and fission terms on the right hand side (*RHS*) by preserving the reaction rates. We can define the reaction rates as:

$$R_f(\vec{r}, L) = \nu\sigma_f(\vec{r}, L)\phi(\vec{r}, L) \tag{C.11}$$

$$R_s(\vec{r}, L \to K) = \sigma_s(\vec{r}, L \to K)\phi(\vec{r}, L) \tag{C.12}$$

Expanding both the reaction rates in the following way:

$$R(\vec{r}, L) = \sum_{j=0}^{M-1} \frac{1}{\rho(j, M-1)} P_j(L, M-1) R_{jg}(\vec{r}), \tag{C.13}$$

where

$$R_{jg}(\vec{r}) = \sum_{L=0}^{M-1} P_j(L, M-1) R(\vec{r}, L). \tag{C.14}$$

By the treatment of orthogonal expansion in Eq. (C.13), the reaction rates are preserved.

The *RHS* of Eq. (C.6) becomes:

$$\begin{aligned} RHS &= \sum_{K=0}^{N-1} P_i(K, N-1) \sum_{g'=1}^{G} \sum_{L=0}^{M-1} \sum_{j=0}^{M-1} \frac{1}{\rho(j, M-1)} P_j(L, M-1) R_{s,jg'}(\vec{r}, K) + \\ &\frac{\chi_{ig}(\vec{r})}{k} \sum_{g'=1}^{G} \sum_{L=0}^{M-1} \sum_{j=0}^{M-1} \frac{1}{\rho(j, M-1)} P_j(L, M-1) R_{f,jg'}(\vec{r}) \\ &= \sum_{g'=1}^{G} \sum_{j=0}^{M-1} \sum_{K=0}^{N-1} P_i(K, N-1) \frac{1}{\rho(j, M-1)} R_{s,jg'}(\vec{r}, K) \sum_{L=0}^{M-1} P_j(L, M-1) + \\ &\frac{\chi_{ig}(\vec{r})}{k} \sum_{g'=1}^{G} \sum_{j=0}^{M-1} \frac{1}{\rho(j, M-1)} R_{f,jg'}(\vec{r}) \sum_{L=0}^{M-1} P_j(L, M-1). \end{aligned} \tag{C.15}$$

Now applying the important property of DLOP or DT:

$$\sum_{K=0}^{N-1} P_l(K, N-1) = \rho(0, N-1)\delta_{0l}. \tag{C.16}$$

Only the zeroth order terms ($j = 0$) remain on the *RHS*. The *RHS* can be simplified as:

$$\begin{aligned} RHS &= \sum_{g'=1}^{G}\sum_{K=0}^{N-1} P_i(K, N-1) R_{s,0g'}(\vec{r}, K) + \frac{\chi_{ig}(\vec{r})}{k}\sum_{g'=1}^{G} R_{f,0g'}(\vec{r}) \\ &= \sum_{g'=1}^{G}\sum_{K=0}^{N-1} P_i(K, N-1)\sum_{L=0}^{M-1}\sigma_s(\vec{r}, L \to K)\phi(\vec{r}, L) + \frac{\chi_{ig}(\vec{r})}{k}\sum_{g'=1}^{G}\sum_{L=0}^{M-1}\nu\sigma_f(\vec{r}, L)\phi(\vec{r}, L) \\ &= \sum_{g'=1}^{G}\sigma_{s,i,g'\to g}(\vec{r})\phi_{g'}(\vec{r}) + \frac{\chi_{ig}(\vec{r})}{k}\sum_{g'=1}^{G}\nu\sigma_{f,g'}(\vec{r})\phi_{g'}(\vec{r}), \end{aligned} \tag{C.17}$$

where the coarse group scalar flux and the coarse group fission and scattering cross-sections are given by:

$$\phi_{g'}(\vec{r}) = \sum_{L=0}^{M-1}\phi(\vec{r}, L), \tag{C.18}$$

$$\nu\sigma_{f,g'}(\vec{r}) = \frac{\sum_{L=0}^{M-1}\nu\sigma_f(\vec{r}, L)\phi(\vec{r}, L)}{\sum_{L=0}^{M-1}\phi(\vec{r}, L)}, \tag{C.19}$$

$$\sigma_{s,i,g'\to g}(\vec{r}) = \frac{\sum_{L=0}^{M-1}\phi(\vec{r}, L)\sum_{K=0}^{N-1} P_i(K, N-1)\sigma_s(\vec{r}, L \to K)}{\sum_{L=0}^{M-1}\phi(\vec{r}, L)}. \tag{C.20}$$

Finally, the diffusion equation with polynomial expansion becomes:

$$-\nabla D_{ig}(\vec{r})\cdot\nabla\phi_{ig}(\vec{r})+\sigma_{t,ig}(\vec{r})\phi_{ig}(\vec{r})=\sum_{g'=1}^{G}\sigma_{s,i,g'\to g}(\vec{r})\phi_{g'}(\vec{r})+\frac{\chi_{ig}(\vec{r})}{k}\sum_{g'=1}^{G}\nu\sigma_{f,g'}(\vec{r})\phi_{g'}(\vec{r}). \quad \text{(C.21)}$$

The zeroth order ($i=0$) calculation is equivalent to the standard coarse group calculation, and Eqs. (C.18)-(C.20) can be determined by the zeroth order calculation. With the elimination of the j's moments on the *RHS*, the higher order equations are decoupled from each other and only depend on the zeroth order (coarse group) flux. This decoupling leads to a short computational time comparable to a common multigroup solution over G coarse groups (higher order equations are solved very quickly since their *RHS* is known) but can give a fine-group energy spectrum by the unfolding of the scalar flux from all the moments:

$$\phi(\vec{r},K)=\sum_{i=0}^{N-1}\frac{1}{\rho(i,N-1)}P_i(K,N-1)\phi_{ig}(\vec{r}). \quad \text{(C.22)}$$

Appendix D. Definitions of Errors

If the problem solved has I spatial points in one or multi dimensional geometry and H fine groups, the relative error (RE) with the fine energy group and spatial mesh point indices h and i are defined as a function of two scalar fluxes as:

$$RE(i,h) = \left| \frac{\phi_1(i,h) - \phi_2(i,h)}{\phi_2(i,h)} \right|, \tag{D.1}$$

In terms of this pointwise relative error, mean relative error (mre), root mean square relative error (rms), and maximum relative error ($err_{\max}$) of the scalar flux are defined as:

$$mre = \frac{1}{I \times H} \sum_{i=1}^{I} \sum_{h=1}^{H} \left[RE(i,h) \times \frac{\phi_H(i,h)}{\phi_{H,avg}} \right], \tag{D.2}$$

where the average scalar flux is:

$$\phi_{H,avg} = \frac{1}{I \times H} \sum_{i=1}^{I} \sum_{h=1}^{H} \phi_H(i,h), \tag{D.3}$$

$$rms = \sqrt{\frac{\sum_{i=1}^{I} \sum_{h=1}^{H} RE(i,h)^2}{I \times H}}, \tag{D.4}$$

$$err_{\max} = \max RE(i,h) \quad \text{for all } i \text{ and } h. \tag{D.5}$$

Similarly for the eigenvalue, define the relative error between two eigenvalues as:

$$RE_k = \left| \frac{k_2 - k_1}{k_2} \right|. \tag{D.6}$$

Appendix E. Review of Fixed Point Iteration Algorithms

E.1 Algorithms of power iteration

The operator form of the k-eigenvalue transport equation is:

$$L\psi = MSD\psi + \frac{1}{k}MFD\psi, \tag{E.1}$$

where L is the transport operator, S and F are scattering and fission operators, M and D are moment-to-discrete and discrete-to-moment operators. The traditional method of solving Eq. (E.1) is the power iteration. Algorithms of the power iteration can be found in many references. A brief review of the power iteration algorithm is as follows:

Algorithm E1: PI

Initial guess of flux moments and eigenvalue

Calculate fission source from initial guesses

Do while ($l<L_{max}$ and ($err_l>tol_l$ or $err_k>tol_k$)) ! Outer iteration

! Gauss-Seidel iteration

! Gauss-Seidel part 1: fast group block forward substitution

Do $g=1,IGF$

Construct source vectors for group g:

$$Q_g^l = \frac{1}{k^{l-1}} \sum_{g'=1}^{IG} MF_g D\psi_{g'}^{l-1} + \sum_{g'=1}^{g-1} MS_{g'g} D\psi_{g'}^{l}.$$

Do while ($n<N_{max}$ and $err_n>tol_n$) ! Within group source iteration

! Inverse of transport operator

$$L\psi_g^{l,n} = Q_g^l + MS_{gg} D\psi_g^{l,n-1}.$$

Calculate err_n

Enddo

$$\psi_g^l = \psi_g^{l,n_{last}}$$

enddo

! Gauss-Seidel part 2: thermal upscattering groups, intermediate loop

Do while ($m<M_{max}$ and $err_m>tol_m$)

Do $g=IGF+1,IG$

Construct source vectors for group g:

$$Q_g^{l,m} = \frac{1}{k^{l-1}} \sum_{g'=1}^{IG} MF_g D\psi_{g'}^{l-1} + \sum_{g'=1}^{IGF} MS_{g'g} D\psi_{g'}^{l} + \sum_{g'=IGF+1}^{g-1} MS_{g'g} D\psi_{g'}^{l,m} + \sum_{g'=g+1}^{IG} MS_{g'g} D\psi_{g'}^{l,m-1}$$

Do while ($n<N_{max}$ and $err_n>tol_n$)

! Within group source iteration

! Inverse of transport operator

$$L\psi_g^{l,m,n} = Q_g^{l,m} + MS_{gg} D\psi_g^{l,m,n-1}.$$

Calculate err_n

Enddo

$$\psi_g^{l,m} = \psi_g^{l,m,n_{last}}$$

enddo

Calculate err_m

Enddo ! End of intermediate level thermal upscattering loop

! End of Gauss-Seidel iteration

$$\psi_g^l = \psi_g^{l,m_{last}}$$

Update fission source using ψ^l, calculate err_l

Update eigenvalue using ψ^l and ψ^{l-1}, calculate err_k

Enddo ! End of outer iteration

!!

IG: total number of energy groups.

IGF: number of fast groups (no upscattering).

l,m,n: indices of outer, intermediate and inner iterations.

err_l, err_m, err_n: maximum relative errors of scalar fluxes between two consecutive iterations, defined in Eq. (D.5).

err_k: relative error of eigenvalue defined in Eq. (D.6).

tol_l, tol_m, tol_n: convergence tolerance of flux moments of different loops.

tol_k: convergence tolerance of eigvenvalue.

L_{max}, M_{max}, N_{max}: maximum number of iteration allowed in the outer, intermediate, and inner iterations.

!!

It can be observed that with upscattering, there are three loops in the standard power iteration: inner iteration of the within-group solver, intermediate loop for upscattering in the Gauss-Seidel iteration, and the outer iteration.

The inner iteration is a problem with external source and within group scattering source. It can be solved using standard source iteration with acceleration methods, i.e., diffusion synthetic acceleration (DSA). It can also be solved using Krylov subspace method with DSA as a preconditioner. Discussion of Krylov methods is beyond the scope of this study and only fixed-point iteration algorithms are discussed here.

The intermediate level Gauss-Seidel iteration simplifies to block forward substitution if the problem does not have upscattering. With upscattering, there is an intermediate upscattering loop. This loop leads to inefficient performance of the whole algorithm. The reason is that the source term in the external source Gauss-Seidel problem is the fission source generated using the $(l\text{-}1)^{th}$ outer iteration value which is just an intermediate value. With an intermediate fission source, converging to the true solution with Gauss-Seidel iteration is unnecessary.

There are a few ways to improve the efficiency of the power iteration with full Gauss-Seidel iteration. The first way is to eliminate the intermediate upscattering loop by setting M_{max}=1 [Gill 2011]. The reason is that within each outer iteration, although full Gauss-Seidel solution is not obtained with an intermediate fission source, the existence of outer

iteration guarantees that the upscattering source can still be updated not in the Gauss-Seidel iteration but in the outer iteration together with the fission source.

A further step to improve the overall efficiency is to set both M_{max}=1 and N_{max}=1 [Evans 2010] [Gill 2011]. In this way besides the elimination of the upscattering loop, the within group source iteration is also eliminated. There is only one outer iteration loop left. While this is more efficient than the power iteration with full Gauss-Seidel iteration, it is not guaranteed to converge in some problems [Evans 2010].

Actually, even in the full power iteration algorithm, the existence of M_{max}, tol_m, N_{max} and tol_n makes the Gauss-Seidel iteration a "peudo Gauss-Seidel" iteration because these parameters prevent full convergence of Gauss-Seidel iteration given an intermediate fission source. To summarize, the three algorithms discussed above are:

Algorithm E1: Power iteration with intermediate upscattering loop and inner source iteration loop (3 levels, indices l, m, n).

Algorithm E2: Power iteration with no upscattering loop (2 levels, indices l, n).

Algorithm E3: Power iteration with no upscattering loop and no within group scattering loop (1 level, index l).

A brief review of differences in the above algorithms is necessary for the recondensation method developed in this dissertation. Instead of Algorithm E1, using Algorithm E2 for leading order coarse group calculation makes the recondensation process more efficient. Actually, in this dissertation, Algorithm E2 is used in all the eigenvalue problems, including fine group reference calculations and leading order coarse group calculations.

E.2 Algorithms of external source problems

Note that in external source problems, there is no outer iteration. Upscattering iteration is necessary in the Gauss-Seidel iteration in multigroup problem. The algorithm can be obtained by (1) eliminating the outer iteration, (2) using external source instead of fission source, and (3) setting M_{max} and N_{max} arbitrarily large as:

Algorithm E4: Gauss-Seidel iteration with upscattering loop for external source problem (2 levels, indices m, n).

Note that tol_{nf}, tol_{nt}, tol_m are convergence tolerance for fast group inner iteration, thermal group inner iteration and upscattering iteration, respectively. M_{max} and N_{max} should be large enough for the Gauss-Seidel iteration. If they are limited to small number, it is possible that the iteration can stop before converging to the full Gauss-Seidel solution.

References

[Adams 2002] M. L. Adams and E. W. Larsen, "Fast Iterative Methods for Discrete-Ordinates Particle Transport Calculations," *Progress in Nuclear Energy*, 40, 3.

[Alcouffe 1977] R. E. Alcouffe, "Diffusion Synthetic Acceleration Methods for the Diamond-Differenced Discrete-Ordinates Equations," *Nuclear Science and Engineering*, 64, 344.

[Attieh 2002] I. K. Attieh and R. E. Pevey, "An Adaptive General Multigroup method," *27th Annual CNS-CNA Student Conference*, Toronto, Ontario, Canada, June 2-5, 2002.
[Bell 1970] G. I. Bell and S. Glasstone, "Nuclear Reactor Theory," Van Nostrand Reinhold, New York.

[Attie 2004] I. K. Attieh, "Generalized Multigroup Method," PhD Dissertation, University of Tennessee, Knoxville.

[Bell 1970] G. I. Bell and S. Glasstone, "Nuclear Reactor Theory," Van Nostrand, Princeton, New Jersey.

[Bowman 2007] S. M. Bowman, "Overview of the SCALE Code System," *Transactions of American Nuclear Society*, 97, 589-591.

[Carbon 1973] D. F. Carbon, "A Model-Atmosphere Opacity Code for the CN Red System," *Astrophysical Journal*, 183, 903-921.

[Carbon 1974] D. F. Carbon, "A Comparison of the Straight-Mean, Harmonic-Mean, and Multiple-Picket Approximations for the Line Opacities in Cool Model Atmospheres," *Astrophysical Journal*, 187, 135-145.

[Ching 1976] J. Ching, E. M. Oblow, and H. Goldstein, "A Discrete Energy Formulation of Neutron Transport Theory Applied to Solving the Discrete Ordinates Equations," *Nuclear Science and Engineering*, 61, 159-169.

[Courant 1962] R. Courant and D. Hilbert, "Methods of Mathematical Physics, Volume I", Wiley-Interscience.

[Cullen 1974] D. E. Cullen, "Application of the Probability Table Method to Multigroup Calculations of Neutron Transport," *Nuclear Science and Engineering*, 55, 387.

[Daubechies 1992] I. Daubechies, "Ten Lectures on Wavelets," SIAM, Philadelphia.

[Deuflhard 2004] P. Deuflhard, "Newton Methods for Nonlinear Problems. Affine Invariance and Adaptive Algorithms." Springer Series in Computational Mathematics, Vol. 35, Springer, Berlin.

[Descotes 2011] V. Descotes and J. Ortensi, "Final Report on Utilization of TRU TRISO Fuel as Applied to HTR Systems Part II: Prismatic Reactor Cross Section Generation," INL/EXT-10-20677, Idaho National Laboratory.

[DOE 2002] US DOE Nuclear Energy Research Advisory Committee, "A Technology Roadmap for Generation IV Nuclear Energy Systems," GIF-002-00.

[Duderstadt 1976] J. Duderstadt and L. Hamilton, "Nuclear Reactor Analysis," John Wiley & Sons, Inc.

[Evans 2010] T. M. Evans, K. T. Clarno and J. E. Morel, "A Transport Acceleration Scheme for Multigroup Discrete Ordinates with Upscattering," *Nuclear Science and Engineering*, 165, 292-304.

[Forget 2007] B. Forget and F. Rahnema, "A Spectral Unfolding Method," *Transactions of American Nuclear Society*, 96, 669.

[Forget 2010] B. Forget and L. Zhu, "Mixed Energy Reactor Simulations using the Discrete Generalized Multigroup Method", *International conference on the Physics of Reactors, advances in Reactor Physics to Power the Nuclear Renaissance*, Pittsburgh, Pennsylvania, USA, May 9-14, 2010.

[Gautschi 2004] W. Gautschi, "*Orthogonal Polynomials: Computation and Approximation,*" Oxford University Press.

[Gibbs 1898] J. W. Gibbs, "Fourier's Series," *Nature* 59, 200 (1898) and 606 (1899).

[Gill 2011] D. F. Gill, Y. Y. Azmy, J. S. Warsa and J. D. Densmore, " Newton's Method for the Computation of k-Eigenvalues in SN Transport Applications," *Nuclear Science and Engineering*, 168, 37-58.

[Giust 2000] F. D. Giust, "Release Notes for HELIOS System 1.6," SSP-00/205, Studsvik Scandpower.

[Gougar 2009] H. D. Gougar, "Results of a Neutronic Simulation of HTR-Proteus Core 4.2 Using PEBBED and Other INL Reactor Physics Tools: FY-09 Report," September 2009.

[Greene 2009] N. M. Greene, L. M. Petrie and R. M. Westfall, "NITAWL: SCALE System Module for Performing Resonance Shielding and Working Library Production," ORNL/TM-2005/39, Version 6, Vol. II, Sect. F2.

[Hébert 2006] A. Hébert, "Towards DRAGON Version4", *paper presented at the Topical Meeting on Advances in Nuclear Analysis and Simulation*, Vancouver, Canada, September 10-14, 2006.

[Hébert 2009] A. Hébert, "Applied Reactor Physics," Presses Internationales Polytechnique.

[Herman 2010] M. Herman and A. Trkov, "ENDF-6 Formats Manual," BNL-90365-2009, Brookhaven National Laboratory.

[Henry 1975] A. F. Henry, "Nuclear Reactor Analysis," MIT Press, Cambridge.

[Hobson 1955] E. W. Hobson, "The Theory of Spherical and Ellipsoidal Harmonics," Chelsea Pub. Co..

[Hollenback 1998] D. F. Hollenback and L. M. Petrie, "Comparison of the CENTRM Resonance Processor to the NITAWL Resonance Processor in Scale," American Nuclear Society Annual Meeting, Nashville, Tennessee, June 7-11, 1998.

[IEEE 1985] "IEEE Standard for Binary Floating-Point Arithmetic," ANSI/IEEE Std 754-1985, IEEE Standards Board and American National Standards Institute.

[Jung 2009] Y. Jung and H. Joo, "Decoupled Planar MOC Solution for Dynamic Group Constant Generation in Direct Three-Dimensional Core Calculations," *International Conference on Mathematics, Computational Methods, Reactor Physics*, Saratoga Springs, New York, May 3-7, 2009.

[Kelley 2003] C. T. Kelly, "Solving Nonlinear Equations with Newton's Method, no 1 in Fundamentals of Algorithms," SIAM, 2003.

[Kim 2007] K. S. Kim, J. Y. Cho, H. C. Lee, J. M. Noh and S. Q. Zee, "Development of a Physics Analysis Procedure for the Prismatic Very High Temperature Gas-Cooled Reactors," Annals of Nuclear Energy, 34, 849.

[Lamarsh 1983] J. R. Lamarsh, "Introduction to Nuclear Reactor Theory," 2nd Edition, Addison-Wesley.

[Lathrop 1969] K. D. Lathrop, "Spatial Differencing of the Transport Equation: Positivity vs. Accuracy," *Journal of Computational Physics*, 4, 475.

[Levitt 1972] L. B. Levitt, "The Probability Table Method for Treating Unresolved Neutron Resonance in Monte Carlo Calculations," *Nuclear Science and Engineering*, 49, 450.

[Lewis 1993] E. E. Lewis and W. F. Miller, Jr., "Computational Methods of Neutron Transport," American Nuclear Society, La Grange Park, Illinois.

[Lewis 2001] E. E. Lewis, G. Palmiotti, T. A. Taiwo, M. A. Smith and N. Tsoulfanidis, "Benchmark Specification for Deterministic 2-D/3-D MOX Fuel Assembly Transport Calculations without Spatial Homogenization (C5G7 MOX)," NEA/NSC/DOC(2010)4, March 28, 2001.

[Liu 1981] Y. H. Liu, "Neutron Transport Calculations Involving a Mixture of Group and Discrete-Energy Fluxes," PhD Dissertation, Columbia University.

[MacFarlane 2000] R. E. MacFarlane and D. W. Muir, "NJOY99.0 Code System for Producing Pointwise and Multigroup Neutron and Photon Cross Sections from ENDF/B Data," PSR480/NJOY99.0, Los Alamos National Laboratory.

[Mukundan 2000] R. Mukundan, "Discrete Orthogonal Moment Features Using Chebyshev Polynomials," *Proc. Of Intnl. Conf. on Image and Vision Computing – IVCNZ'00,* p20-25, New Zealand, Nov. 2000.

[Mukundan 2001] R. Mukundan, S. H. Ong, and P. A. Lee, "Discrete vs. continuous orthogonal moments for image analysis," *Proc. Of Intnl. Conf. on Imaging Systems, Science and Technology – CISST'2001*, p23-29, Las Vegas, June 2001.

[Mukundan 2004] R. Mukundan, "Some Computational Aspects of Discrete Orthonormal moments," *IEEE Trans. Image Process.* 13, 1055-1059.

[Müller 1966] C. Müller, "Spherical Harmonics," Lecture Notes in Mathematics, Vol. 17, Springer.

[Neuman 1974] C. P. Neuman and D. I. Schonbach, "Discrete (Legendre) orthogonal polynomials—A Survey," *Int. J. Numer. Methods Eng.*, 8, 743.

[Nikiforov 1988] A. V. Nikiforov, V. B. Uvarov, "Special Functions of Mathematical Physics," Birkhauser, Bessel, Boston.

[Nikiforov 1991] A. V. Nikiforov, S. K. Suslov and V. B. Uvarov, "Classical Orthogonal Polynomials of a Discrete Variable," Springer, New York.

[Nikolaev 1976] M. N. Nikolaev, "Comments on the Probability Table Method," *Nuclear Science and Engineering*, 61, 286.

[Ortensi 2010] J. Ortensi, Personal communication, Idaho National Laboratory, 2010.

[Querci 1974] F. Querci, M. Querci and T. Tsuji, "Model Atospheres for C Type Stars," *Astron. & Astrophys.* 31, 265-282.

[Rahnema 2008] F. Rahnema, S. Douglass, and B. Forget, "Generalized Energy Condensation Theory," *Nuclear Science and Engineering*, 160, 41.

[Roberts 2010] D. R. Roberts, M. Ouisloumen, V. N. Kucukboyaci and K. N. Ivanov, "Development of Iterative Transport-Diffusion Methodology for LWR Analysis," *International conference on the Physics of Reactors, advances in Reactor Physics to Power the Nuclear Renaissance*, Pittsburgh, Pennsylvania, USA, May 9-14, 2010.

[Smith 1980] K. S. Smith, "Spatial Homogenization Methods for Light Water Reactor Analysis," PhD Dissertation, Massachusetts Institute of Technology.

[Smith 2002] K. S. Smith and J. D. Rhodes III, "Full-core, 2-D, LWR core calculation with CASMO-4E," *Proc. Int. Conf. on the New Frontiers of Nuclear Technology: Reactor Physics, Safety and High-Performance Computing (PHYSOR 2002)*, 13A-04, Oct. 7-10, Seoul, Korea.

[Stamm'ler 1983] R. J. J. Stamm'ler and M. J. Abbate, "Methods of Steady-State Reactor Physics in Nuclear Design," Academic Press, 1983.

[Williams 1995] M. L. Williams and M. Asgari, "Computation of Continuous-Energy Neutron Spectra with Discrete Ordinates Transport Theory," *Nuclear Science and Engineering*, 121, 173-201.

[Williams 2000] M. L. Williams, "Submoment Expansion of Neutron-Scattering Sources," *Nuclear Science and Engineering*, 134, 218-226.

[Williams 2009] M. L. Williams, M. Asgari, D. F. Hollenbach, "CENTRM: A One-Dimensional Neutron Transport Code for Computing Pointwise Energy Spectra," ORNL/TM-2005/39, Version 6, Vol. II, Sect. F18.

[Williams 2009, 2] M. L. Williams and D. F. Hollenback, "PMC: A Program to Produce Multigroup Cross Sections Using Pointwise Energy Spectra from CENTRM," ORNL/TM-2005/39, Version 6, Vol. II, Sect. F19.

[Wu 2010] H. Wu, L. Cao, Y. Zheng and W. Yang, "The Wavelet Function Expansion Method for Solving the Neutron Transport Equation," *International conference on the Physics of Reactors, advances in Reactor Physics to Power the Nuclear Renaissance*, Pittsburgh, Pennsylvania, USA, May 9-14, 2010.

[Yamamoto 2004] A. Yamamoto, Y. Kitamura, T. Ushio and N. Sugimura, "Convergence Improvement of Coarse Mesh Rebalance Method for Neutron Transport Calculations," *Journal of Nuclear Science and Technology*, 41, 781.

[Zerkle 1997] M. L. Zerkle, I. K. Abu-Shumays, M. W. Ott, and J. P. Winwood, "Theory and Application of the RAZOR Two-Dimensional Continuous Energy Lattice Physics Code,"*Proc. Joint Int. Conf. Mathematical Methods and Supercomputing for Nuclear Applications*, Saratoga Springs, New York, October 5–9, 1997, Vol. 1, p. 417, American Nuclear Society.

[Zhong 2005] Z. Zhong, "Continuous Energy, Multi-Dimensional Discrete Ordinates Transport Calculations for Problem Dependent Resonance Treatment," PhD dissertation, Purdue University.

[Zhong 2006] Z. Zhong, T. J. Downar and Y. Xu, "Continuous-Energy Multidimensional SN Transport for Problem-Dependent Resonance Self-Shielding Calculations," *Nuclear Science and Engineering*, 154, 190-201.

[Zhu 2010] L. Zhu and B. Forget, "A Discrete Generalized Multigroup Energy Expansion Theory," *Nuclear Science and Engineering*, 166, 239.

[Zhu 2011] L. Zhu and B. Forget, "An Energy Recondensation Method Using the Discrete Generalized Multigroup Energy Expansion Theory," *Annals of Nuclear Energy*, 38, 1718.

[Zhu 2011, 2] L. Zhu and B. Forget, "A Nonlinear Energy Acceleration Method," *Transactions of American Nuclear Society*, 104, 317, 2011.